Technische Universität Wien

DIPLOMARBEIT

Phase Behaviour of Symmetrical Binary Mixtures in a Field

Ausgeführt am Institut für
Theoretische Physik
der Technischen Universität Wien
unter der Anleitung von
Ao. Univ. Prof. Dr. Gerhard Kahl

durch
Jürgen Köfinger
Kl. Krummnußbaum 146, 3671 Marbach/Donau

20. 10. 2004

Meinen Eltern.

Abstract

In an effort to gain more insight into the phase behaviour of binary mixtures in an external field, we solve the Ornstein-Zernike equation with the mean spherical approximation closure relation for the symmetrical binary Yukawa mixture in the field $\Delta\mu$, i.e. the difference of the chemical potentials of the two components, and present examples for two different types of phase diagrams in the space spanned by the temperature, the concentration and the number density, i.e. a mixed field-density space, and in the (temperature, pressure, $\Delta\mu$)-space, i.e. a field space. Advanced Metropolis Monte Carlo simulation methods, that allow to sample coexisting phases in a single run, and histogram reweighting techniques are applied to obtain quantitative results for coexistence lines and critical points for one of the aforementioned types.

Contents

Chapter 1

Introduction

Nearly all liquids of every day life are mixtures, often of a large number of components, like paint, blood, drugs, drinks, gas, and oil. It is evident from their omnipresence that the knowledge of the phase behaviour is important for production processes, technical applications, the design of liquids with certain properties, and for the developement of new drugs to give a few examples.

Already mixtures of only two components, so called binary mixtures, are very complex and have too many unknown parameters, so that reasonable models that provide quantitative results are out of reach. Only by applying simplifications and approximations we can find models that can be treated in theoretical frameworks and that give results that allow us to predict the phase behaviour of more complex mixtures at least at a qualitative level.

The **symmetrical binary mixture** is considered to be the simplest model for a fluid consisting of two components. This symmetry is due to the same size of the particles of both species and that the interaction of like particles is the same in both components. The interaction of dislike particles is different and is characterised by a single parameter δ which therefore determines the topology of the phase diagram. The symmetrical mixture can also be used as a model for a one-component fluid of particles with an additional internal degree of freedom [1], like magnetic [2, 3, 4, 5] and dipolar [6, 7] fluids, and the Ising-spin fluid [8, 9, 10].

Most studies of the phase behaviour of the symmetrical binary mixure were restricted to the case that no external field is applied [11, 12, 13]. The types of phase diagrams for systems without an external field can be distinguished by the way the demixing critical line, i.e. the λ-line, intersects the vapour-liquid coexistence line. Usually they are classified in three types labelled I, II, and III.

Pini *et al.* [14] are to our knowledge the first authors that presented isothermal cuts of the phase diagram of a symmetrical binary mixture in an external field. They applied mean field theory and hierarchical reference theory to a symmetrical binary mixture of particles that interact via hard-core Yukawa potentials.

The first aim of this thesis is to extend the inisight into the phase behaviour of these systems

by applying standard integral equation theory to the symmetrical binary Yukawa mixture, and present comprehensive phase diagrams in the temperature, concentration, density space and in the space of temperature, pressure, and the difference of the chemical potentials of the components. We have chosen the mean spherical approximation (MSA) as closure relation for the Ornstein-Zernike equation. This method provides semi-quantitive results but has the advantage that we can solve the Ornstein-Zernike equation for our system to a large extent analytically which reduces the numerical effort [15, 16, 17, 18]. The phase diagrams that we present for two subtypes of type II are to our knowledge the first representations of integral equation results for binary mixtures in a three-dimensional thermodynamic space.

The second aim of this work is to obtain quantitative results for the phase diagram of the system in an external field by Metropolis Monte Carlo simulation [19, 20, 21]. We used the mulitcanonical sampling technique [22] in the framwork of the grand canonical ensemble and histrogram reweighting methods [23, 24] for data analysis [25]. We present simulation results for parts of isothermal cuts and values of critical points in the non-equimolar region which represent to our knowledge the first Monte Carlo simulation data for a symmetrical binary system in an external field.

The thesis is organised as follows: We present a review of the basic concepts of thermodynamics and statistical mechanics in chapter 2 and introduce the model for the symmetrical binary Yukawa mixture in chapter 3. The theoretical foundations of integral equation theory are summarized in chapter 4 and the Monte Carlo simulation method is explained in chapter 5. The MSA results are compiled in chapter 6 and Monte Carlo results in chapter 7.

Chapter 2

Basic Concepts

2.1 Introduction

A **thermodynamic system** is considered to be a substance that is separated from its surroundings in a specific way. The systems are classified by the way they can interact with each other, i.e. by the quantities they can exchange. **Isolated** systems do not interact with each other at all, on the contrary to **open** systems that can exchange energy and particles. **Closed** systems are not allowed to exchange any particles but there is the possibility of energy transfer via a diathermic wall or the exchange of volume.

Let us assumce the substance in consideration consists of N spherically symmetrical, identical particles and each particle has three translational degrees of freedom. Therefore the microscopic state of the system is given by $3N$ configurational coordinates $\mathbf{r}^N = \{\mathbf{r}_1 \dots \mathbf{r}_N\}$ and $3N$ momenta $\mathbf{p}^N = \{\mathbf{p}_1 \dots \mathbf{p}_N\}$. The enterity of all possible microscopic states of a system defines the **phase-space**. The Hamilton function of the system is

$$\mathcal{H}(\mathbf{p}^N, \mathbf{r}^N) = \mathcal{K}(\mathbf{p}^N) + \mathcal{U}(\mathbf{r}^N) \tag{2.1}$$

with the kinetic energy $\mathcal{K}(\mathbf{p}^N)$ depending only on the momenta and the potential energy $\mathcal{U}(\mathbf{r}^N)$ depending on the configuration.

Taking only two-body interactions into account the **total potential energy** $\mathcal{U}(\mathbf{r}^N)$ can be written as a sum over the pair potentials $\phi(\mathbf{r}_i, \mathbf{r}_j)$ and is then called to be **pairwise-additive**. The value of $\phi(\mathbf{r}_i, \mathbf{r}_j)$ is the potential energy of two particles alone at the coordinates $\mathbf{r}_i$ and $\mathbf{r}_j$. *Spherically symmetrical* particles are described by *spherically symmetrical* pair potentials which therefore only depend on the distance $r_{ij} = |\mathbf{r}_i - \mathbf{r}_j|$ between the particles. Bringing all these properties together we can write the total potential energy as

$$\mathcal{U}(\mathbf{r}^N) = \sum_{i=1}^{N} \sum_{j=i+1}^{N} \phi(r_{ij}). \tag{2.2}$$

2.2 The Ensemble Average

Gibbs introduced the concept of an **ensemble** which is a collection of a large number of copies of the system (so called replicas). These replicas have the same macroscopic parameters but they are in different microscopic states distributed according to the **phase-space probability density** $f^{(N)}(\mathbf{r}^N, \mathbf{p}^N; t)$.

The probability that the system is in a certain microscopic state at a time t can be expressed as the probability $f^{(N)}(\mathbf{r}^N, \mathbf{p}^N; t)\mathrm{d}\mathbf{r}^N\mathrm{d}\mathbf{p}^N$ that the corresponding point in phase-space is located in an infinitely small phase-space element $\mathrm{d}\mathbf{r}^N\mathrm{d}\mathbf{p}^N$ at the phase-space coordinates $(\mathbf{r}^N, \mathbf{p}^N)$ at the time t.

For a system in equilibrium the probability density $f^{(N)}$ is time independent and we call it $p(\mathbf{r}^N, \mathbf{p}^N)$. The expectation A of an observable $A(\mathbf{r}^N, \mathbf{p}^N)$ is obtained by the so called **ensemble average**, i.e. we measure the quantity of interest in the systems of the ensemble and calculate the average.

Ensembles are distinguished by their interactions with so called reservoirs and therefore by the variables that define the macroscopic state of the system. To illustrate that we fix the temperature of a diathermic system by bringing it in contact with a so called energy **reservoir** (or heat bath) which is an infinitely large system at a constant temperature T. This defines the canonical ensemble consisting of systems with fixed particle number N, volume V, and fixed temperature T.

2.3 The Canonical and the Grand Canonical Ensemble

2.3.1 The Canonical Ensemble Average

As mentioned in section (2.2) a system in the canonical ensemble has fixed particle number N, fixed volume V and is in thermodynamic equilibrium with a heat bath at temperature T. We define the inverse temperature $\beta = \frac{1}{k_\mathrm{B}T}$ with k_B being Boltzmann's constant.

The **canonical equilibrium probability density** is given by

$$p(\mathbf{r}^N, \mathbf{p}^N) = \frac{1}{N!h^{3N}} \frac{e^{-\beta\mathcal{H}(\mathbf{r}^N, \mathbf{p}^N)}}{Q_N(V,T)} \tag{2.3}$$

with the **canonical partition function**

$$Q_N(V,T) = \frac{1}{N!h^{3N}} \int\int \mathrm{d}\mathbf{r}^N\mathrm{d}\mathbf{p}^N e^{-\beta\mathcal{H}(\mathbf{r}^N, \mathbf{p}^N)}. \tag{2.4}$$

h is Planck's constant and the prefactor h^{-3N} ensures that $f^{(N)}(\mathbf{r}^N, \mathbf{p}^N; t)\mathrm{d}\mathbf{r}^N\mathrm{d}\mathbf{p}^N$ and $Q_N(V,T)$ go over to the corresponding quantities of quantum statistics. The factor $1/N!$ corrects for the indistinguishability of the particles.

For the Hamilton function (2.1) the integration over the momenta in equation (2.4) can be per-

formed analytically. The partition function becomes

$$Q_N(V,T) = \frac{1}{N!\Lambda^{3N}} Z_N(V,T) \tag{2.5}$$

with the configurational part of the partition function $Z_N(V,T)$ defined as

$$Z_N(V,T) = \int \mathrm{d}\mathbf{r}^N e^{-\beta \mathcal{U}(\mathbf{r}^N)}. \tag{2.6}$$

Above we have introduced the **de Broglie thermal wavelength** Λ which is defined as

$$\Lambda = \left(\frac{2\pi\beta\hbar^2}{m}\right)^{\frac{1}{2}}. \tag{2.7}$$

The ensemble average of an observable $A(\mathbf{r}^N, \mathbf{p}^N)$ in the canonical ensemble is given by

$$\begin{aligned} \langle A \rangle &= \int\int \mathrm{d}\mathbf{r}^N \mathrm{d}\mathbf{p}^N p(\mathbf{r}^N, \mathbf{p}^N) A(\mathbf{r}^N, \mathbf{p}^N) \\ &= \frac{1}{N!h^{3N} Q_N(V,T)} \int\int \mathrm{d}\mathbf{r}^N \mathrm{d}\mathbf{p}^N A(\mathbf{r}^N, \mathbf{p}^N) e^{-\beta \mathcal{H}(\mathbf{r}^N, \mathbf{p}^N)} \\ &= \frac{1}{\int\int \mathrm{d}\mathbf{r}^N \mathrm{d}\mathbf{p}^N e^{-\beta \mathcal{H}(\mathbf{r}^N, \mathbf{p}^N)}} \int\int \mathrm{d}\mathbf{r}^N \mathrm{d}\mathbf{p}^N A(\mathbf{r}^N, \mathbf{p}^N) e^{-\beta \mathcal{H}(\mathbf{r}^N, \mathbf{p}^N)}. \end{aligned} \tag{2.8}$$

2.3.2 The Grand Canonical Ensemble Average

A system in the grand canonical ensemble has fixed temperature T, fixed volume V, and fixed chemical potential μ.

The **grand canonical partition function** is given by

$$Q(\mu,V,T) = \sum_{N=0}^{\infty} \frac{1}{h^{3N} N!} \int\int \mathrm{d}\mathbf{r}^N \mathrm{d}\mathbf{p}^N e^{-\beta(\mathcal{H}(\mathbf{p}^N, \mathbf{r}^N) - \mu N)} \tag{2.9}$$

and can be rewritten for the Hamilton function (2.1) as

$$Q(\mu,V,T) = \sum_{N=0}^{\infty} \frac{1}{\Lambda^{3N} N!} \int \mathrm{d}\mathbf{r}^N e^{-\beta(\mathcal{U}(\mathbf{r}^N) - \mu N)}. \tag{2.10}$$

The ensemble average of an observable $A(\mathbf{r}^N, \mathbf{p}^N)$ in the grand canonical ensemble is given by

$$\langle A \rangle = \sum_{N=0}^{\infty} \frac{1}{N!h^{3N} Q(\mu,V,T)} \int\int \mathrm{d}\mathbf{r}^N \mathrm{d}\mathbf{p}^N A(\mathbf{r}^N, \mathbf{p}^N) e^{-\beta(\mathcal{H}(\mathbf{r}^N, \mathbf{p}^N) - \mu N)}. \tag{2.11}$$

2.3.3 Thermodynamic Potentials

The macroscopic quantities that define the thermodynamic state of a system are called **state variables**. A **thermodynamic potential** is a function of the state variables that is capable of describing the thermodynamic behaviour of a system. All thermodynamic equilibrium properties can be calculated by derivatives of the potential which give the so called **equations of state**. Every thermodynamic potential can be expressed as logarithm of the corresponding partition function.

The **Helmholtz free energy** is the thermodynamic potential of the canonical ensemble and therefore it is proportional to the logarithm of the canonical partition function

$$F = -\frac{1}{\beta} \ln Q_N(V,T). \tag{2.12}$$

Introducing the partition function of a gas of non interacting particles, i. e. the ideal gas,

$$Q_N^{\mathrm{id}}(V,T) = \frac{1}{N!\Lambda^{3N}} V^N \tag{2.13}$$

we can rewrite the canonical partition function as

$$Q_N(V,T) = \frac{Z_N(V,T)}{V^N} Q_N^{\mathrm{id}}(V,T). \tag{2.14}$$

Thus the free energy can be written as a sum of the free energy of the ideal gas F^{id} (ideal part) and the excess part F^{ex} that contains the contributions to F caused by the interaction of particles

$$F = F^{\mathrm{id}} + F^{\mathrm{ex}}. \tag{2.15}$$

Using Stirling's approximation for large N the **ideal free energy** is

$$\beta F^{\mathrm{id}} = \ln \rho + 3 \ln \Lambda - 1 \tag{2.16}$$

and the **excess free energy** in the canonical ensemble is given by

$$F^{\mathrm{ex}} = -\frac{1}{\beta} \ln \frac{Z_N(V,T)}{V^N}. \tag{2.17}$$

We also can split up the **internal energy** U

$$U = U^{\mathrm{id}} + U^{\mathrm{ex}} \tag{2.18}$$

in an ideal part $U^{\mathrm{id}} = \frac{3}{2} N k_{\mathrm{B}} T$ and the excess part

$$U^{\mathrm{ex}} = \frac{1}{Z_N(V,T)} \int \mathrm{d}\mathbf{r}^N \mathcal{U}(\mathbf{r}^N) e^{-\beta \mathcal{U}(\mathbf{r}^N)}. \tag{2.19}$$

2.4 Structural Functions

2.4.1 n-Particle Density

The **n-particle density** is defined as

$$\rho_N^{(\mathrm{n})}(\mathbf{r}_1, \ldots, \mathbf{r}_n) \equiv \rho_N^{(n)}(\mathbf{r}^n) = \left\langle \sum_{i_1=1}^{N} \sum_{i_2=i_1+1}^{N} \cdots \sum_{i_n=i_{n-1}+1}^{N} \prod_{j=1}^{n} \delta(\mathbf{r}_j - \mathbf{r}'_{i_j}) \right\rangle. \tag{2.20}$$

Multiplying $\rho_N^{(n)}(\mathbf{r}^n)$ by its normalisation constant $\frac{(N-n)!}{N!}$ we can write the probability $p_N^{(n)}(\mathbf{r}^n)$ of finding n particles in a volume $\mathrm{d}\mathbf{r}^n$ at the coordinates $\mathbf{r}^n$ as

$$p_N^{(n)}(\mathbf{r}^n) = \frac{(N-n)!}{N!} \rho_N^{(n)}(\mathbf{r}^n) \mathrm{d}\mathbf{r}^n. \tag{2.21}$$

In the canonical ensemble the n-particle density is given by

$$\rho_N^{(n)}(\mathbf{r}^n) = \frac{N!}{(N-n)!}\frac{1}{N!h^{3N}Q_N(V,T)}\int\int \mathrm{d}\mathbf{r}^{(N-n)}\mathrm{d}\mathbf{p}^N e^{-\beta\mathcal{H}(\mathbf{r}^N,\mathbf{p}^N)}. \tag{2.22}$$

If the Hamilton function $\mathcal{H}(\mathbf{r}^N,\mathbf{p}^N)$ is of form (2.1) the ensemble average simplifies to

$$\rho_N^{(\mathrm{n})}(\mathbf{r}) \quad = \quad \frac{N!}{(N-n)!}\frac{1}{Z_N}\int \mathrm{d}\mathbf{r}^{(N-n)}e^{-\beta\mathcal{U}(\mathbf{r}^N)}. \tag{2.23}$$

For the 1-particle density of a spatially homogeneous system we get

$$\int \rho_N^{(1)}(\mathbf{r})\mathrm{d}\mathbf{r} = \rho V = N \Rightarrow \rho = \frac{N}{V}. \tag{2.24}$$

2.4.2 n-Particle Distribution Function

The **n-particle distribution function** is defined as

$$g_N^{(\mathrm{n})}(\mathbf{r}^n) = \frac{1}{\rho_N^{(1)}(\mathbf{r}_1)\ldots\rho_n^{(1)}(\mathbf{r}_n)}\rho_N^{(\mathrm{n})}(\mathbf{r}^n), \tag{2.25}$$

and reduces for a spatially homogeneous system to

$$g_N^{(\mathrm{n})}(\mathbf{r}^n) = \frac{1}{\rho^n}\rho_N^{(\mathrm{n})}(\mathbf{r}^n). \tag{2.26}$$

The **pair distribution function** $g_N^{(2)}(\mathbf{r}_1,\mathbf{r}_2)$ for a spatially homogeneous and isotropic system only depends on the distance $r = |\mathbf{r}_1 - \mathbf{r}_2|$ and is then called **radial distribution function** $g(r)$. For separation distances much larger than the range of the interaction potential the pair distribution function approaches the ideal-gas limit

$$\lim_{r\to\infty} g(r) = 1 - \frac{1}{N} \tag{2.27}$$

which reads in the thermodynamic limit

$$\lim_{r\to\infty} g(r) = 1. \tag{2.28}$$

We can use the radial distribution function to calculate the mean number of particles in a spherical shell around a reference particle. If the shell extends from a distance r to $r+\mathrm{d}r$ from the reference particle, the mean number of particles in this shell is given by

$$n(r)\mathrm{d}r = 4\pi r^2\rho g(r)\mathrm{d}r. \tag{2.29}$$

Another useful correlation function is the **total correlation function** $h(\mathbf{r})$ which is defined as

$$h(\mathbf{r}) = g(\mathbf{r}) - 1. \tag{2.30}$$

For mixtures of n components we introduce the **partial pair distribution function** $g_{ij}(\mathbf{r})$. The radial distribution function $g_{ij}(r)$ is related to the probability that for a particle of component i a particle of component j can be found in a distance r. The total correlation function between two particles of species i and j is $h_{ij}(\mathbf{r}) = g_{ij}(\mathbf{r}) - 1$.

2.4.3 Structure Factor

The **static structure factor** is an autocorrelation function of special importance because it can be directly measured through scattering experiments with neutrons or X-rays. The static structure factor is defined as

$$S(\mathbf{k}) = \frac{1}{N}\langle \rho_{\mathbf{k}}\, \rho_{-\mathbf{k}} \rangle \tag{2.31}$$

with $\rho_{\mathbf{k}}$ being the Fourier transform of the 1-particle density $\rho(\mathbf{r})$

$$\rho_{\mathbf{k}} = \int \mathrm{d}\mathbf{r}\, \rho(\mathbf{r}) e^{-\mathrm{i}\mathbf{k}\cdot\mathbf{r}}. \tag{2.32}$$

For a spatially homogeneous and isotropic fluid the structure factor can be written as Fourier transform of the **total correlation function** $h(r) = g(r) - 1$

$$S(\mathbf{k}) = 1 + \rho \int \mathrm{d}\mathbf{r}\, h(r) e^{-\mathrm{i}\mathbf{k}\cdot\mathbf{r}}. \tag{2.33}$$

The above definitions are easily extended to mixtures with n components labelled i and j. The **partial structure factors** are defined as

$$S_{ij}(\mathbf{k}) = \frac{1}{N}\langle \rho^i_{\mathbf{k}}\, \rho^j_{-\mathbf{k}} \rangle \tag{2.34}$$

and can be written as integrals over the **partial pair distribution functions** $g_{ij}(r)$

$$S_{ij}(\mathbf{k}) = \delta_{ij} + (\rho_i \rho_j)^{\frac{1}{2}} \int \mathrm{d}\mathbf{r}\, e^{-\mathrm{i}\mathbf{k}\cdot\mathbf{r}} [g_{ij}(r) - 1]. \tag{2.35}$$

2.4.4 The Equation of State

As mentioned in section (2.3.3) an **equation of state** is a relation between the macroscopic properties that defines the thermodynamic state of a system. Given the equation of state all other thermodynamic properties can be derived. For a pairwise-additive interaction potential (equation (2.2)) all thermodynamic properties can be written as integrals over the radial distribution function. We introduce the pressure p and the isothermal compressibility χ_{T}.

The **energy equation** is given by

$$\frac{U^{\mathrm{ex}}}{N} = 2\pi\rho \int_0^\infty \mathrm{d}r\, \phi(r) g(r) r^2. \tag{2.36}$$

The **pressure** or **virial equation** reads

$$\frac{\beta p}{\rho} = 1 - \frac{2}{3}\pi\beta\rho \int_0^\infty \mathrm{d}r\, \frac{\mathrm{d}\phi(r)}{\mathrm{d}r} g(r) r^3. \tag{2.37}$$

The **compressibility equation** can only be derived in the grand canonical ($TV\mu$) ensemble. The result is also valid for interparticle forces which are not pairwise-additive:

$$\frac{\rho\chi_{\mathrm{T}}}{\beta} = 1 + \rho \int \mathrm{d}\mathbf{r}\, [g(\mathbf{r}) - 1] \tag{2.38}$$

If we know the radial distribution function exactly the equations of state yield the same thermodynamic properties. Usually this is not the case. Depending on which equation we use to derive thermodynamic properties we call it the energy, the pressure, or the compressibility route.

2.5 Phase Transitions

2.5.1 Equilibrium

Let us assume we have two systems I and II of a n-component fluid. These systems are thermodynamically open, i.e. they can exchange energy and particles. They are in **thermodynamic equilibrium** with each other if the temperature, the pressure, and the chemical potentials are the same in each system.

$$T^{(\mathrm{I})} = T^{(\mathrm{II})} \qquad p^{(\mathrm{I})} = p^{(\mathrm{II})} \qquad \mu_i^{(\mathrm{I})} = \mu_i^{(\mathrm{II})} \qquad \text{for} \quad i = 1 \dots n \tag{2.39}$$

These conditions are called **thermal**, **mechanic**, and **material equilibrium**.

2.5.2 Phase Stability

A **phase** can be described as a spatially homogeneous state of matter. Phases can differ in many respects, such as structure, density, composition, order or symmetry for example. The requirement of **thermal stability** is expressed by

$$-T \left(\frac{\partial^2 F}{\partial T^2} \right)_{V,N} = c_{\mathrm{V}} > 0. \tag{2.40}$$

where c_{V} is the specific heat at constant volume V.
A one-component system can only be in a single phase if it is **mechanically stable**

$$V \left(\frac{\partial^2 F}{\partial V^2} \right)_{T,N} = \chi_{\mathrm{T}}^{-1} \geq 0. \tag{2.41}$$

Using the more familiar expression

$$\chi_{\mathrm{T}} = -\frac{1}{V} \left(\frac{\partial V}{\partial p} \right)_{T,N} \tag{2.42}$$

for the isothermal compressibility we can see that the condition of mechanical stability states that the pressure p cannot decrease with decreasing volume V. The limit of stability is given by $\chi_{\mathrm{T}}^{-1} = 0$ and defines the so called **spinodal line** (or surface in general) in the space of state variables.

A mixture also has to have **material stability** which is expressed by

$$\left(\frac{\partial^2 G}{\partial x_i^2} \right)_{T,p,N} \geq 0 \tag{2.43}$$

with x_i being the mol fraction of species i.

If mechanical stability is violated, that is the isothermal compressibility is negative, the free energy of the fluid is lowered by splitting in two phases with different densities. The violation of material stability leads to a separation into phases with different concentrations in order to lower the Gibbs free energy.

2.5.3 Phase Coexistence

At the **phase transition** two (or more) phases are in thermodynamic equilibrium that is in coexistence. Therefore the system consists of two (or more) regions which are themselves spatially homogeneous. For a mixture of n components where n_p phases are in coexistence the **variance** or **degree of freedom** $\mathcal{F}$ is given by **Gibbs' phase rule**

$$\mathcal{F} = n + 2 - n_\mathrm{p}. \tag{2.44}$$

The variance is the number of intensive variables of the system that can be changed without destroying phase coexistence. As example we consider a one-component fluid ($n = 1$). The state is defined by the two intensive variables temperature T and pressure p. If we have a vapour-liquid transition two phases are in coexistence ($n_\mathrm{p} = 2$). Therefore the degree of freedom is $\mathcal{F} = 1$ and we can vary the pressure for example. Thus the temperature $T(p)$ is a function of the pressure which defines a one dimensional coexistence line in the $T-p$ plane. This is an example for a **phase diagram**, a term that is usually used for any visualisation of the phase behaviour of a system.

At a phase transition the thermodynamic potential has a singularity. If any of the first derivatives of the thermodynamic potential has a finite discontinuity it is called a **first-order phase transition**. At a **continuous** or **critical phase transition** the first derivatives are continuous and at least one of the second derivatives shows a discontinuity or divergence [26].

2.5.4 The Order Parameter

Phase transitions can also be characterised by the behaviour of an **order parameter** which was introduced by Landau in the late 1930s. At a first order phase transition the order parameter changes discontinuously as one crosses the coexistence curve. At a continuous phase transition the symmetry of the system is always broken and the order parameter becomes non zero. An order parameter describing the vapour-liquid transition is the difference of the particle number densities of the vapour and the liquid phase.

2.5.5 Critical Phenomena

At a critical point a continuous phase transition occurs, specified by the critical temperature T_c and the critical pressure p_c. In the following we define a measure for the deviation of the temperature T from T_c as

$$t = \frac{T - T_\mathrm{c}}{T_\mathrm{c}}. \tag{2.45}$$

Some of the second derivatives of the thermodynamic potential which correspond to thermodynamic properties (like specific heat c_V and isothermal compressibility χ_T) show divergencies at a critical point. The behaviour of these quantities close to the critical point ($t \to \pm 0$) is described via a power-law. Introducing **critical exponents** some of them are summarised for fluid systems in table 2.1 [26], where we introduce the **correlation length** ξ. One possible definition for this quantity is given by the length scale of the exponential decay $e^{-r/\xi}$ with distance r of the order parameter correlation function.

The critical exponents depend only on a few fundamental parameters, e.g. for short-range interactions the critical exponents depend on the dimensionality of space d and the symmetry of

specific heat (at constant volume)	$c_{\mathrm{V}} \sim \lvert t\rvert^{-\alpha}$
liquid-gas density difference	$(\rho_{\mathrm{liq}} - \rho_{\mathrm{vap}}) \sim (-t)^{\beta}$
isothermal compressibility	$\chi_{\mathrm{T}} \sim \lvert t\rvert^{-\gamma}$
critical isotherm ($t = 0$)	$p - p_{\mathrm{c}} \sim \lvert\rho_{\mathrm{liq}} - \rho_{\mathrm{vap}}\rvert^{\delta}\mathrm{sgn}(\rho_{\mathrm{liq}} - \rho_{\mathrm{vap}})$
correlation length	$\xi \sim \lvert t\rvert^{-\nu}$
pair correlation function at T_{c}	$g(\mathbf{r}) \sim \frac{1}{r^{d-2+\eta}}$

Table 2.1: Definitions for critical exponents for fluid systems.

the order parameter. Therefore models can be assigned to so called **universality classes** which comprise systems with the same set of critical exponents and therefore show the same critical behaviour. These classes are named after their most prominent member like the 2d and 3d Ising, 3d X-Y, 3d-Heisenberg, and the 2d Potts universality class.

2.5.6 Field Space

Griffith and Wheeler [27] introduced the concepts of **fields** and **densities** in addition to the concept of **intensive** and **extensive** quantities. Extensive variables add up if two identical systems are combined whereas intensive quantities do not change. Temperature, pressure, and number density are intensive, the particle number and the volume are extensive quantities. Intensive variables are now further classified in fields and densities. Fields are quantities that have the same value at first-order phase transitions like temperature and pressure whereas densities have different values.

A system with q independent thermodynamic quantities can be characterised by $q + 1$ fields f_i. One of these fields can be regarded as a function of the others and is therefore called **potential**. For the coexistence of two phases I and II, $(q + 1)$ field equations have to be fulfilled

$$f_i^{(\mathrm{I})} = f_i^{(\mathrm{II})} \qquad i = 0 \ldots q \tag{2.46}$$

which defines a $(q - 1)$ dimensional hypersurface in the q dimensional field space. In a system of n components we need $n + 1$ independent quantities ($q = n + 1$). For a binary mixture ($q = 3$) we get 2-dimensional coexistence surfaces in the 3-dimensional field space.

A $(q - 1)$-dimensional hypersurface can ...

1. end in a $(q - 2)$-dimensional hypersurface if the limit of the definition of a field is reached, e.g. if one of the components is no longer present.

2. cut another $(q - 1)$-dimensional hypersurface in a $(q - 2)$-dimensional "triple-point" hypersurface.

3. end in a $(q - 2)$-dimensional "critical-point" hypersurface.

At a **critical end-point** two phases become critical while in coexistence with a third phase (the so called spectator phase). Therefore in field space a line of triple-points meets a line of critical points.

At a **tricritical point** three phases become one critical phase which means that in field space three lines of critical points meet a line of triple-points.

A phase diagram in field space has less information than a phase diagram in a mixed field-density space. The advantage is that properties like critical end-points can be easily identified[28].

Chapter 3

The Symmetrical Binary Mixture

3.1 The Binary Yukawa Mixture

The hard-core Yukawa potential consists of a hard-core and an attractive tail (see figure 3.1). The interaction potential of a binary Yukawa mixture is defined as

$$\phi_{ij}(r) = \begin{cases} \infty & r < \sigma_{ij} \\ -\frac{\sigma_{ij}\varepsilon_{ij}}{r} e^{-z(r-\sigma_{ij})} & r \geq \sigma_{ij} \end{cases} \qquad i,j = 1,2 \tag{3.1}$$

where the σ_i are the hard-core diameters of particles of species i,

$$\sigma_{ij} = \frac{\sigma_i + \sigma_j}{2} \tag{3.2}$$

gives the distance of closest approach between particles of species i and j, and the ε_{ij} measure the interaction strength between them. z is the so called inverse range parameter that scales the range of the potential.

Such a mixture is called symmetrical if the hard-core diameters are equal and if the interaction strength of like particles is the same for the two components, i.e.

$$\varepsilon \equiv \varepsilon_{11} = \varepsilon_{22}, \tag{3.3}$$

and only the interaction between dislike particles is different. Therefore we introduce the ratio of the interaction strengths of dislike to like particles, δ, which is defined as

$$\delta \equiv \frac{\varepsilon_{12}}{\varepsilon} = \frac{\varepsilon_{21}}{\varepsilon}. \tag{3.4}$$

We choose for the inverse range parameter

$$z = \frac{1.8}{\sigma}. \tag{3.5}$$

To this mixture we apply the field

$$\Delta\mu = \mu_1 - \mu_2 \tag{3.6}$$

which is the difference of the chemical potentials of the two species.

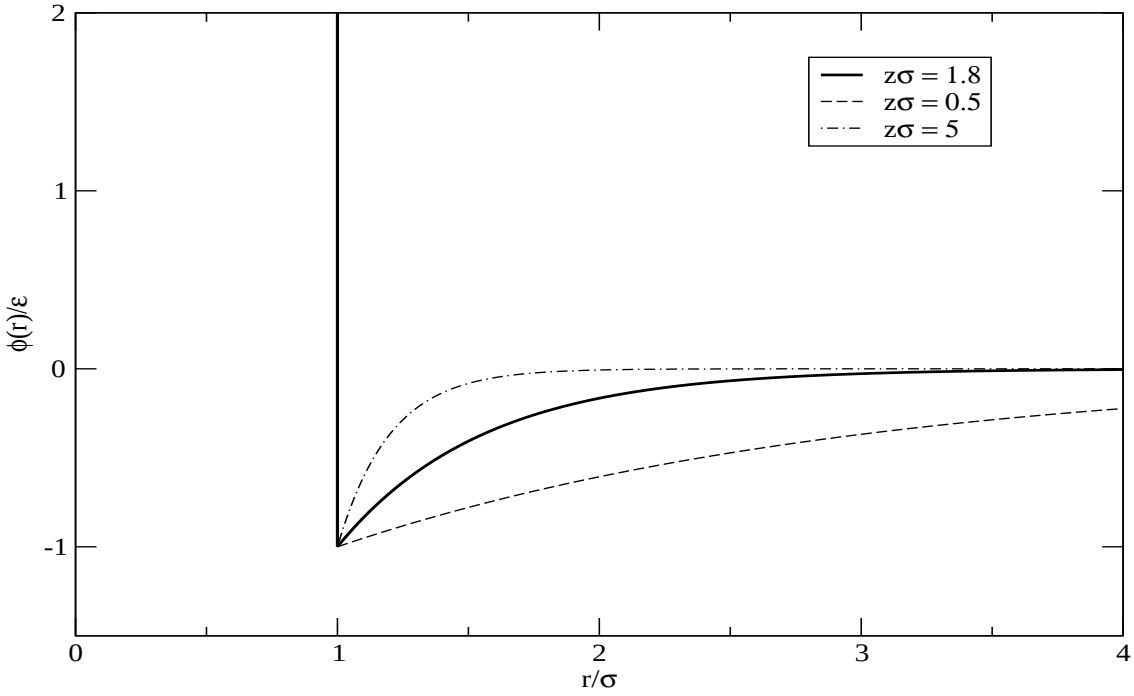

Figure 3.1: The hard-core Yukawa potential for different values of the inverse range parameter z.

3.2 General Properties

In mixtures we have in addition to the vapour-liquid transition, transitions between mixed and demixed fluids and between and an A rich and a B rich phase. The latter two are called mixing-demixing and demixing transition, respectively.

The phase diagrams of a symmetrical binary mixture can be distinguished by the way the demixing critical line, i.e. the so called λ-line, intersects the vapour-liquid coexistence line [11] .

- **Type I:** The λ-line intersects the vapour-liquid curve in a critical end point.
- **Type II:** The λ-line ends in a tricritical point and we find a triple point.
- **Type III:** The λ-line ends in a tricritical point we do not have a triple point.

At the triple point mentioned above and denoted in figure 3.2 a vapour coexists with a mixed liquid and a demixed liquid, which itself consists of an A rich and a B rich phase. Therefore it is a point where four phases are in coexistence and we call it **quadruple point**.

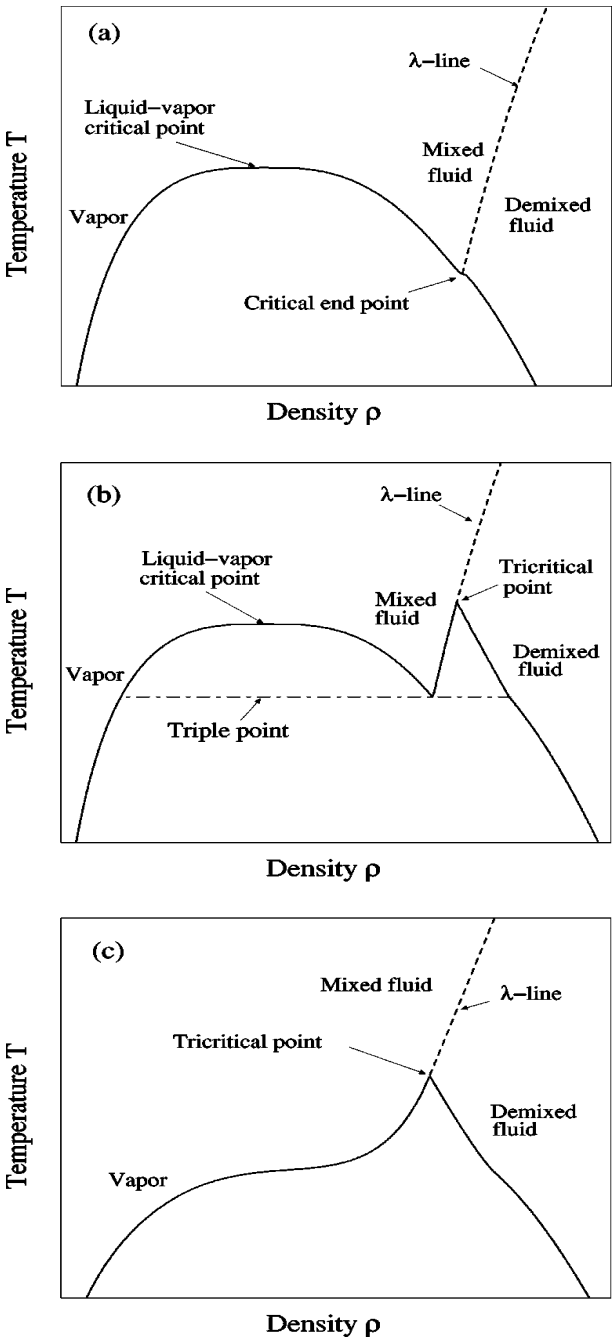

Figure 3.2: Schematic representations of the phase diagram of the symmetrical binary mixture for $\Delta\mu = 0$, labelled I, II, and III from top to bottom [11].

3.2.1 Reduced Units

Values of variables in tables and figures are presented in reduced units which are given by

$$T^* = \frac{k_B T}{\varepsilon} \tag{3.7}$$

$$\rho^* = \rho\sigma^3 \tag{3.8}$$

$$p^* = \frac{p\sigma^3}{\varepsilon} \tag{3.9}$$

$$\tag{3.10}$$

In the following we omit the star. Chemical potentials are given in units of $k_B T$.

Chapter 4

Integral Equation Theory

4.1 Ornstein-Zernike Equation

The Ornstein-Zernike equation [29, 30, 31] can be considered the defining relation for the **direct correlation function** $c^{(2)}(\mathbf{r}_1, \mathbf{r}_2)$:

$$h^{(2)}(\mathbf{r}_1, \mathbf{r}_2) = c^{(2)}(\mathbf{r}_1, \mathbf{r}_2) + \int \mathrm{d}^3 r_3 \rho^{(1)}(\mathbf{r}_3) h^{(2)}(\mathbf{r}_1, \mathbf{r}_3) c^{(2)}(\mathbf{r}_3, \mathbf{r}_2) \tag{4.1}$$

Inserting this expression for the total correlation function $h^{(2)}$ into the right hand side and iterating this replacement leads to the infinite sum

$$\begin{aligned} h^{(2)}(\mathbf{r}_1, \mathbf{r}_2) &= c^{(2)}(\mathbf{r}_1, \mathbf{r}_2) + \int \mathrm{d}^3 r_3 \rho^{(1)}(\mathbf{r}_3) c^{(2)}(\mathbf{r}_1, \mathbf{r}_3) c^{(2)}(\mathbf{r}_3, \mathbf{r}_2) + \\ &+ \iint \mathrm{d}^3 r_3 \mathrm{d}^3 r_4 \rho^{(1)}(\mathbf{r}_3) \rho^{(1)}(\mathbf{r}_4) c^{(2)}(\mathbf{r}_1, \mathbf{r}_3) c^{(2)}(\mathbf{r}_3, \mathbf{r}_4) c^{(2)}(\mathbf{r}_4, \mathbf{r}_2) + \ldots . \end{aligned} \tag{4.2}$$

The first term on the right hand side is the direct correlation function of two particles at positions $\mathbf{r}_1$ and $\mathbf{r}_2$. The other terms account for the indirect correlation between the two particles which is caused by the correlation mediated by an increasing number of particles located at $(\mathbf{r}_3, \mathbf{r}_4 \ldots)$. For a spatially homogeneous and isotropic system the Ornstein-Zernike equation simplifies to

$$h(r) = c(r) + \rho \int d^3 r' h(r') c(|\mathbf{r} - \mathbf{r}'|). \tag{4.3}$$

A Fourier transform of both sides of the Ornstein-Zernike equation (4.3) leads to

$$\tilde{h}(q) = \tilde{c}(q) + \rho \tilde{c}(q) \tilde{h}(q) \tag{4.4}$$

$$= \frac{\tilde{c}(q)}{1 - \rho \tilde{c}(q)} \quad , \tag{4.5}$$

which is a very convenient form because the integral equation reduces to an algebraic equation for the Fourier transforms of the direct and the total correlation function.

The Ornstein-Zernike equation can be generalised to mixtures of n components:

$$h_{ij}(r) = c_{ij}(r) + \sum_{k=1}^{n} \rho_k \int \mathrm{d}^3 r' h_{ik}(r') c_{kj}(|\mathbf{r} - \mathbf{r}'|) \qquad i, j = 1 \ldots n \tag{4.6}$$

Closure Relation

The Ornstein-Zernike equation (4.3) relates two unknown functions $h(r)$ and $c(r)$. A **closure relation** is an additional equation which provides a relation between the functions $h(r)$, $c(r)$, and the pair potential $\phi(r)$. The cluster expansion of the radial distribution function leads to

$$g(r) = e^{-\beta\phi(r)+h(r)-c(r)+B(r)}. \tag{4.7}$$

The **bridge function** $B(r)$ stands for an infinite sum of terms represented by so called "bridge diagrams" [30]. If we knew the bridge function exactly, then equation (4.7) would be the exact closure. Unfortunately the exact $B(r)$ is not known for any system. Therefore approximations have to be applied which leads to several different closure relations like Percus-Yevick, hypernetted chain, and the mean spherical approximation.

Mean Spherical Approximation

The **mean spherical approximation** (MSA) was introduced by Lebowitz and Percus as generalisation of the mean spherical model of Ising spin systems [32]. It is often used as closure relation for potentials with a hard core (hard core diameter σ) and a (predominantly attractive) tail $\overline{\phi}(r)$. The MSA closure relation is given by

$$\phi(r) = \begin{cases} \infty & r < \sigma \\ \overline{\phi}(r) & r \geq \sigma \end{cases} \tag{4.8}$$

$$\begin{array}{rcll} g(r) & = & 0 & r < \sigma \\ c(r) & = & -\beta\overline{\phi}(r) & r \geq \sigma. \end{array} \tag{4.9}$$

The first expression of equations (4.9) is called core condition. It represents the impenetrability of the potentials and is an exact expression, whereas the second relation is only true in the limit of infinite separation ($\lim_{r\to\infty} c(r) = -\beta\overline{\phi}(r)$). The Ornstein-Zernike equation in combination with the mean spherical approximation as closure can be solved analytically for a number of potentials including hard-core Yukawa.

4.2 The Yukawa Mixture

The hard-core Yukawa potentials for a n-component mixture can be parameterised as

$$\phi_{ij}(r) = \begin{cases} \infty & r < \sigma_{ij} \\ -\frac{\sigma_{ij}\varepsilon_{ij}}{r} e^{-z(r-\sigma_{ij})} & r \geq \sigma_{ij} \end{cases} \qquad i,j = 1 \ldots n \tag{4.10}$$

z is the inverse range parameter and the ε_{ij} measure the interaction strength. The hard-core diameter of the particles of component i is σ_i. The distance of closest approach between particles of species i and j therefore is $\sigma_{ij} = (\sigma_i+\sigma_j)/2$. The mean spherical approximation for this mixture reads

$$\begin{array}{rcll} h_{ij}(r) & = & -1 & r < \sigma_{ij} \\ c_{ij}(r) & = & K_{ij}\frac{e^{-z(r-\sigma_{ij})}}{r} & r \geq \sigma_{ij} \end{array} \tag{4.11}$$

with

$$K_{ij} = \frac{\sigma_{ij}\ \varepsilon_{ij}}{k_B T}. \tag{4.12}$$

Blum and Høye [17][18] proposed an analytic solution of Baxter's factorised version [33] of the Ornstein-Zernike equation with the mean spherical approximations as closure. We use the expression introduced by Arrieta *et. al.* [15][16] and write the Ornstein-Zernike equation as

$$\begin{aligned} 2\pi r c_{ij}(r) &= -Q'_{ij}(r) + \sum_l \rho_l \int_{\lambda_{lj}}^{\infty} Q_{jl}(t) Q'_{il}(r+t) \mathrm{d}t \\ 2\pi r h_{ij}(r) &= -Q'_{ij}(r) + 2\pi \sum_l \rho_l \int_{\lambda_{jl}}^{\infty} (r-t) h_{il}(|r-t|) Q_{lj}(t) \mathrm{d}t. \end{aligned} \tag{4.13}$$

The $Q_{ij}(r)$ are the so called **factor correlation functions** and the λ_{ij} are defined as $\lambda_{ij} = (\sigma_j - \sigma_i)/2$.

The two sets of equations (4.13) have $3n^2$ unknowns $\{c_{ij}\}$, $\{h_{ij}\}$ and $\{Q_{ij}\}$ but each set only consists of n^2 equations. The mean spherical approximation closure of equation (4.11) provides the needed n^2 additional equations. Considering equations (4.13) under the conditions given by equations (4.11) the factor correlation functions have to have the following form:

$$Q_{ij}(r) = Q^0_{ij}(r) + \frac{1}{z} D_{ij} e^{-z(r-\sigma_{ij})} \tag{4.14}$$

$$Q^0_{ij}(r) = \begin{cases} \frac{a_{ij}}{2}(r-\sigma_{ij})^2 + b_{ij}(r-\sigma_{ij}) + \frac{1}{z} C_{ij} \left(e^{-z(r-\sigma_{ij})} - 1 \right) & \lambda_{ji} \le r < \sigma_{ij} \\ 0 & r \ge \sigma_{ij} \end{cases} . \tag{4.15}$$

To determine the factor correlation functions we have to know the coefficients $\{a_{ij}\}$, $\{b_{ij}\}$, $\{C_{ij}\}$, and $\{D_{ij}\}$. It is mathematically more convenient not to use equations (4.13) directly but rewrite them as

$$\begin{aligned} \sum_{lmk} A^{(1)}_{mkjl} G_{km} D_{ml} D_{il} + \sum_{lm} A^{(2)}_{mjl} D_{ml} D_{il} + \sum_l A^{(3)}_{jl} D_{il} + A^{(4)}_{ij} = 0 \\ \sum_{lmk} B^{(1)}_{mklj} G_{km} D_{mj} G_{il} + \sum_{mk} B^{(2)}_{mkij} G_{km} D_{mj} + \\ + \sum_{lm} B^{(3)}_{mlj} D_{mj} G_{il} + \sum_m B^{(4)}_{mij} D_{mj} + \sum_l B^{(5)}_{lj} G_{il} + B^{(6)}_{ij} = 0. \end{aligned} \tag{4.16}$$

These are $2n^2$ nonlinear algebraic equations with $2n^2$ unknown coefficients $\{D_{ij}\}$ and $\{G_{ij}\}$. The coefficients $A^{(\ )}_{\dots}$ and $B^{(\ )}_{\dots}$ only depend on σ_i, ε_{ij}, z, ρ_i and T and can be found in appendix A. The $\{G_{ij}\}$ are integrals of the radial distribution function $g_{ij}(r)$

$$G_{ij} = z \int_0^{\infty} r e^{-z(r-\sigma_{ij})} g_{ij}(r) \mathrm{d}r. \tag{4.17}$$

Equations (4.16) have to be solved numerically and therefore an initial estimate for the solution is needed. The $A^{(4)}_{ij}$ are the only coefficients that depend on the energy-related quantities ε_{ij} and T and we expand them into a Taylor series from the infinite temperature limit up to the first non zero terms which gives two systems of linear equations

$$\begin{aligned} \sum_l A^{(3)}_{jl} D_{il} &= -A^{(4)}_{ij} \\ \sum_l B^{(5)}_{lj} G_{il} &= -B^{(6)}_{ij}. \end{aligned} \tag{4.18}$$

These equations provide a very good initial estimate.

The coefficients $\{a_{ij}\}$, $\{b_{ij}\}$, and $\{C_{ij}\}$ of the factor correlation functions can be expressed by the solutions to equations (4.16) (see appendix A).

Physical Solutions

Pastore [34] proved that whenever the Ornstein-Zernike equation with the MSA closure has a solution, this solution is unique and physical. The uniqueness is only valid within the class of correlation functions that correspond to positive and finite structure factors. Because of the fact that we do not solve the Ornstein-Zernike equations directly but use equations (4.16) we have to demand the invertibility of the matrix of factor correlation functions. This condition requires that

$$\Delta(t) = \det\left(\delta_{ij} + \sqrt{\rho_i \rho_j}\hat{Q}_{ij}(t)\right) \tag{4.19}$$

has no zeros in the complex right half-plane of the t variable. The $\hat{Q}_{ij}(t)$ are the Laplace transforms of the factor correlation functions

$$\hat{Q}_{ij}(t) = \int_{\lambda_{ji}}^{\infty} e^{-tr} Q_{ij}(r)\mathrm{d}r. \tag{4.20}$$

If t is real then $\Delta(t)$ is a real and continuous function and $\lim_{t\to\infty}\Delta(t) = 1$. So if $\Delta(0) \leq 0$ then $\Delta(t)$ has to cross the t-axis at least once. In this case the solution is rejected. We use this as simplified criterion for a physical solution although accepting the solution for $\Delta(0) > 0$ is only a practical rule.

4.3 Thermodynamic Properties

With the mean spherical approximation as closure, energy derived properties are usually more accurate than by any other route [36]. In the following we will present expressions for the excess (over the hard-sphere reference system) pressure and chemical potential. The corresponding properties of the reference system are given by the **Carnahan-Mansoori-Starling-Leland** equation of state (CMSL). Introducing $\xi_i = \pi/6 \sum_j \rho_j \sigma_j^i$ and $\eta = \xi_3$, i. e. the packing fraction, the CMSL expression for the pressure of the hard-sphere mixture is

$$\frac{p^{\mathrm{CMSL}}}{\rho k_B T} = \frac{1}{1-\eta} + \frac{18(\xi_1\xi_2 + \xi_2^2)}{\pi\rho(1-\eta)^2} + \frac{6\eta\xi_2^3}{\pi\rho(1-\eta)^3} \tag{4.21}$$

and the chemical potential of component i is given by

$$\begin{aligned}\frac{\mu_i^{\mathrm{CMSL}}}{k_B T} = \ln\left(\frac{\rho_i}{1-\eta}\right) + \frac{\frac{\pi}{6}\rho\sigma_i^3 + 3\sigma_i\xi_2 + 3\sigma_i^2\xi_1}{1-\eta} + \frac{3\sigma_i^3\xi_1\xi_2 + 3\sigma_i^3\xi_2^2}{(1-\eta)^2} + \\ + \frac{3\sigma_i^2\xi_2^2}{\eta(1-\eta)^2} + \frac{3\sigma_i^2\xi_2^2\ln(1-\eta)}{\eta^2} - \frac{(\sigma_i^3\xi_2^3)(2-5\eta+\eta^2)}{\eta^2(1-\eta)^3} - \frac{2\sigma_i^3\xi_2^3\ln(1-\eta)}{\eta^3}.\end{aligned} \tag{4.22}$$

(4.23)

The excess pressure calculated by the energy route is given by

$$\frac{\Delta p_E}{\rho k_B T} = \frac{\pi}{3}\rho\sum_{ij} x_i x_j \sigma_{ij}^3 \{[g_{ij}(\sigma_{ij})]^2 - [g_{ij}^0(\sigma_{ij})]^2\} + J \tag{4.24}$$

where

$$g_{ij}^0(\sigma_{ij}) = \frac{1}{\sigma_{ij}(1-\eta)^3}[\frac{3}{2}\sigma_i\sigma_j\xi_2 + \sigma_{ij}(1-\eta)] \tag{4.25}$$

$$g_{ij}(\sigma_{ij}) = \frac{1}{2\pi\sigma_{ij}}(b_{ij} - C_{ij}) \tag{4.26}$$

$$J = \frac{2\pi}{3}\rho\sum_{ij} x_i x_j K_{ij}\left(G'_{ij} - \frac{1}{z}G_{ij}\right) \tag{4.27}$$

$$G'_{ij} = -z\int_{\sigma_{ij}}^{\infty} \mathrm{d}r\, r^2 e^{-z(r-\sigma_{ij})} g_{ij}(r). \tag{4.28}$$

The excess chemical potential for the component i is

$$\frac{\Delta\mu_i}{k_B T} = -\frac{2\pi}{z}\sum_j \rho_j K_{ij} G_{ij} - \frac{1}{2}\sum_j \rho_j[\tilde{c}_{ij}(0) - \tilde{c}_{ij}^0(0)] \tag{4.29}$$

with

$$\tilde{c}_{ij}(0) = 4\pi\int_0^{\infty} r^2 c_{ij}(r)\mathrm{d}r. \tag{4.30}$$

while the $\tilde{c}_{ij}^0(0)$ correspond to the hard-sphere case (see appendix A).

Chapter 5

Monte Carlo Simulations

5.1 Introduction

The Monte Carlo simulation method [19][20][21] is used to obtain estimates for the ensemble average of observables which only depend on the configurational variables.

To introduce the concepts of Monte Carlo simulation we work in the **canonical ensemble** which means that the system has fixed particle number N, volume V and temperature T.
The Hamilton function of the system is $\mathcal{H}(\mathbf{p}^N, \mathbf{r}^N) = \mathcal{K}(\mathbf{p}^N) + \mathcal{U}(\mathbf{r}^N)$ with the the kinetic energy $\mathcal{K}(\mathbf{p}^N)$ and the potential energy $\mathcal{U}(\mathbf{r}^N)$. Macroscopic properties are calculated as ensemble averages of observables

$$\langle A \rangle = \frac{\int \mathrm{d}\mathbf{p}^N \mathrm{d}\mathbf{r}^N A(\mathbf{p}^N, \mathbf{r}^N) \exp(-\beta \mathcal{H}(\mathbf{p}^N, \mathbf{r}^N))}{\int \mathrm{d}\mathbf{p}^N \mathrm{d}\mathbf{r}^N \exp(-\beta \mathcal{H}(\mathbf{p}^N, \mathbf{r}^N)} . \tag{5.1}$$

If the observable of interest only depends on the configurational variables the ensemble average reduces to

$$\langle A \rangle = \frac{\int \mathrm{d}\mathbf{r}^N A(\mathbf{r}^N) \exp(-\beta \mathcal{U}(\mathbf{r}^N))}{\int \mathrm{d}\mathbf{r}^N \exp(-\beta \mathcal{U}(\mathbf{r}^N))} . \tag{5.2}$$

We can define the *configurational part of the partition function* as

$$Z \equiv \int \mathrm{d}\mathbf{r}^N \exp(-\beta \mathcal{U}(\mathbf{r}^N)). \tag{5.3}$$

5.2 Theoretical Background

5.2.1 The Estimator

The ensemble average of an observable can be estimated by generating configurations $\mathbf{r}_\mu^N$ corresponding to a probability distribution $p(\mathbf{r}_\mu^N)$ and evaluating the so called **estimator**

$$\begin{aligned} \langle A \rangle &\approx \frac{\sum_{\mu=1}^n A(\mathbf{r}_\mu^N) p^{-1}(\mathbf{r}_\mu^N)(\exp(-\beta \mathcal{U}(\mathbf{r}_\mu^N))}{\sum_{\mu=1}^n p^{-1}(\mathbf{r}_\mu^N) \exp(-\beta \mathcal{U}(\mathbf{r}_\mu^N))} \\ &\equiv \frac{\sum_{\mu=1}^n A_\mu p_\mu^{-1} \exp(-\beta \mathcal{U}_\mu)}{\sum_{\mu=1}^n p_\mu^{-1} \exp(-\beta \mathcal{U}_\mu))} . \end{aligned} \tag{5.4}$$

If all configurations have equal probabilities (i.e. the probability distribution is constant for all configurations) equation (5.4) reduces to

$$\langle A \rangle \approx \frac{\sum_{\mu=1}^{n} A_\mu \exp(-\beta \mathcal{U}_\mu)}{\sum_{\mu=1}^{n} \exp(-\beta \mathcal{U}_\mu))}. \tag{5.5}$$

This is the so called **simple** or **direct sampling** which is not very efficient for most cases. The reason is that most of the randomly generated configurations $\mathbf{r}_\mu^N$ will have large energies $\mathcal{U}_\mu$. So the factor $e^{-\beta \mathcal{U}_\mu}$ is small for these configurations and they do not contribute very much to the average.
Rewriting equation (5.2) as

$$\langle A \rangle = \int \mathrm{d}\mathbf{r}^N A(\mathbf{r}^N) \frac{\exp(-\beta \mathcal{U}(\mathbf{r}^N))}{\int \mathrm{d}\mathbf{r}'^N \exp(-\beta \mathcal{U}(\mathbf{r}'^N))} = \int \mathrm{d}\mathbf{r}^N A(\mathbf{r}^N) \frac{\exp(-\beta \mathcal{U}(\mathbf{r}^N))}{Z} \tag{5.6}$$

we can see that the **Boltzmann distribution**

$$p_\mu = \frac{\exp(-\beta \mathcal{U}_\mu)}{Z} \tag{5.7}$$

is the probability density of finding the system in the configuration μ. If we are able to generate configurations that are distributed according to the Boltzmann distribution, then the average could be simply estimated by

$$\langle A \rangle \approx \frac{1}{n} \sum_{\mu=1}^{n} A_\mu. \tag{5.8}$$

This is achieved by producing the sequence of configurations via a so called **Markov process**.

5.2.2 Metropolis Monte Carlo Simulation

In a **Markov process** [37][20] a new state ν is randomly generated out of a state μ with a probability $P(\mu \to \nu)$. These **transition probabilities** have to fulfil three conditions to satisfy the definition of a Markov process. The first is that they have to be time independent. Second, they do not depend on the previous history of the process but only on the two states μ and ν. The last condition they have to fulfil is the **sum rule**

$$\sum_{\nu} P(\mu \to \nu) = 1 \tag{5.9}$$

which expresses the fact that the process has to generate a state although the initial state and the generated state can be identical, i.e. $P(\mu \to \mu)$ need not to be zero.

In a Monte Carlo simulation we use a Markov process repeatedly to generate a so called **Markov chain** of states.

The Master Equation

The **master equation** governs the stochastic dynamics of Markov processes. It is a very important and general equation of statistical physics that has been applied to many different problems in physics, chemistry, and biology like population dynamics, laser physics, Brownian motion, semiconductors, to name a few examples.

We define the probability that the system is in a state μ at the time t as weight $w_\mu(t)$. The fact that the system has to be in some state at each moment t is expressed by

$$\sum_\mu w_\mu(t) = 1 \qquad \forall t. \tag{5.10}$$

A macroscopic quantity can be calculated as **expectation** of an observable at a time t

$$\langle A \rangle_t = \sum_\mu A_\mu w_\mu(t). \tag{5.11}$$

The set of weights $\{w_\mu(t)\}$ is the solution of the following set of differential equations which is called the **master equation**

$$\frac{\mathrm{d}w_\mu}{\mathrm{d}t} = \sum_\nu \left[w_\nu(t) P(\nu \to \mu) - w_\mu(t) P(\mu \to \nu) \right], \tag{5.12}$$

with the time independent transition probabilities $P(\mu \to \nu)$.

The master equation gives the rate of change $\frac{\mathrm{d}w_\mu}{\mathrm{d}t}$ of the probability of finding the system in a state μ at a time t, which is given by the weight $w_\mu(t)$. This rate is built up by transitions into the state μ from all other states ν which is given by the first term, and due to transitions out of the state μ into all other states ν which is expressed by the second term on the right-hand side of equation (5.12).

Equilibrium

If the system is in thermodynamic equilibrium the weights $\{w_\mu(t)\}$ are time independent. These constant weights imply that the terms on the right-hand side of equation (5.12) cancel one another. Because of the mathematical properties of equation (5.12) and with (5.9) as constraint, the rate $\frac{\mathrm{d}w(t)}{\mathrm{d}t}$ will vanish in the limit $t \to \infty$ for all solutions of the master equation. Thus we can define **equilibrium occupation probabilities** as

$$p_\mu = \lim_{t \to \infty} w_\mu(t). \tag{5.13}$$

The master equation for a system in equilibrium reduces to

$$\sum_\nu \left[p_\nu P(\nu \to \mu) - p_\mu P(\mu \to \nu) \right] = 0 \tag{5.14}$$

which can be rewritten as

$$\sum_\nu p_\mu P(\mu \to \nu) = \sum_\nu p_\nu P(\nu \to \mu) \tag{5.15}$$

and which leads in combination with the sum rule (5.9) to

$$p_\mu = \sum_\nu p_\nu P(\nu \to \mu). \tag{5.16}$$

If we use transition probabilities $P(\mu \to \nu)$ satisfying equation 5.16 in a Markov process, p_μ will be a equilibrium distribution of the generated states. To guarantee that, starting from an arbitrary state, we generate this equilibrium distribution one has to impose the additional conditions of ergodicity and detailed balance.

Ergodicity and Detailed Balance

In an **ergodic** Markov process one is able to reach every state from any other state. To prevent the system from getting caught in a **dynamic equilibrium** [20] one imposes **detailed balance**

$$p_\mu P(\mu \to \nu) = p_\nu P(\nu \to \mu). \tag{5.17}$$

This equation expresses that the transition from state μ to state ν occurs as often as the transition from state μ to state ν. The above equation can be written as

$$\frac{P(\mu \to \nu)}{P(\nu \to \mu)} = \frac{p_\nu}{p_\mu}. \tag{5.18}$$

To guarantee that we generate states according to a given probability distribution the transition probabilities have to satisfy detailed balance (5.18), the sum rule (5.9), and the condition of ergodicity.

Acceptance Ratios

Detailed balance only fixes the ratios of the transition probabilities. This means that we are free to choose the $P(\mu \to \nu)$. We only have to adjust $P(\nu \to \mu)$ so that the equation for detailed balance (5.18) is satisfied and to tune $P(\mu \to \mu)$ to fulfil the sum rule (5.9).

We take advantage of this freedom of choosing the transition probabilities by introducing the **selection probability** $s(\mu \to \nu)$ and the **acceptance ratio** $a(\mu \to \nu)$, via

$$P(\mu \to \nu) = s(\mu \to \nu)\, a(\mu \to \nu). \tag{5.19}$$

The selection probability $s(\mu \to \nu)$ is the probability that a state ν is generated out of a state μ. The acceptance ratio $a(\mu \to \nu)$ is the probability that the generated state ν is accepted as the new state of the system.

If we were able to construct an algorithm that only generates states according to the probability distribution we could accept every new state, i.e. we would have acceptance ratios $a(\mu \to \nu) = 1$ for all pairs of states μ and ν. Such algorithms are difficult to find. By introducing acceptance ratios we are completely free to choose an algorithm for generating states.

Metropolis Algorithm

One possible choice for the selection probabilities $s(\mu \to \nu)$ is to set them all equal which leads to

$$\frac{P(\mu \to \nu)}{P(\nu \to \mu)} = \frac{s(\mu \to \nu)\, a(\mu \to \nu)}{s(\nu \to \mu)\, a(\nu \to \mu)} = \frac{a(\mu \to \nu)}{a(\nu \to \mu)}. \tag{5.20}$$

It is possible to maximise the acceptance ratios by giving the larger one the largest possible value (which is 1 for a probability) and to adjust the other one to satisfy detailed balance (5.18).

Now we put the pieces together. The probability distribution we want to generate is the Boltzmann distribution

$$p_\mu = \frac{\exp(-\beta \mathcal{U}_\mu)}{Z}. \tag{5.21}$$

The condition of detailed balance with equal selection probabilities therefore is

$$\frac{P(\mu \to \nu)}{P(\nu \to \mu)} = \frac{a(\mu \to \nu)}{a(\nu \to \mu)} = \frac{e^{-\beta \mathcal{U}_\nu}}{e^{-\beta \mathcal{U}_\mu}} = e^{-\beta(\mathcal{U}_\nu - \mathcal{U}_\mu)}. \tag{5.22}$$

For the acceptance ratios of the Metropolis algorithm in the canonical ensemble follows

$$a(\mu \to \nu) = \begin{cases} e^{-\beta(\mathcal{U}_\nu - \mathcal{U}_\mu)} & \text{if } \mathcal{U}_\nu - \mathcal{U}_\mu > 0 \\ 1 & \text{otherwise} \end{cases} \tag{5.23}$$

and can be written as

$$a(\mu \to \nu) = \min\left(1, e^{-\beta \Delta \mathcal{U}}\right) \tag{5.24}$$

with $\Delta \mathcal{U} = \mathcal{U}_\nu - \mathcal{U}_\mu$.

5.2.3 Trial Moves

Starting from a state μ, we generate new states ν by so called **trial moves**. The only condition that has to be fulfilled is that every point of the state space can be reached from any other state in a finite number of Markov processes. This is the condition of **ergodicity**. The trial moves do not need to correspond to any physical movement of the particles in real space.

In the **canonical ensemble** one usually uses **displacements of particles** as trial moves. If our cubic box is of length L and Δ is the maximum of the allowed displacement the rule for the trial moves is

$$\mathbf{r}_i \to \mathbf{r}_i + \Delta \xi_i \qquad i = 1 \ldots N \tag{5.25}$$

where ξ_i is a three dimensional vector of real random numbers between -1 and 1. The upper limit of Δ is given by half the box length. (For a discussion of how to choose a value for Δ see [19].)

5.2.4 Simulation in the Grand Canonical Ensemble

A system in the **grand canonical ensemble** is thermodynamically open which means that we allow transfer of particles and energy between the system and a reservoir. Therefore we have a fixed volume V, fixed inverse temperature β, and a fixed chemical potential μ. The particle number N and the energy E are allowed to fluctuate. To incorporate fluctuations in the number of particles we use **trial insertions** and **deletions** of particles. The acceptance ratios are

$$a(N \to N-1) = \min\left(1, \frac{N}{V} e^{-\beta[\mathcal{U}(\mathbf{r}^{N-1}) - \mathcal{U}(\mathbf{r}^N) - \mu]}\right) \tag{5.26}$$

$$a(N \to N+1) = \min\left(1, \frac{V}{N+1} e^{-\beta[\mathcal{U}(\mathbf{r}^{N+1}) - \mathcal{U}(\mathbf{r}^N) + \mu]}\right). \tag{5.27}$$

As a consequence not only the particle number but also the energy fluctuates.

The acceptance probabilities given by equations (5.26) and (5.27) can be easily generalised to **mixtures** by using the chemical potentials for each species. In the grand canonical ensemble these chemical potentials are fixed, and in addition to fluctuations in the total particle number and in the energy also the concentrations fluctuate. These fluctuations are already incorporated by the trial insertions and deletions, but for optimisation reasons we introduce a **trial flip** where

a particle of one component changes to a particle of another component. For a binary mixture with components A and B the acceptance ratios for the flip moves are given by

$$a(\mathrm{A} \to \mathrm{B}) = \min\left(1, e^{-\beta[\mathcal{U}(\mathbf{r}^{N_\mathrm{A}-1}, \mathbf{r}^{N_\mathrm{B}+1}) - \mathcal{U}(\mathbf{r}^{N_\mathrm{A}}, \mathbf{r}^{N_\mathrm{B}}) - (\mu_\mathrm{B} - \mu_\mathrm{A})]}\right) \tag{5.28}$$

$$a(\mathrm{B} \to \mathrm{A}) = \min\left(1, e^{-\beta[\mathcal{U}(\mathbf{r}^{N_\mathrm{A}+1}, \mathbf{r}^{N_\mathrm{B}-1}) - \mathcal{U}(\mathbf{r}^{N_\mathrm{A}}, \mathbf{r}^{N_\mathrm{B}}) - (\mu_\mathrm{A} - \mu_\mathrm{B})]}\right). \tag{5.29}$$

5.2.5 Technical Details

Periodic Boundary Conditions

The smaller the simulation box is, the bigger is the fraction of particles being at the surface of this box. To minimise surface effects one usually applies **periodic boundary conditions**. The volume containing the particles serves as primitive cell of an infinite periodic lattice.
Each particle interacts with all other particles in its own cell and with all particles (including all images of itself) in the other cells. The total potential energy $\mathcal{U}$ for a pairwise additive potential can be written as

$$\mathcal{U} = \frac{1}{2} \sum_{\substack{i,j,\mathbf{n} \\ i \neq j \text{ for } \mathbf{n}=\mathbf{0}}} \phi(|\mathbf{r}_{ij} + \mathbf{n}L|), \tag{5.30}$$

where L is the side length of the cubic box and $\mathbf{n}$ a vector of three integer numbers. $\mathbf{n}L$ is therefore a lattice vector.

Truncation of Interactions and Background Corrections

If the total potential energy is dominated by contributions of particles which are closer to each other than a distance r_c the term **short-range interaction** is used. It is possible to ignore the interactions of particles separated more than this distance by truncating the potential at r_c. To minimise the resulting error one can apply a **background correction**. Then the total potential energy is written as sum of pair potentials ϕ_c with a maximum range r_c and a background (or long range) correction

$$\mathcal{U} = \sum_{i<j} \phi_\mathrm{c}(r_{ij}) + \frac{N\rho}{2} \int_{r_\mathrm{c}}^{\infty} \mathrm{d}r 4\pi r^2 \phi(r). \tag{5.31}$$

We have assumed that $g(r) = 1$ for $r > r_c$. This tail correction is only finite for interaction potentials that decay faster than r^{-3}. If the cutoff radius r_c is less than half the box length we only have to consider the interactions of a particle with the nearest periodic images of the other particles. This is called **nearest-image convention**.

Beside this **simple truncation** one can additionally shift the potential so that it vanishes at the cutoff radius. This is mostly used in molecular dynamics simulations [19]. Another method is the so called **minimum image convention** where one does not have a spherical cutoff. Instead each particle interacts with the nearest image of the other particles in the periodic lattice. It can be visualised by drawing the primitive cell (the original simulation box) with the particle of interest in the centre. Only the particles in this "virtual" box are used to calculate the interaction energy for the particle in the centre.

Cell List Method

To minimise the computational effort of the energy calculations of a short-range interaction potential we build up the simulation box of equally sized cubic cells with box length r_c (or slightly larger). Therefore each particle only interacts with the particles in its own cell and in the 26 neighbouring cells. The numerical effort of the cell list method, which is also called linked-list method, scales with the particle number N.

5.3 Histogram Reweighting

5.3.1 Single Histogram Reweighting

Let us assume we want to estimate the **excess internal energy** $U^{\mathrm{ex}}(\beta)$

$$U^{\mathrm{ex}}(\beta) = \langle \mathcal{U} \rangle \approx \frac{\sum_{\mu=1}^{n} \mathcal{U}_\mu p_\mu^{-1} e^{-\beta \mathcal{U}_\mu}}{\sum_{\mu=1}^{n} p_\mu^{-1} e^{-\beta \mathcal{U}_\mu}}. \tag{5.32}$$

In a simulation at the inverse temperature β_1 we generate n configurations corresponding to the Boltzmann probability distribution $p_\mu = \frac{e^{-\beta_1 \mathcal{U}_\mu}}{Z}$. We can get an estimate for the excess internal energy at another inverse temperature β with

$$U^{\mathrm{ex}}(\beta) = \frac{\sum_{\mu=1}^{n} \mathcal{U}_\mu e^{-(\beta-\beta_1)\mathcal{U}_\mu}}{\sum_{\mu=1}^{n} e^{-(\beta-\beta_1)\mathcal{U}_\mu}}. \tag{5.33}$$

This equation is the basis of **single histogram reweighting** [23].

Histograms

For a system with discrete energy states E_i we can collect the data of our simulation in a **histogram**. Therefore we count how often states with a certain internal energy E_i are sampled which gives the energy histogram $N(E_i)$. This can be used to write the equation (5.33) as

$$E(\beta) \approx \frac{\sum_i E_i N(E_i) e^{-(\beta-\beta_1)E_i}}{\sum_i N(E_i) e^{-(\beta-\beta_1)E_i}}. \tag{5.34}$$

This is where the name histogram reweighting comes from.

The use of histograms for a continuous quantity $\mathcal{Q}$ causes an loss of information because one has to use bins with a certain size $\mathrm{d}\mathcal{Q}$ and count how often states occur with a value between $\mathcal{Q}$ and $\mathcal{Q} + \mathrm{d}\mathcal{Q}$.

In a Monte Carlo simulation we are able to sample only a small region of the phase-space and therefore the temperature range for which single histogram reweighting provides reliable results is restricted.

Let us assume we perform a simulation at an inverse temperature β_1 and that we want to use the obtained energy histogram to extrapolate to an inverse temperature β. We will only get accurate estimates for observables if the sampled configurations also sufficiently cover the region of phase-space that would have been sampled in a simulation at the inverse temperature β. More precisely,

the energy histogram of the simulation data has to be significantly larger than 1 in the energy range where the energy distribution at the inverse temperature β would also be significantly larger than 1. In short, the energy distributions have to overlap sufficiently.

5.3.2 Multi Histogram Reweighting

Let us assume we have data of two simulations at different temperatures with overlapping energy distributions and that each of the energy histograms has poor statistics in the overlapping region. Using single histogram reweighting for any of the data sets would give a poor estimate for the excess internal energy U^{ex} for temperatures corresponding to energy distributions covering the overlap.

Multi histogram reweighting [24] is a method that makes it possible to combine the data of arbitrarily many simulations without adding up statistical errors.

If the **energy density of states** $\rho(\mathcal{U})$ is known the calculation of the excess internal energy can be written as

$$U^{\mathrm{ex}}(\beta) = \int \mathrm{d}\mathbf{r}^N \mathcal{U} \, \frac{e^{-\beta\mathcal{U}}}{Z} = \int \mathrm{d}\mathcal{U} \, \mathcal{U} \, \rho(\mathcal{U}) \, \frac{e^{-\beta\mathcal{U}}}{Z}. \tag{5.35}$$

$\rho(\mathcal{U})\mathrm{d}\mathcal{U}$ is the number of states of the system with energies between $\mathcal{U}$ and $\mathcal{U}+\mathrm{d}\mathcal{U}$. The probability of generating a state with an energy between $\mathcal{U}$ and $\mathcal{U}+\mathrm{d}\mathcal{U}$ is given by

$$p(\mathcal{U})\mathrm{d}\mathcal{U} = \frac{e^{-\beta\mathcal{U}}}{Z}\rho(\mathcal{U})\mathrm{d}\mathcal{U}. \tag{5.36}$$

For the sake of simplicity we concentrate on a system with discrete energy states E_j. This does not influence the final results and therefore we drop the index j.

The probability distribution $p(E)$ of sampling a state with the energy E is given by

$$p(E) = \frac{e^{-\beta E}}{Z}\rho(E) \tag{5.37}$$

and therefore the density of states is

$$\rho(E) = p(E)\frac{Z}{e^{-\beta E}}. \tag{5.38}$$

We perform simulations at the inverse temperatures β_i producing n_i samples in simulation i. The probability distribution is estimated by

$$p_i^{\mathrm{est}}(E) = \frac{N_i(E)}{n_i} \tag{5.39}$$

where $N_i(E)$ is the energy histogram of the ith simulation. This estimate will fluctuate around the expectation value. We assume that the number of points in a bin (the number of sampled states with the energy E) is distributed according to a Poisson distribution. Using the fact that for a Poisson distribution the variance is equal to the expectation value we can obtain the variance of the estimate for the probability distribution by

$$\overline{{p_i^{\mathrm{est}}}^2(E)} - \overline{p_i^{\mathrm{est}}(E)}^2 = \frac{\overline{N_i(E)^2} - \overline{N_i(E)}^2}{n_i^2} = \frac{\overline{N_i(E)}}{n_i^2} = \frac{\overline{p_i^{\mathrm{est}}(E)}}{n_i}. \tag{5.40}$$

The quantities with a bar are averages taken over many simulation runs. The density of states is estimated by

$$\rho_i^{\rm est}(E) = p_i^{\rm est}(E)\frac{Z_i}{e^{-\beta_i E}} = \frac{N_i(E)}{n_i}\frac{Z_i}{e^{-\beta_i E}}. \tag{5.41}$$

$\rho_i^{\rm est}(E)$ is an estimate for $\rho(E)$ in the energy range covered by $N_i(E)$. We want to combine these estimates for the whole range of energies covered by the histograms $N_i(E)$. We do this by a weighted sum.

$$\rho^{\rm est}(E) = \sum_i w_i(E)\rho_i^{\rm est}(E) \qquad \sum_i w_i(E) = 1 \tag{5.42}$$

To determine the weights $w_i(E)$ we demand that the variance of this estimate is minimised. Using the fact that the fluctuations of estimates in different simulations are uncorrelated the variance can be written as

$$\overline{{\rho^{\rm est}}^2(E)} - \overline{\rho^{\rm est}(E)}^2 = \sum_i w_i^2(E)\left(\overline{\rho_i^{\rm est}(E)^2} - \overline{\rho_i^{\rm est}(E)}^2\right). \tag{5.43}$$

If we express the density of states by the corresponding probability distributions and if we use equation (5.40) the equation above becomes

$$\begin{aligned}\overline{{p^{\rm est}}^2(E)} - \overline{p^{\rm est}(E)}^2 &= \sum_i w_i^2(E)\left(\frac{Z_i}{Z}\right)^2 e^{-2E(\beta-\beta_i)}\frac{\overline{p_i^{\rm est}(E)}}{n_i} \\ &= p(E)\sum_i w_i^2(E)\left(\frac{Z_i}{Z}\right)e^{-E(\beta-\beta_i)}\frac{1}{n_i}.\end{aligned} \tag{5.44}$$

To determine the weights we combine this equation with the condition that $\sum_i w_i(E) = 1$. The right-hand side then is of the form

$$\sum_i w_i^2(E) f_i = \sum_{i\neq k} w_i^2(E) f_i + \left(1 - \sum_{i\neq k} w_i(E)\right)^2 f_k. \tag{5.45}$$

Differentiating this equation with respect to $w_j(E)$ with $j \neq k$ and setting it equal to zero gives

$$\frac{w_j(E)}{w_k(E)} = \frac{f_k}{f_j} \Rightarrow w_j(E) \propto f_j^{-1}. \tag{5.46}$$

Therefore we obtain for the weights

$$w_j(E) = \frac{\frac{Z}{Z_i}e^{(\beta-\beta_i)E}n_i}{\sum_i \frac{Z}{Z_i}e^{(\beta-\beta_i)E}n_i} \tag{5.47}$$

and for the probability distribution

$$p^{\rm est}(E) = \frac{\sum_i n_i p_i^{\rm est}(E)}{\sum_i \frac{Z}{Z_i}e^{(\beta-\beta_i)E}n_i} = \frac{\sum_i N_i(E)}{\sum_i \frac{Z}{Z_i}e^{(\beta-\beta_i)E}n_i}. \tag{5.48}$$

We have to determine the Z_i by

$$Z_k = \int {\rm d}\mathbf{r}^N e^{-\beta_k E} = \sum_E \rho^{\rm est}(E)e^{-\beta_k E} = \sum_E p(E)\frac{Z}{e^{-\beta_k E}}e^{-\beta_k E} \tag{5.49}$$

$$= \sum_E \frac{\sum_i N_i(E)}{\sum_i Z_i^{-1}e^{(\beta_k-\beta_i)E}n_i}. \tag{5.50}$$

This set of equations for the Z_i is solved iteratively. We can obtain an estimate for the partition function Z at the inverse temperature β by

$$Z = \sum_E \frac{\sum_i N_i(E)}{\sum_i Z_i^{-1} e^{(\beta-\beta_i)E} n_i}. \tag{5.51}$$

5.4 Multicanonical Sampling

Multicanonical Sampling [25] is a method to overcome probability barriers in Monte Carlo simulations. Such barriers appear for example at first order phase transitions and lead to probability distributions with multiple, widely separated maxima. At vapour-liquid phase coexistence away from the critical point the probability distribution of the particle number $p(N)$ shows two strong peaks. If we use a standard Monte Carlo method we will only be able to sample one of the peaks and we will not cross over to the other peak because of the probability, i.e. free energy, barrier.

The multicanonical Monte Carlo method belongs to the group of **biased sampling techniques** which were first introduced to calculate free energies [38]. Berg and Neuhaus [22] showed that such techniques can be used to overcome probability barriers at first order phase transitions. In the case of the vapour-liquid transition this is achieved by enhancing regions of low probability by the use of a **preweighting function** $\eta(N)$ depending on the particle number N. We use an **effective Hamilton function**

$$\tilde{\mathcal{H}}(\mathbf{r}^N, N) = \mathcal{H}(\mathbf{r}^N, N) + \eta(N) \tag{5.52}$$

with

$$\mathcal{H}(\mathbf{r}^N, N) = \mathcal{U}(\mathbf{r}^N) - \mu N. \tag{5.53}$$

The particle number distribution for the Hamilton function $\mathcal{H}(\mathbf{r}^N, N)$ is given by

$$p(N) = \frac{1}{Z} \int \mathrm{d}\mathbf{r}^N e^{-\beta \mathcal{H}(\mathbf{r}^N, N)} \tag{5.54}$$

and therefore the particle number distribution for the effective Hamilton function can be obtained by

$$\tilde{p}(N) = \frac{1}{\tilde{Z}} \int \mathrm{d}\mathbf{r}^N e^{-\beta \tilde{\mathcal{H}}(\mathbf{r}^N, N)} \tag{5.55}$$

$$= \frac{1}{\tilde{Z}} \int \mathrm{d}\mathbf{r}^N e^{-\beta(\mathcal{H}(\mathbf{r}^{\mathcal{N}}, \mathcal{N}) + \eta(N))} \tag{5.56}$$

$$= \frac{1}{\tilde{Z}} \int \mathrm{d}\mathbf{r}^N \frac{e^{-\beta \mathcal{H}(\mathbf{r}^N, N)}}{e^{\beta \eta(N)}}. \tag{5.57}$$

If we perform a simulation using the effective Hamilton function (5.52) we will sample the particle number probability distribution $\tilde{p}(N)$. To obtain the desired Boltzmann distribution we have to unfold the weight function by

$$p(N) = e^{\beta \eta(N)} \tilde{p}(N). \tag{5.58}$$

A Monte Carlo simulation method is efficient if we get good statistics with little numerical effort. Therefore the most efficient preweighting function is $\eta(N) = \ln p(N)$ because then the simulation performs a one-dimensional random walk in the density, which leads to a flat histogram.

5.5 Wang-Landau Algorithm

The Wang-Landau method [39] is an iterative algorithm for finding a preweighting function (for short: weight function). We start with a flat weight function $\eta(N)$ which is updated at each Monte Carlo step by

$$e^{\beta\eta_{\text{new}}(N)} = f e^{\beta\eta_{\text{old}}(N)} \Leftrightarrow \beta\eta_{\text{new}}(N) = \ln f + \beta\eta_{\text{old}}(N). \tag{5.59}$$

The iteration factor f has to fulfil $f > 1$. In parallel to updating the weight function we count how often states with a certain particle number are visited which gives the histogram $H(N)$. If the histogram of visited states $H(N)$ is "flat enough" the iteration factor f is decreased, for example by

$$\ln(f_{\text{new}}) = \frac{\ln(f_{\text{old}})}{2}. \tag{5.60}$$

One possible condition for flatness is that each particle number is sampled at least 80% of the mean number of visited states per particle number.

Detailed balance is violated so we have a non-equilibrium simulation.

5.6 Critical Phenomena

5.6.1 Finite Size Scaling

A critical point is characterised by singularities in the thermodynamic potential and discontinuities or divergencies in their second derivatives. These singularities only occur in the thermodynamic limit. The finite size of the simulation box causes that the divergencies of thermodynamic properties in the critical region are smeared out. The effects caused by the finite size of the simulation box are summarised by the term **finite size effects** [40, 41].

Finite size scaling, a discipline on its own right and therefore beyond the scope of this work, is a sophisticated technique to extract the values of critical exponents and to locate critical points from a finite system. Its validity can be proved by **renormalisation group theory**.

To explain the principles of finite size scaling we have a closer look at the critical behaviour of the specific heat. We use the expressions of table 2.1

$$c_{\text{V}} \sim |t|^{-\alpha} \qquad \xi \sim |t|^{-\nu} \tag{5.61}$$

to write for the specific heat at constant volume c_{V} in the critical region

$$c_{\text{V}} \sim \xi^{\frac{\alpha}{\nu}}. \tag{5.62}$$

At the critical point the correlation length ξ diverges. In a simulation box of finite size the correlation length cannot exceed the box length L and is therefore cut off. As a consequence the singularity of the specific heat at the critical point is smeared out which we express by writing

$$c_{\text{V}} = \xi^{\frac{\alpha}{\nu}} c_{\text{V}}^0(L/\xi). \tag{5.63}$$

ξ denotes the value of the correlation length in the infinite system. The function $c_{\text{V}}^0(L/\xi)$ is constant for $\xi << L$ and it is proportional to $(L/\xi)^{\frac{\nu}{\alpha}}$ for $\xi > L$. We now introduce the **scaling**

variable x

$$x^\nu = \frac{L}{\xi} \propto |t|^\nu L \tag{5.64}$$

and use the expression for the correlation length ξ of equations (5.61) to rewrite equation (5.63) as

$$\begin{aligned} c_\mathrm{V} &= L^{\frac{\alpha}{\nu}} \left(\frac{L}{\xi}\right)^{-\frac{\alpha}{\nu}} c_\mathrm{V}^0(L/\xi) \\ &= L^{\frac{\alpha}{\nu}} (x^\nu)^{-\frac{\alpha}{\nu}} c_\mathrm{V}^0(x^\nu) \\ &= L^{\frac{\alpha}{\nu}} x^{-\alpha} c_\mathrm{V}^0(x^\nu). \end{aligned} \tag{5.65}$$

We define a new function

$$\tilde{c}_\mathrm{V}(x) = x^{-\alpha} c_\mathrm{V}^0(x^\nu) \tag{5.66}$$

and extend the definition of $\tilde{c}_\mathrm{V}(x)$ to negative values of x to get for the specific heat

$$c_\mathrm{V} = L^{\frac{\alpha}{\nu}} \tilde{c}_\mathrm{V}(tL^{\frac{1}{\nu}}). \tag{5.67}$$

The **scaling function** for the specific heat, $\tilde{c}_\mathrm{V}(tL^{\frac{1}{\nu}})$, has no hidden L dependencies and should be the same for all system sizes.

To determine the critical exponent α and the critical temperature T_c we do simulations in the critical region at different system sizes for a set of different temperatures, calculate c_V and use equation (5.67) to get the scaling function $\tilde{c}_\mathrm{V}(tL^{\frac{1}{\nu}})$. Then we vary the critical exponents and the critical temperature until the scaling functions for the different system sizes coincide on top of each other. This gives us the correct critical exponent and critical temperature.

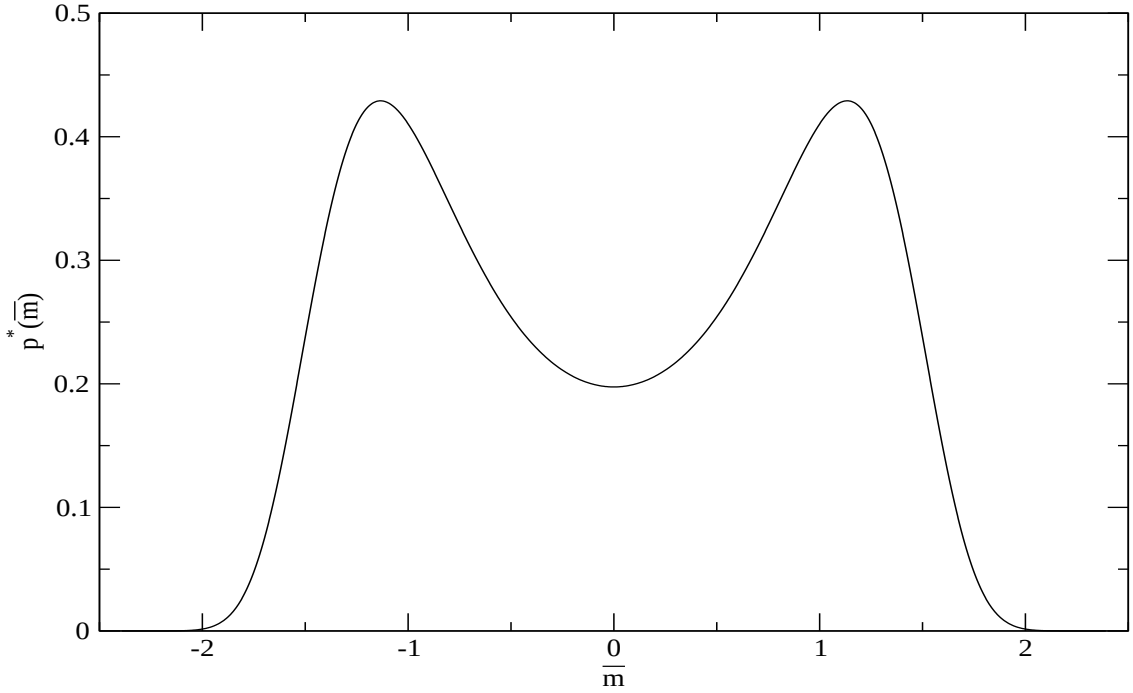

Figure 5.1: The universal fixed point order parameter distribution function [43] for a cubic system with periodic boundary conditions. The distribution has been shifted and scaled to obtain unit variance.

5.6.2 Critical Order Parameter Distribution

Not only the behaviour of the expressions in table 2.1 is universal in the critical region but also the probability density function for the fluctuating order parameter. Once we know it we can determine the critical point by comparison of the measured distribution functions to the form of the universal function. Hilfer and Wilding [42] used finite size scaling and Monte Carlo methods to determine probability density functions for the 2d and 3d Ising model (see figure 5.1). One should bear in mind that the universal order parameter distribution function depends on the geometry of the box and the boundary conditions.

Chapter 6

MSA Phase Diagram

We have calculated the phase diagrams for $\delta = 0.67$ and $\delta = 0.69$ by solving the Ornstein-Zernike equation with the MSA as closure. The calculations were performed with `Mathematica` [44]. The expressions for the pressure and the chemical potentials, which were used to determine phase coexistence are compiled in section 4.3. The two phase diagrams, which belong to type II, show different behaviour and therefore we call them type α and type β respectively.

The legend for the coloured plots is as following:

The coexistence lines for $\Delta\mu = 0$, which means that no field is applied, are **turquoise**. **Blue** is used for isothermal cuts. The **brown** lines mark coexistence points which are separated from each other by a constant distance in the concentration-density plane. To illustrate the behaviour of the critical lines the mean value of these coexistence points is **red** for critical lines starting at the **equimolar critical point** and **orange** for critical lines starting at a **tricritical point**. Triple lines are thick and **aqua** coloured. Additionally, in figure 6.1 and 6.2, some coexistence points of the triple lines are connected by straight, thin, **aqua** lines in the projection of the phase diagram on the concentration-density plane as a guide to the eye.

6.1 Mixed Field-Density Space

The phase diagrams in the (T, c, ρ)-space (along with projections) for type α and β are presented in figure 6.1 and 6.2 respectively.

The phase diagrams for the case that no field is applied and projections of critical and triple lines are shown in figure 6.3 and 6.4. Additionally dashed lines separate different temperature regimes, in which the isothermal cuts have the same topology. Examples for these cut are shown in figure 6.5 and 6.6.

Critical Lines

The most striking difference between the two types is the form of the **critical lines** (see figure 6.1 and 6.2).

- **Type** α: The vapour-liquid critical line going through the equimolar critical point ends in critical end points. The demixing critical line splits at a tricritical point in two mixing-demixing critical lines.
- **Type** β: The vapour-liquid critical line extends from concentration $c = 0$ (pure fluid of B particles) to the equimolar vapour-liquid critical point at $c = 0.5$ and further to $c = 1$ (pure fluid of A particles). The demixing critical line splits at the tricritical point in two mixing-demixing critical lines that end on the vapour-liquid surface in critical end points.

The critical end point property has been suspected from the form of the tie lines in the (T, c, ρ)-space (see appendix B) but can more easily be identified by looking at the phase diagram in field space (see section 6.2).

Triple Lines

The difference in the form of the critical lines is related to the different shapes of the **triple lines** (see also section 6.3). In our mixed field-density space a triple line is represented by three lines of coexistence points. At a certain temperature these coexistence points are given by the coexistence densities and the coexistence concentrations of the three phases. We point out that the term triple line is used for the set of the three lines and also for each line belonging to this set. Taking the symmetry of the system into account we only consider the diagram for $c \leq 0.5$ in the further discussion.

For each value of δ, that corresponds to one of the two types α or β, we have two triple lines that start at the equimolar plane ($c = 0.5$) and one triple line that starts at a much lower concentration. The two types of phase behaviour have in common that always two of the three triple lines meet in a **critical end point**. The phase diagram for a certain value of δ belongs to type α if the two triple lines starting at the equimolar plane meet, and to type β if the triple line starting at lower concentration meets the triple line of the remaining two, that starts at the higher density (see figure 6.1 and 6.2).

Temperature Regimes

In the different temperature regimes denoted in figure 6.3 and 6.4 the isothermal cuts have, for a certain type, the same topology. The limits of these regimes are given in the following table ordered from lower to higher temperatures.

Type α	Type β
quadruple point	quadruple point
equimolar vapour-liquid critical point	minimum of the mixing-demixing critical line
critical end point of the vapour-liquid critical line	critical end point of the mixing-demixing critical line
minimum of the mixing-demixing critical line	equimolar vapour-liquid critical point
tricritical point	tricritical point

Examples for the isothermal cuts corresponding to the different temperature regimes are given in in figures 6.5 and 6.6.

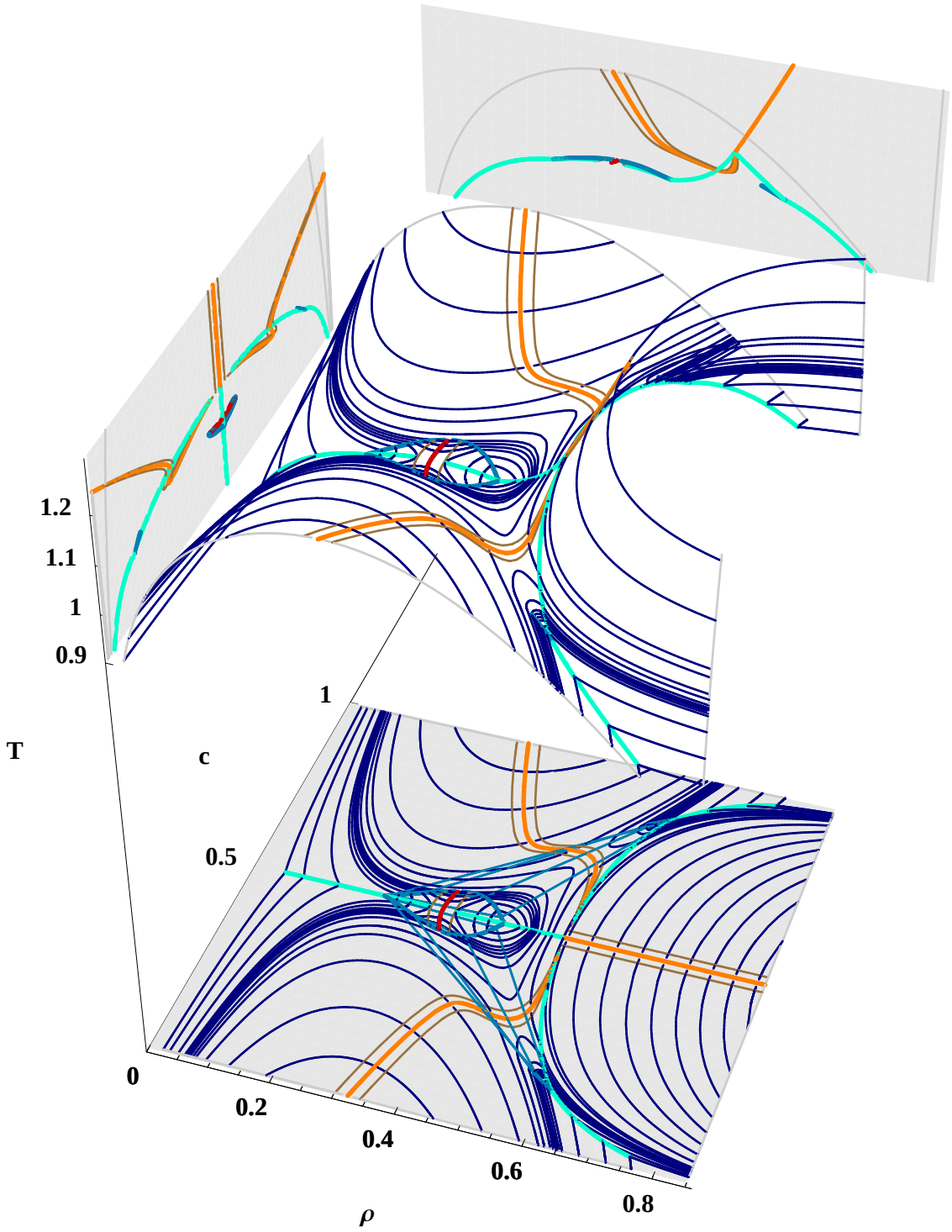

Figure 6.1: (T, c, ρ) phase diagram and projections for $\delta = 0.67$ (type α).

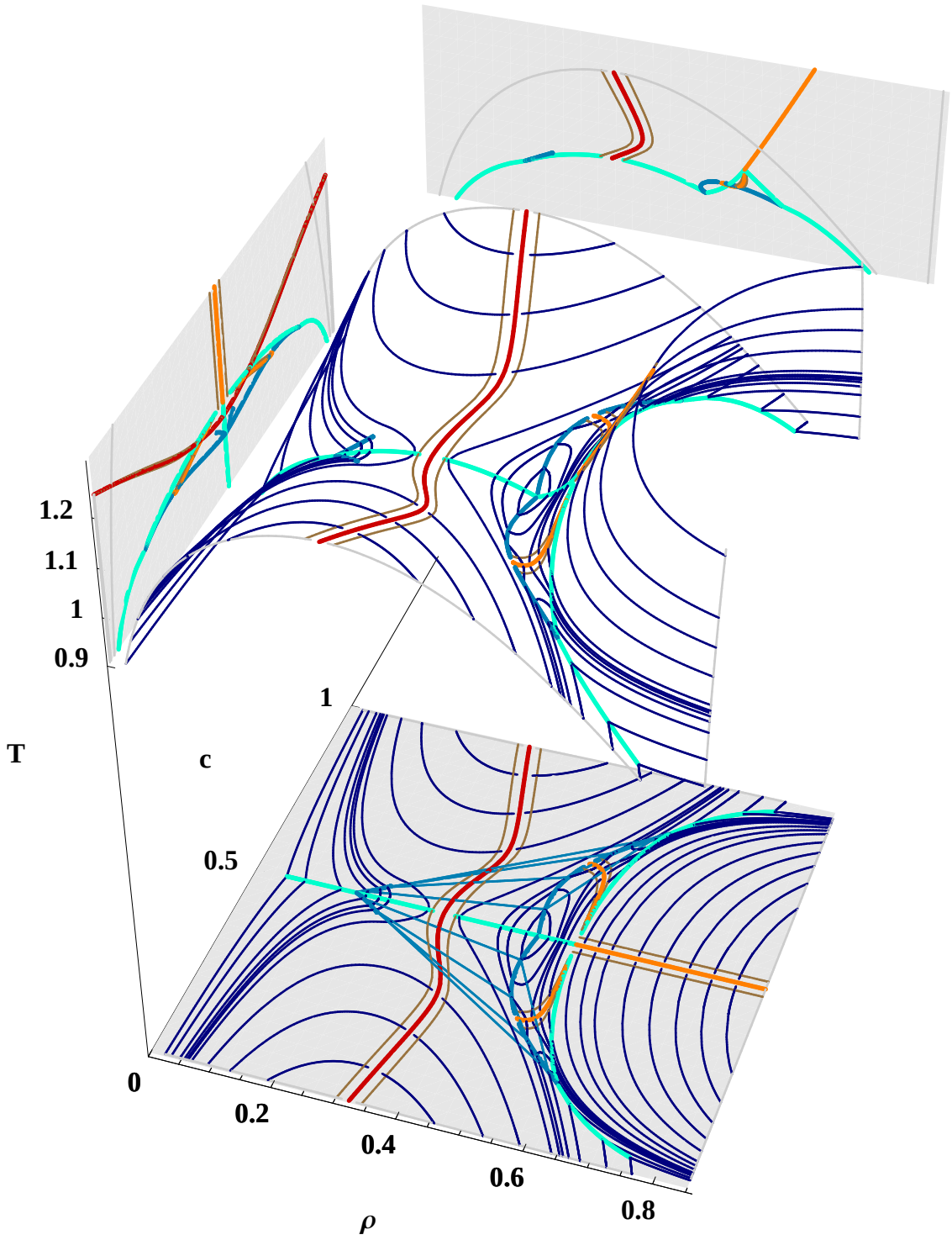

Figure 6.2: (T, c, ρ) phase diagram and projections for $\delta = 0.69$ (type β).

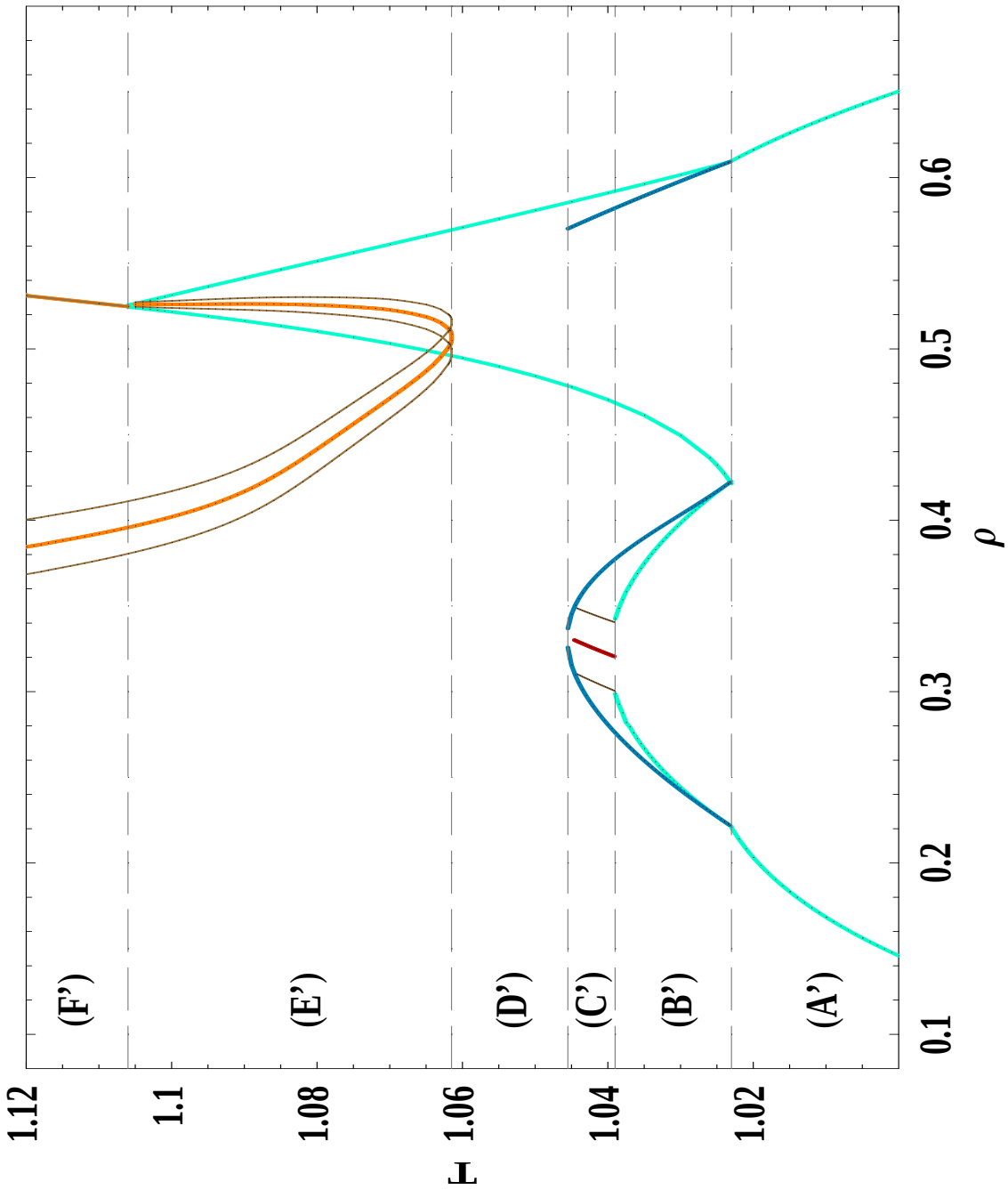

Figure 6.3: Projection of the coexistence lines for $\Delta\mu = 0$ and of critical and triple lines for $\delta = 0.67$. The gray dashed lines indicate the limits of the different temperature regimes denoted from (A') to (F').

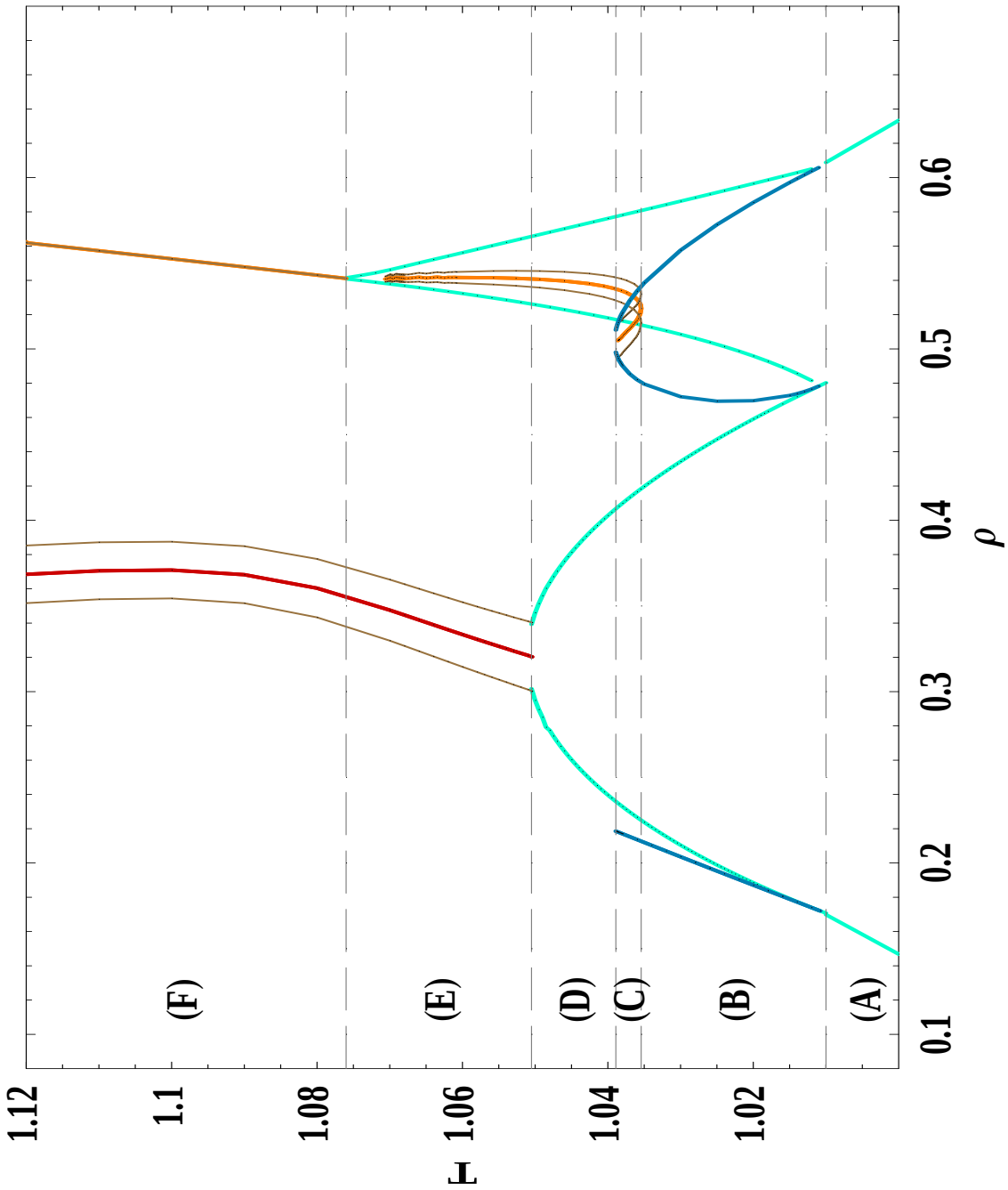

Figure 6.4: Projection of the coexistence lines for $\Delta\mu = 0$ and of critical and triple lines for $\delta = 0.69$. The gray dashed lines indicate the limits of the different temperature regimes denoted from (A) to (F).

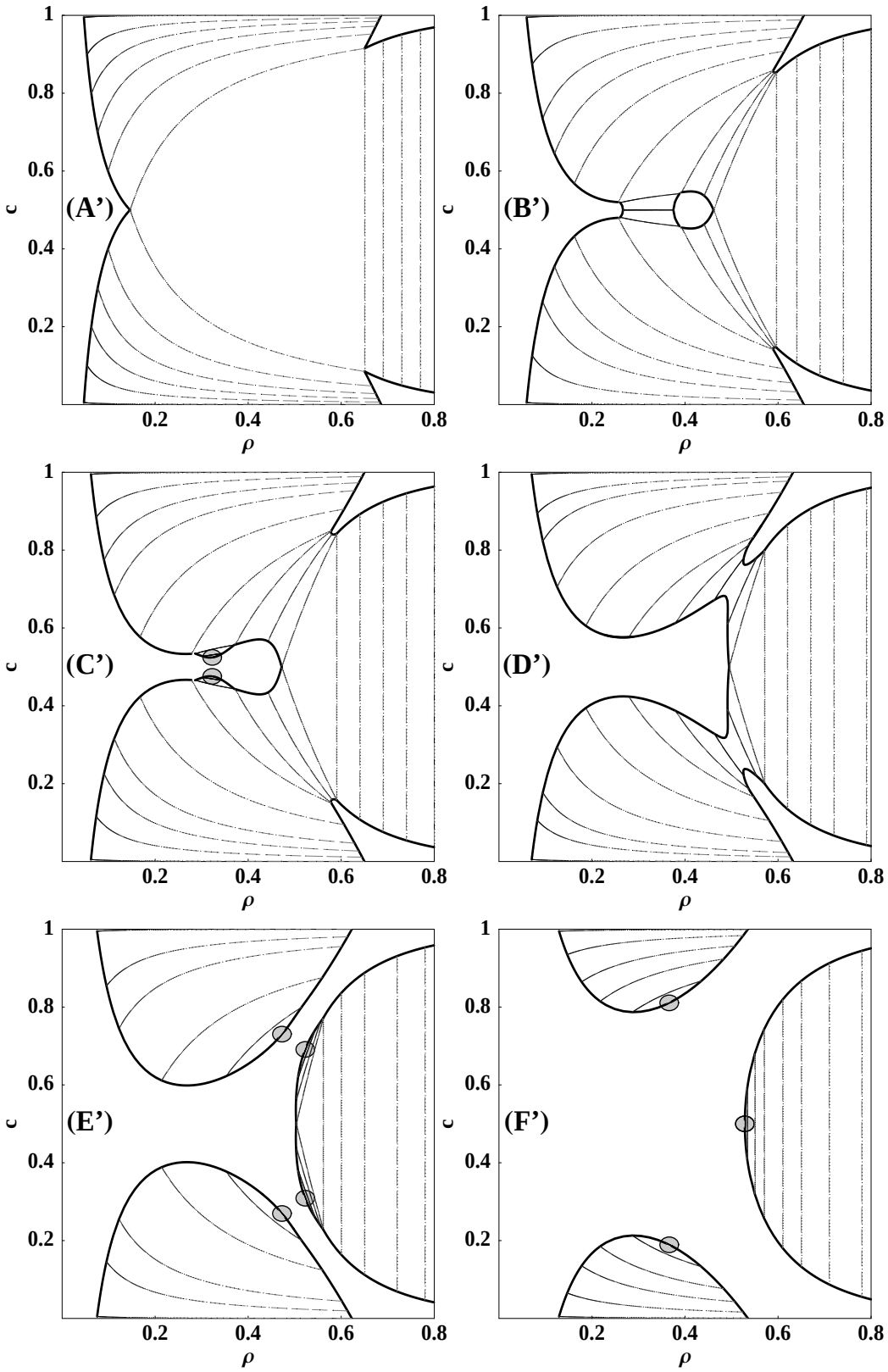

Figure 6.5: Isothermal cuts for $\delta = 0.67$ at $T = 1.0(\mathbf{A}), 1.035(\mathbf{B}), 1.041(\mathbf{C}), 1.06(\mathbf{D}), 1.07(\mathbf{E}), 1.115(\mathbf{F})$. The gray disks denote critical points and the gray, dashed lines are tie lines.

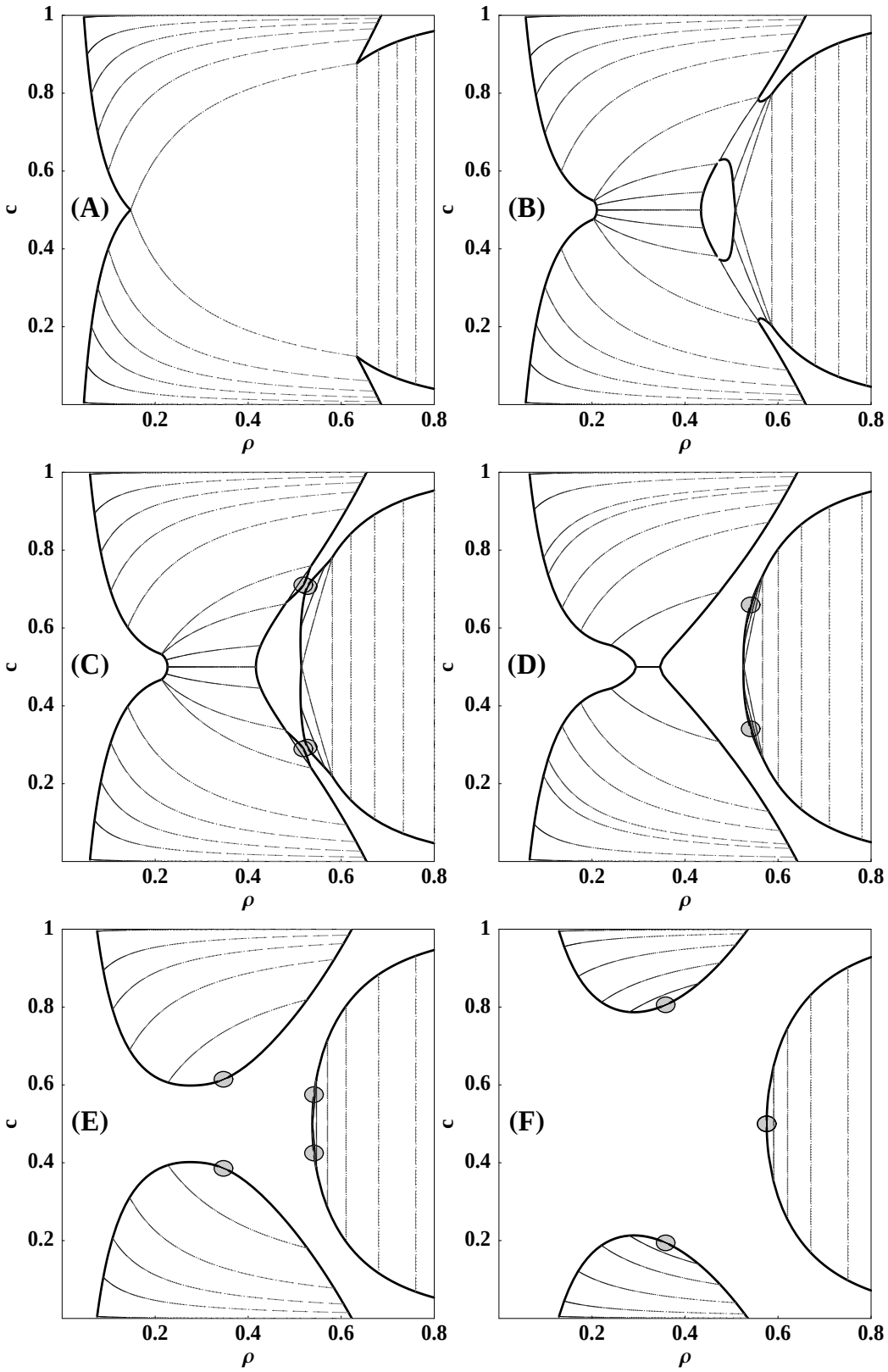

Figure 6.6: Isothermal cuts for $\delta = 0.69$ at $T = 1.0(\mathbf{A}), 1.03(\mathbf{B}), 1.036(\mathbf{C}), 1.05(\mathbf{D}), 1.07(\mathbf{E}), 1.15(\mathbf{F})$. The gray disks denote critical points and the gray, dashed lines are tie lines.

6.2 Field Space

The phase diagram in $(T, \Delta\mu, p)$ field space for the type α is presented in figure 6.7, for type β in 6.8, and figures 6.9 to 6.12 give detailed views. Projections of the complete phase diagrams and of the interesting regions are shown if figures 6.13 to 6.24. As mentioned above some of the features of the phase diagrams presented in section 6.1 are more obvious in the field space representation (see chapter 2.5.6).

For the discussion of the different properties of type α and type β we concentrate on figures 6.11 and 6.12.

The phase diagrams for both types α and β are composed of four surfaces of coexisting phases, namely of

- a vapour-liquid surface,
- two mixing-demixing surfaces, and a
- demixing surface.

The two types have in common that the vapour-liquid sheet intersects with the two mixing-demixing surfaces in two triple lines, and that the latter two sheets intersect with the demixing surface in a line, which also constitutes a triple line. The latter is a special case that emerges from the symmetry of our system. Generally three surfaces intersect in a single point, i.e. in a **quadruple point**, like the vapour-liquid surface and the two mixing-demixing sheets do for both types.

- **Type** α: The phase diagram in the low pressure region is dominated by the mixing-demixing surfaces and the vapour-liquid surface builds a small "pocket" to low pressure values. The vapour-liquid critical line meets the triple lines in critical end points.
- **Type** β: In contrast to type α the phase diagram of type β is dominated at low pressure by the vapour-liquid surface and the two mixing-demixing sheets build a "pocket" to higher pressure values. The mixing-demixing critical lines meet the corresponding triple lines at the vapour-liquid surface and therefore end in critical end points.

Tuning the value of δ we should be able to find the **transition phase diagram** between type α and type β. We suspect that getting closer to the value $\delta_{\alpha\beta}$ that corresponds to the transition diagram, the critical end points, and therefore also the triple lines, should get closer to the critical line of the dominating coexistence surface until they merge into a tricritical point.

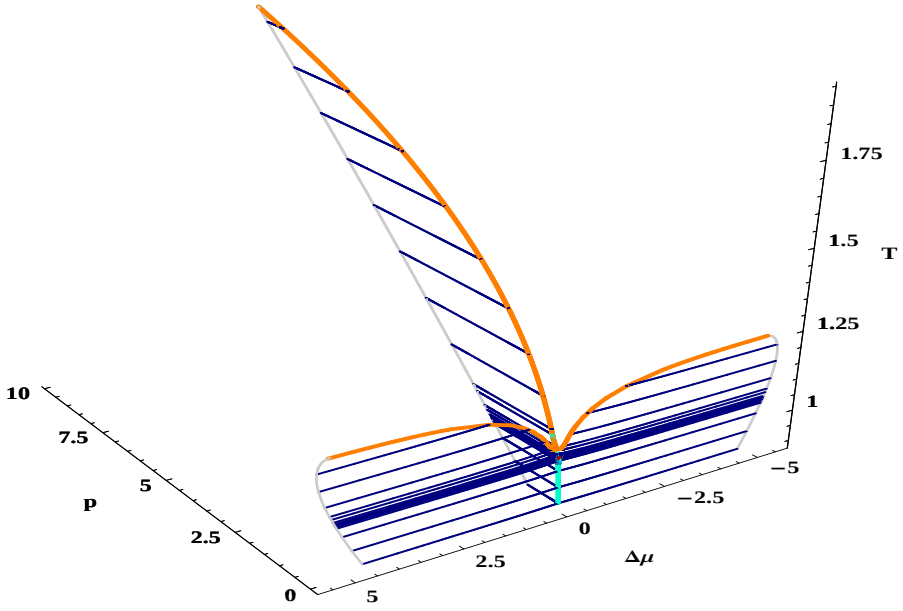

Figure 6.7: Phase diagram for $\delta = 0.67$ in (T, $\Delta\mu$, p)-space.

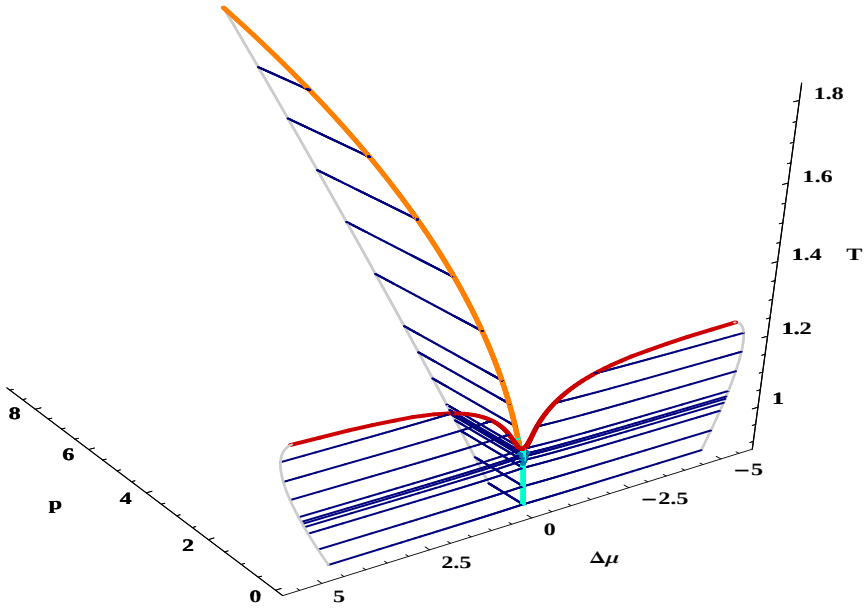

Figure 6.8: Phase diagram for $\delta = 0.69$ in (T, $\Delta\mu$, p)-space.

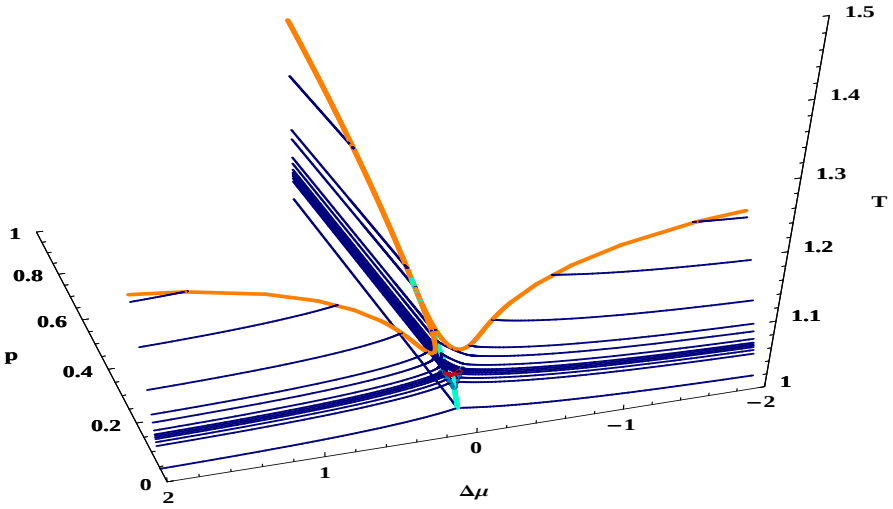

Figure 6.9: Close-up view of the phase diagram for $\delta = 0.67$.

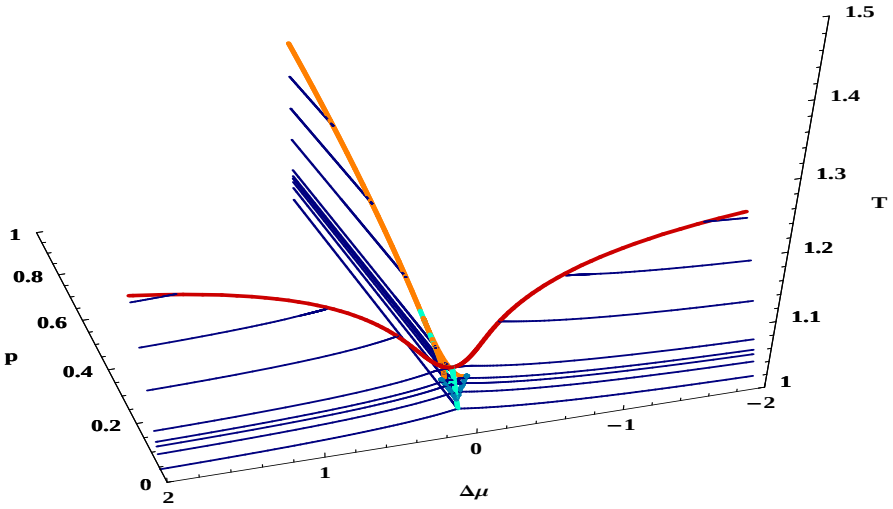

Figure 6.10: Close-up view of the phase diagram for $\delta = 0.69$.

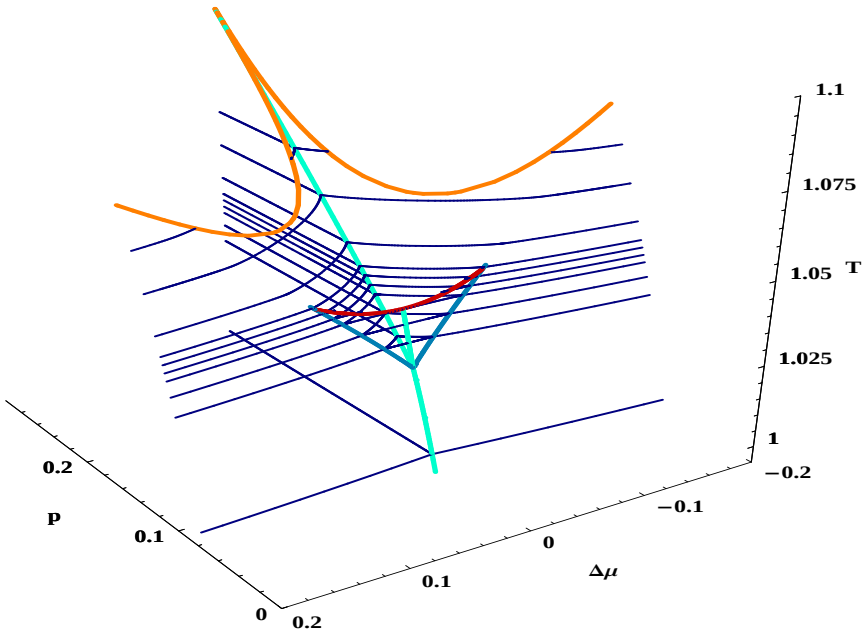

Figure 6.11: The interesting region for $\delta = 0.67$.

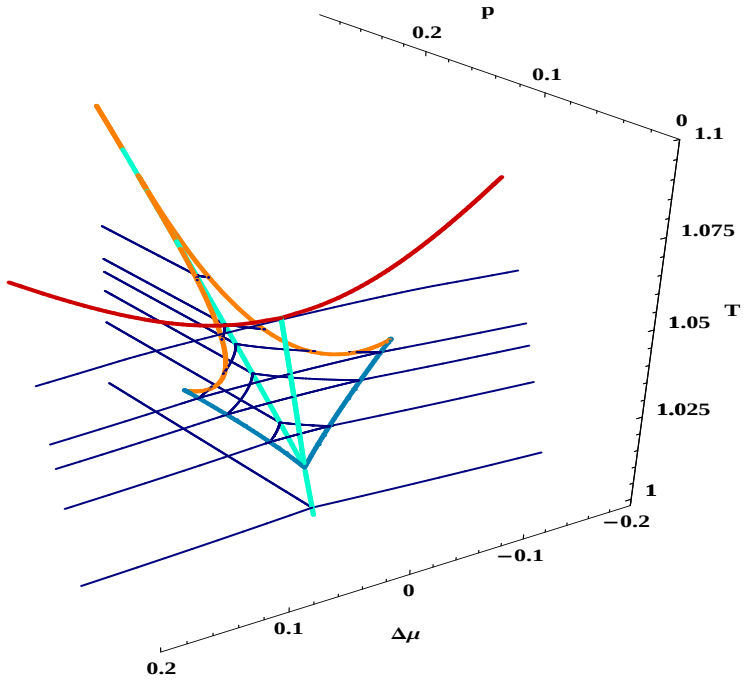

Figure 6.12: The interesting region for $\delta = 0.69$.

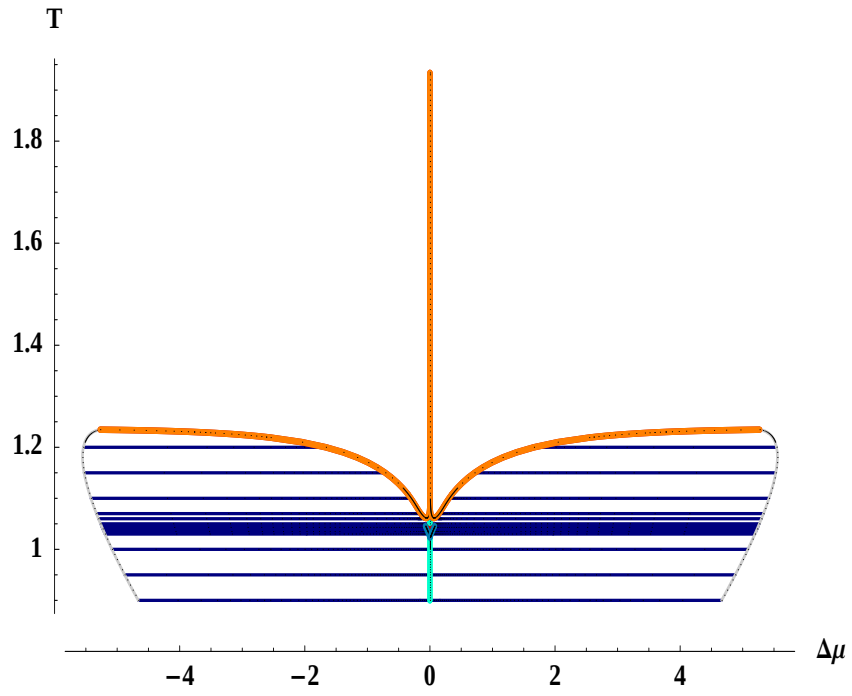

Figure 6.13: Projection of the phase diagram for $\delta = 0.67$ onto the $(T, \Delta\mu)$-plane.

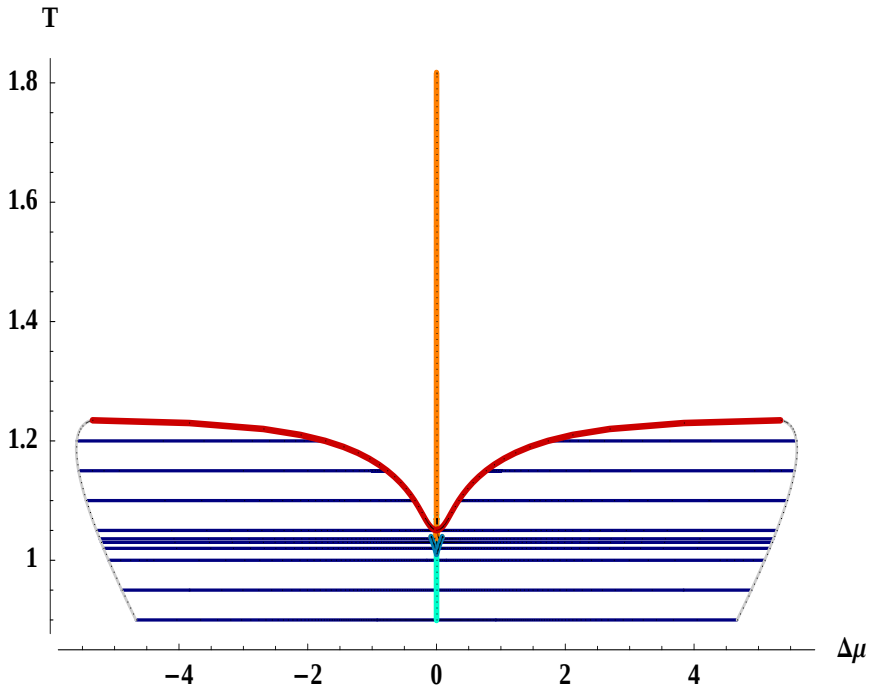

Figure 6.14: Projection of the phase diagram for $\delta = 0.69$ onto the $(T, \Delta\mu)$-plane.

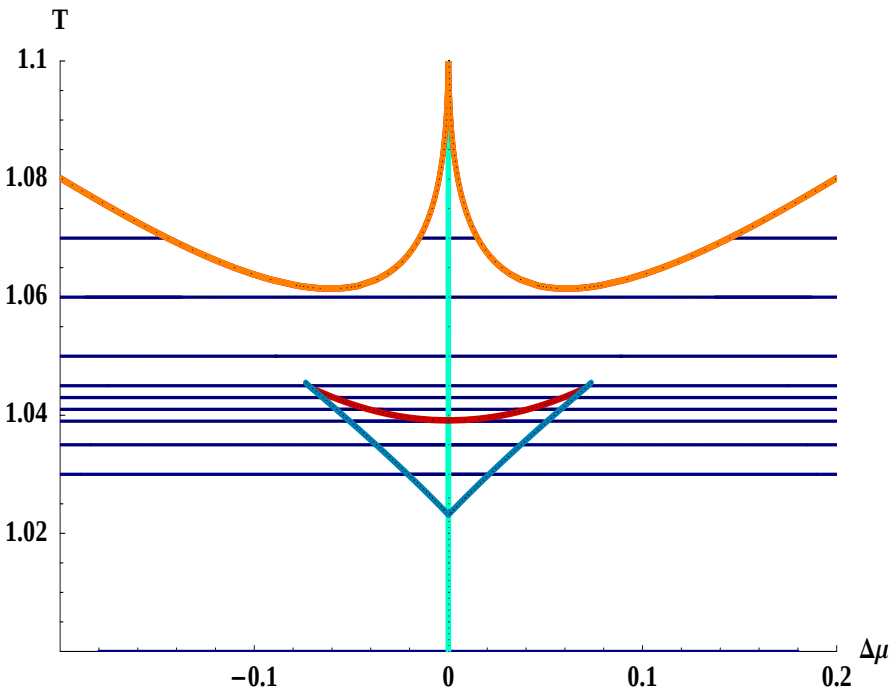

Figure 6.15: Close-up view of the projection of the phase diagram for $\delta = 0.67$ onto the $(T, \Delta\mu)$-plane.

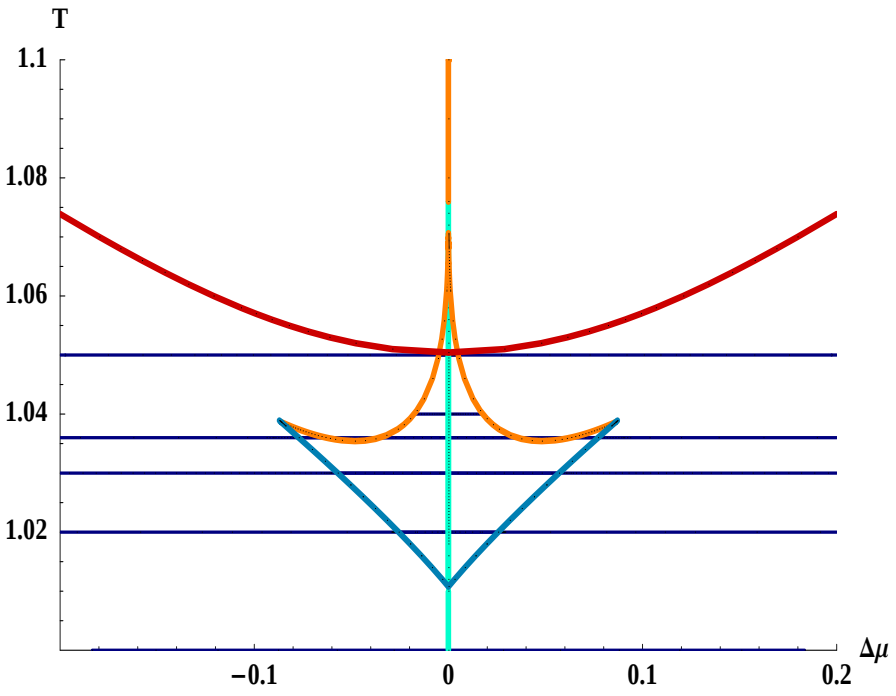

Figure 6.16: Close-up view of the projection of the phase diagram for $\delta = 0.69$ onto the $(T, \Delta\mu)$-plane.

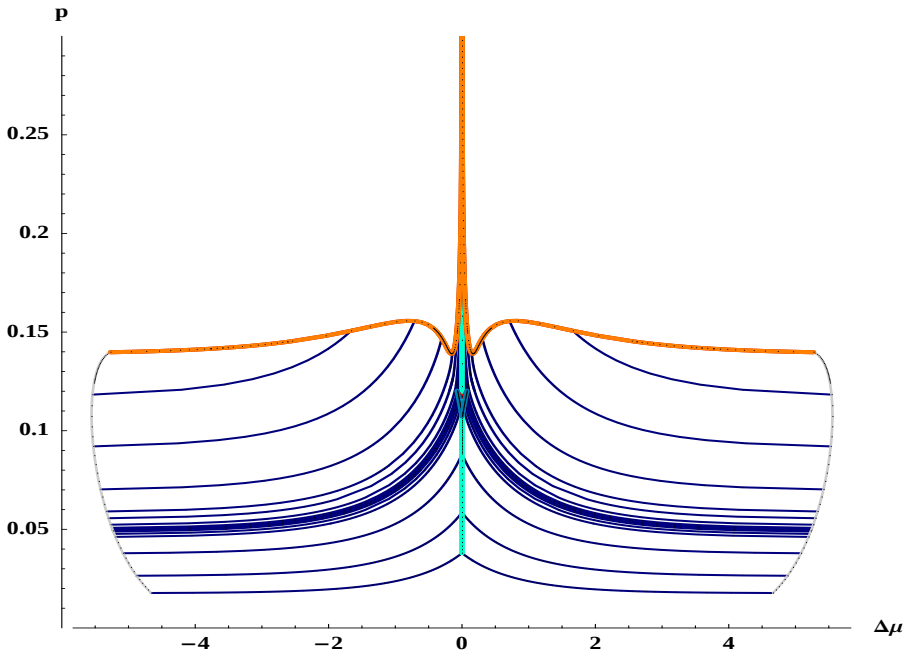

Figure 6.17: Projection of the phase diagram for $\delta = 0.67$ onto the $(p, \Delta\mu)$-plane.

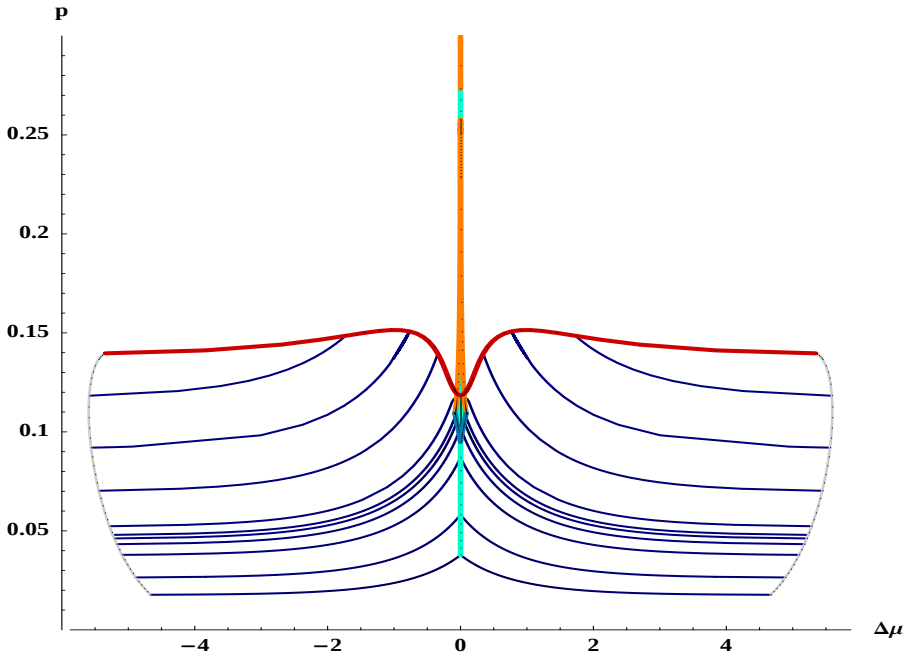

Figure 6.18: Projection of the phase diagram for $\delta = 0.69$ onto the $(p, \Delta\mu)$-plane.

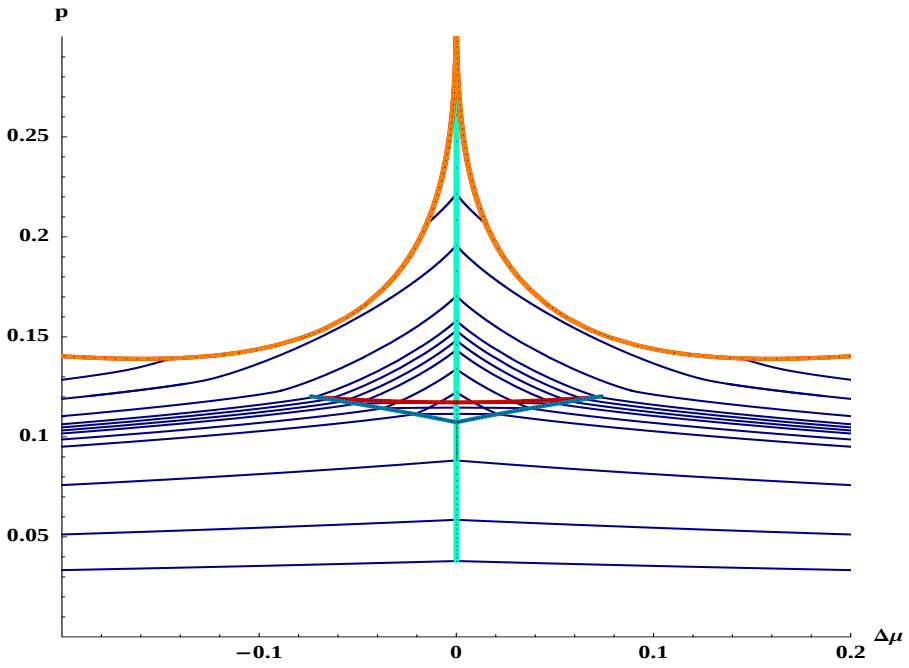

Figure 6.19: Close-up view of the projection of the phase diagram for $\delta = 0.67$ onto the $(p, \Delta\mu)$-plane.

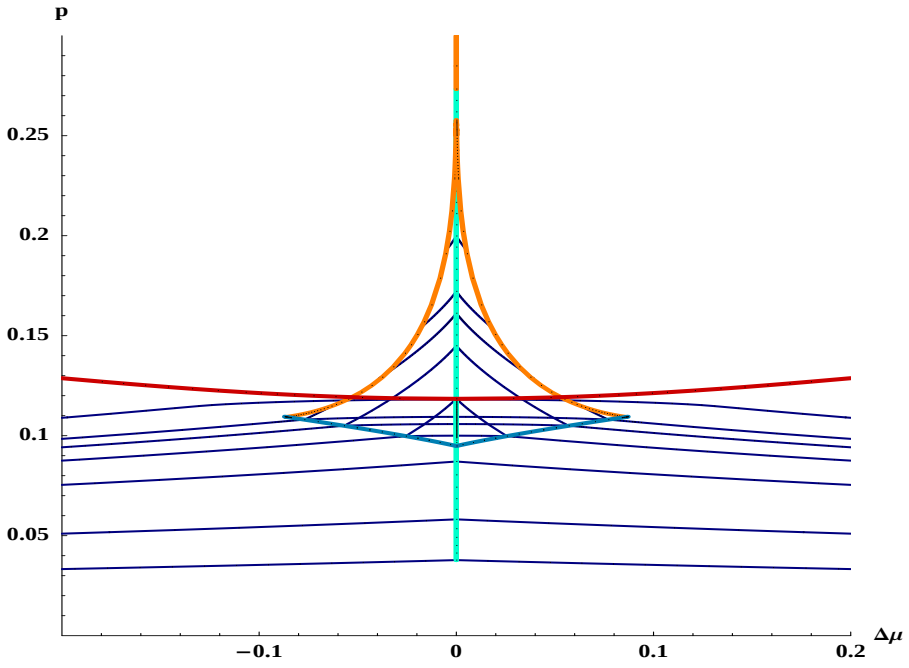

Figure 6.20: Close-up view of the projection of the phase diagram for $\delta = 0.69$ onto the $(p, \Delta\mu)$-plane.

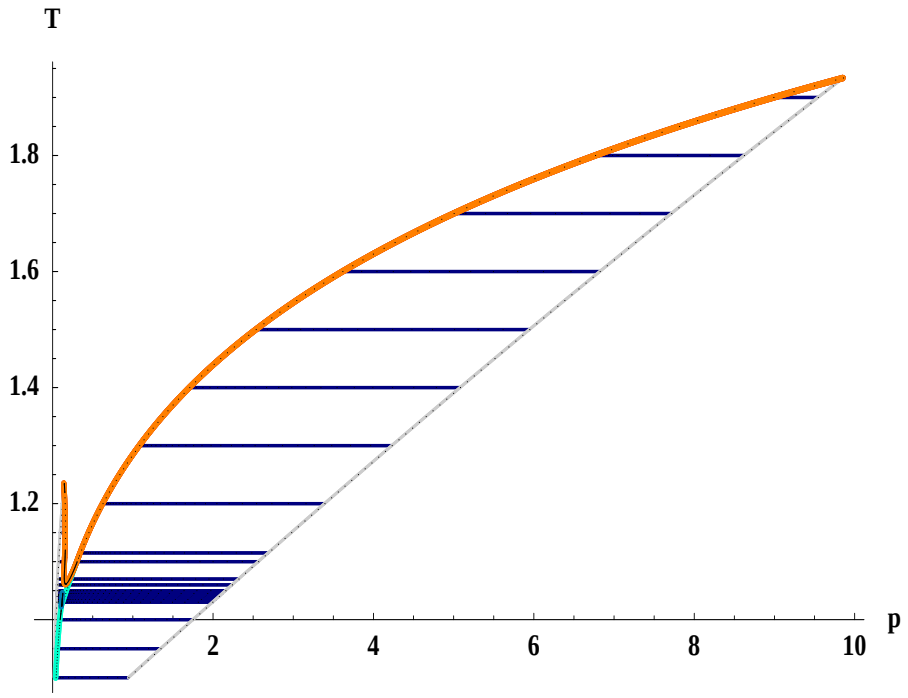

Figure 6.21: Projection of the phase diagram for $\delta = 0.67$ onto the (T, p)-plane.

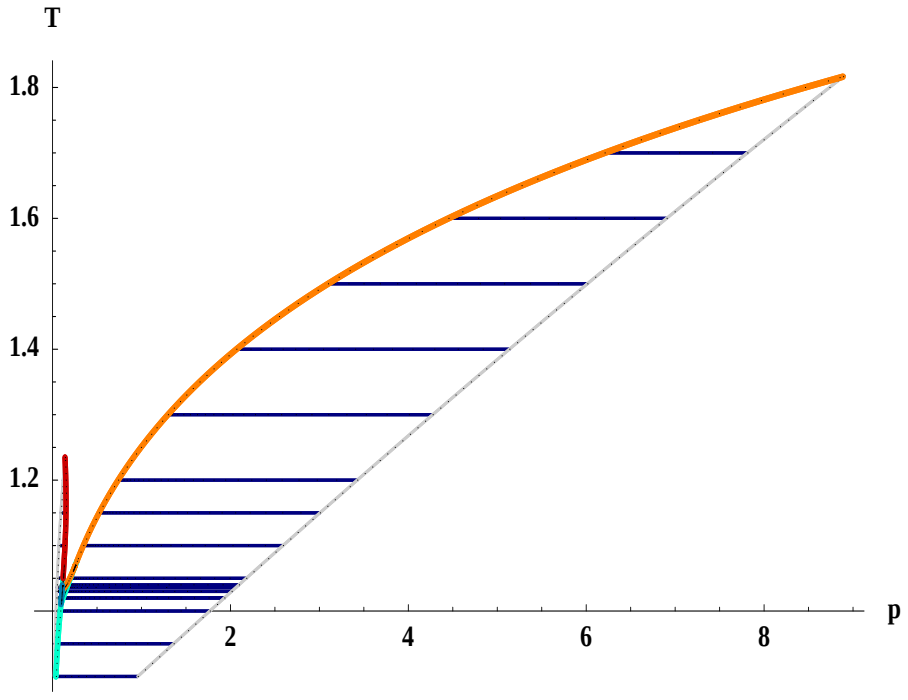

Figure 6.22: Projection of the phase diagram for $\delta = 0.69$ onto the (T, p)-plane.

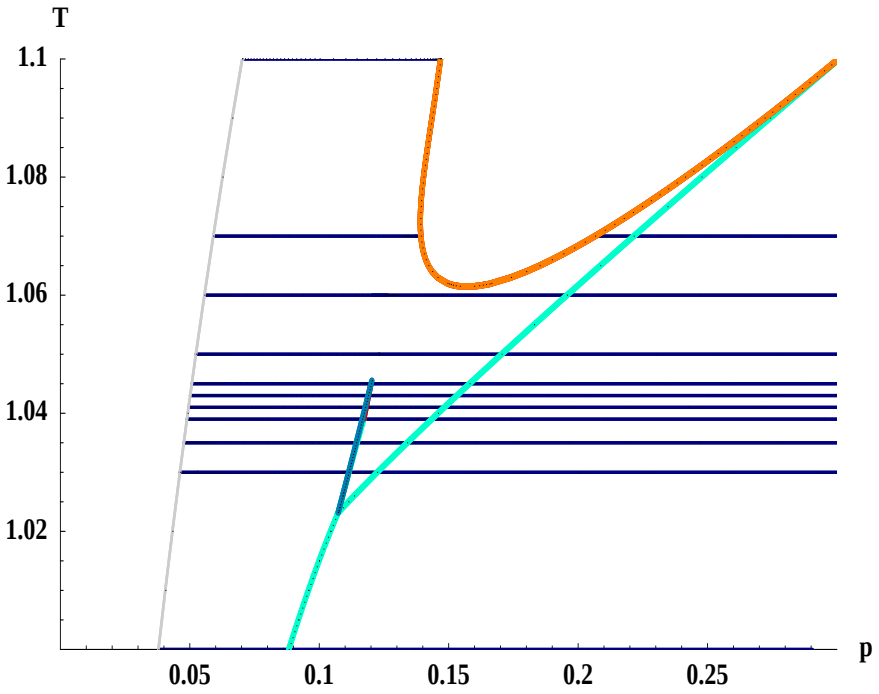

Figure 6.23: Close-up view of the projection of the phase diagram for $\delta = 0.67$ onto the (T, p)-plane.

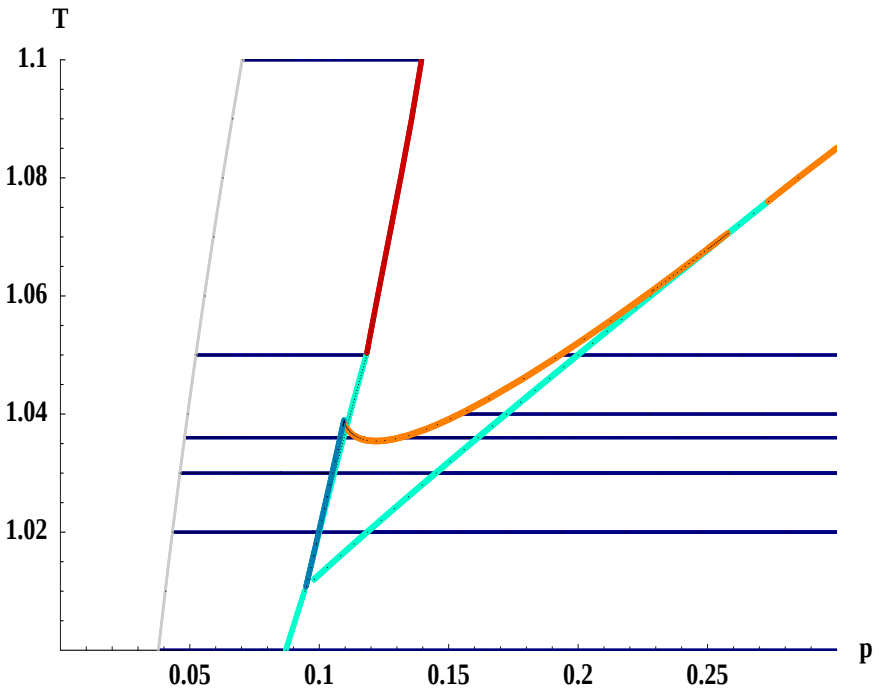

Figure 6.24: Close-up view of the projection of the phase diagram for $\delta = 0.69$ onto the (T, p)-plane.

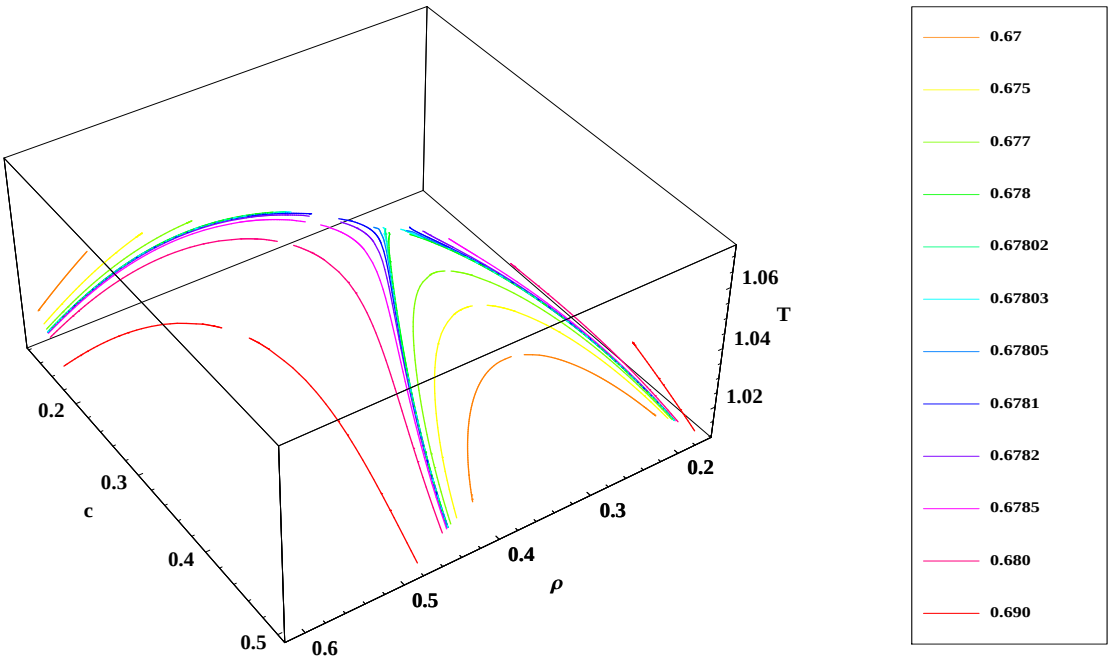

Figure 6.25: Triple Lines for different values of δ in the mixed field-density space.

6.3 Triple Lines

As we explained in section 6.1 we can decide if a phase diagram belongs to type α or β by the behaviour of the triple lines.

In the following plots, which should shed some light onto the transition between type α and β, we present triple lines for different values of δ (see figure 6.25) in the (T, c, ρ)-space and in $(T, \Delta\mu, p)$-space. At the transition between the two types of phase behaviour in the mixed density-field space, the triple lines in one of the symmetry halfs have to meet in a single point which therefore would be a **tricritical point**. From figure 6.26 we estimate for the value of δ for the transition diagram $\delta_{\alpha\beta} = 0.678(0)$.

We know from the mixed field-density space representation of the triple lines (figures 6.25 to 6.30) that at the transition between type α and type β the triple lines reach to higher temperature values than at any other value of δ. Only this knowledge allows it to identify the transition in the field space diagrams of figures 6.31 to 6.34.

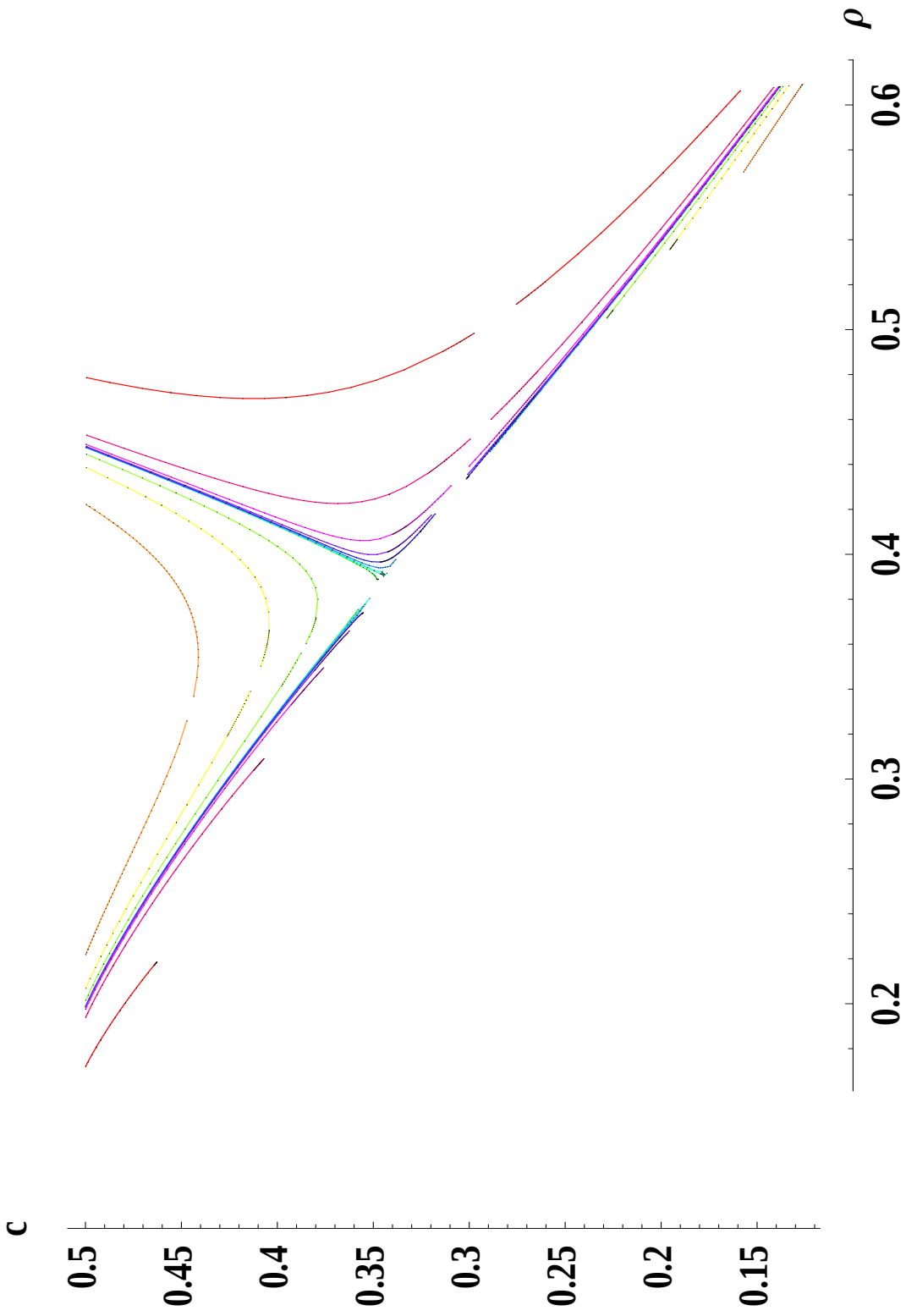

Figure 6.26: Projections of the triple lines for different values of δ onto the c-ρ plane.

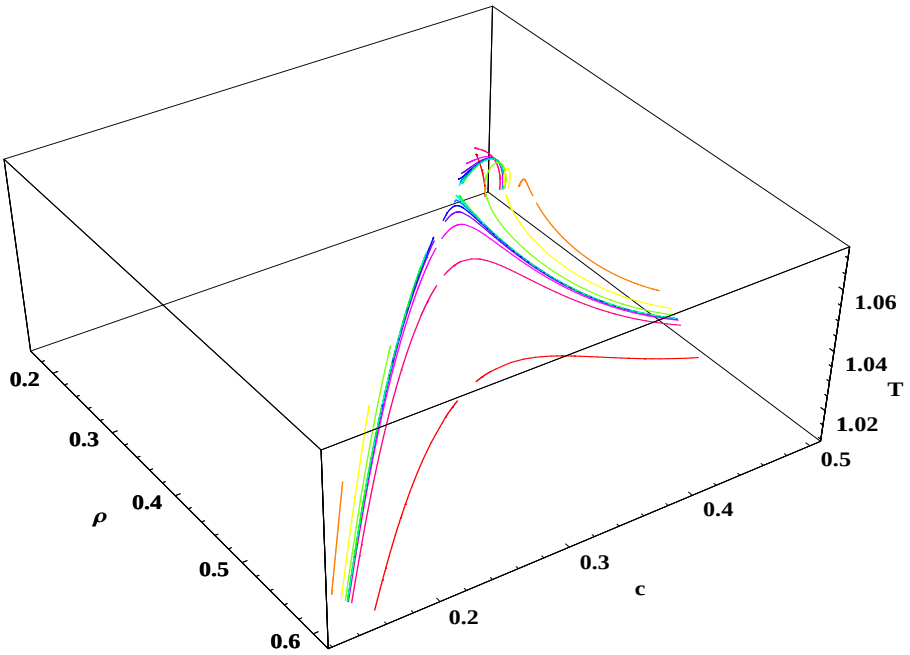

Figure 6.27: Mixed field-density space representation of triple lines with view from the high density region.

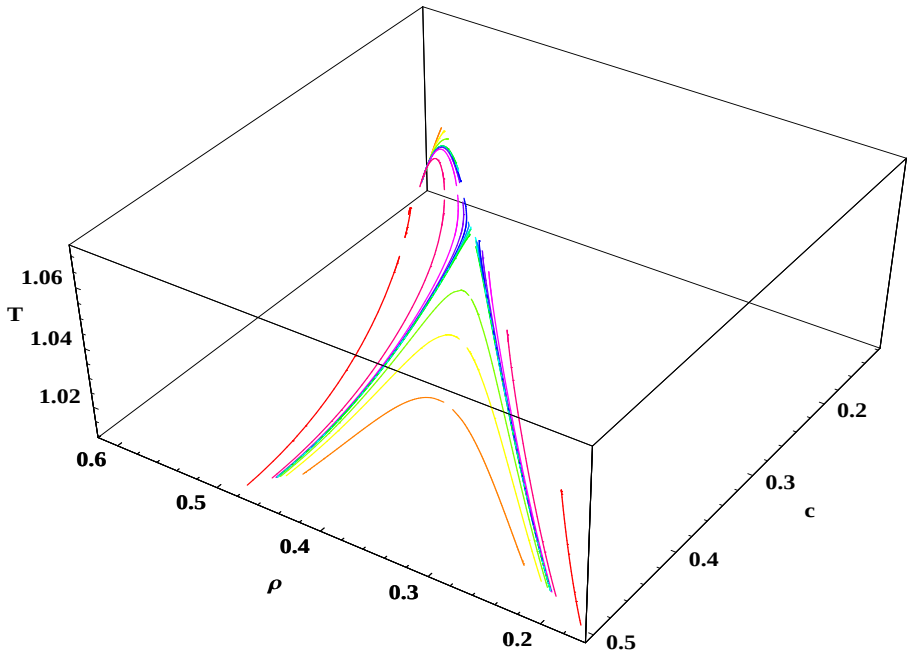

Figure 6.28: Mixed field-density space representation of triple lines with view from the equimolar plane.

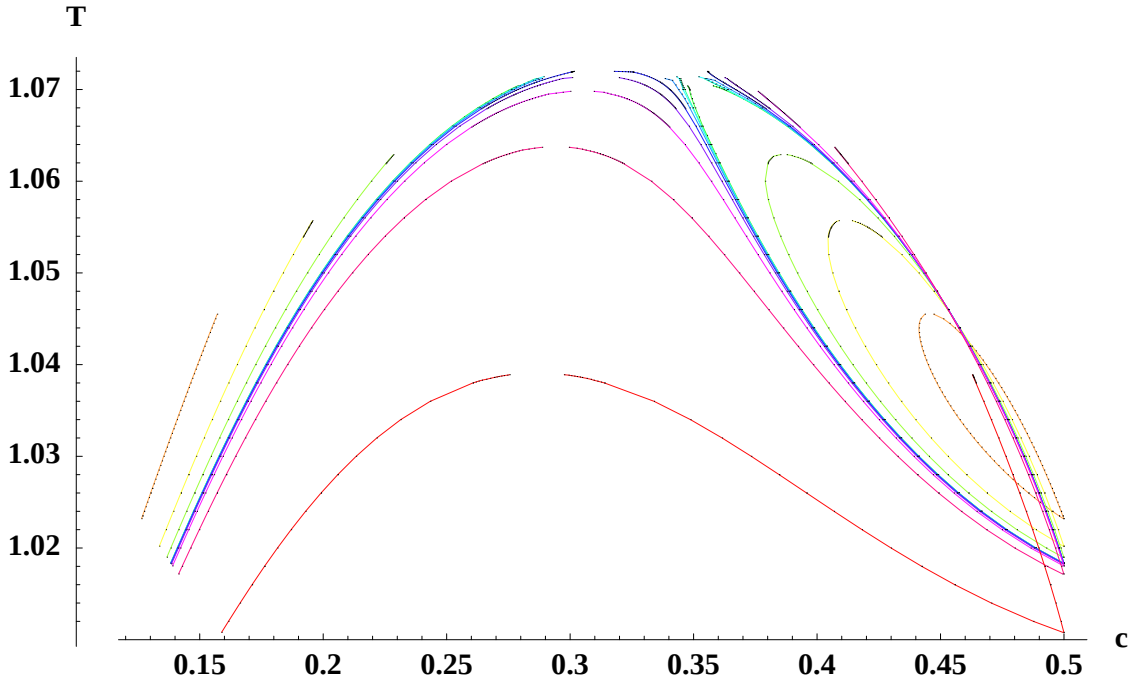

Figure 6.29: Projections of the triple lines for different values of δ onto the T-c plane.

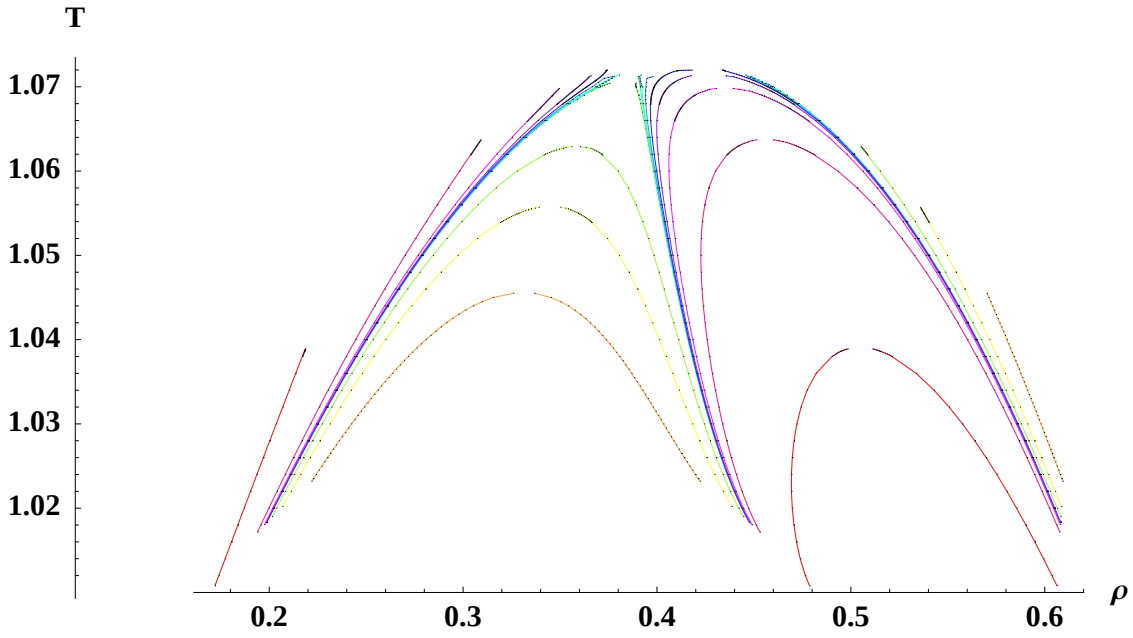

Figure 6.30: Projections of the triple lines for different values of δ onto the T-ρ plane.

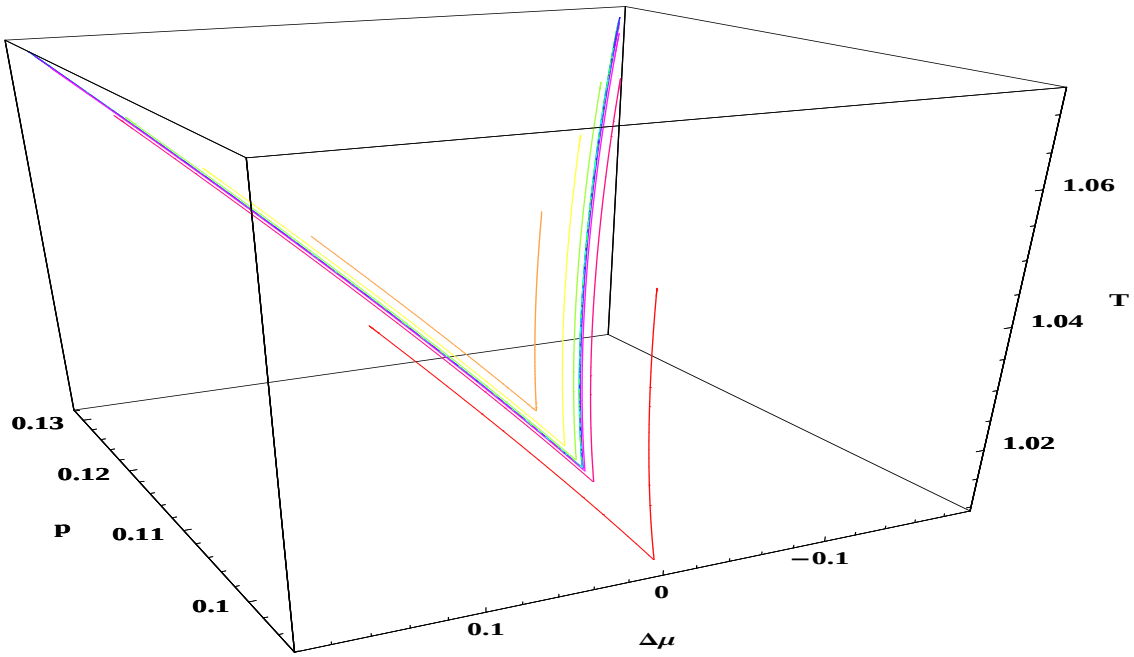

Figure 6.31: The triple lines of figure 6.25 in field space.

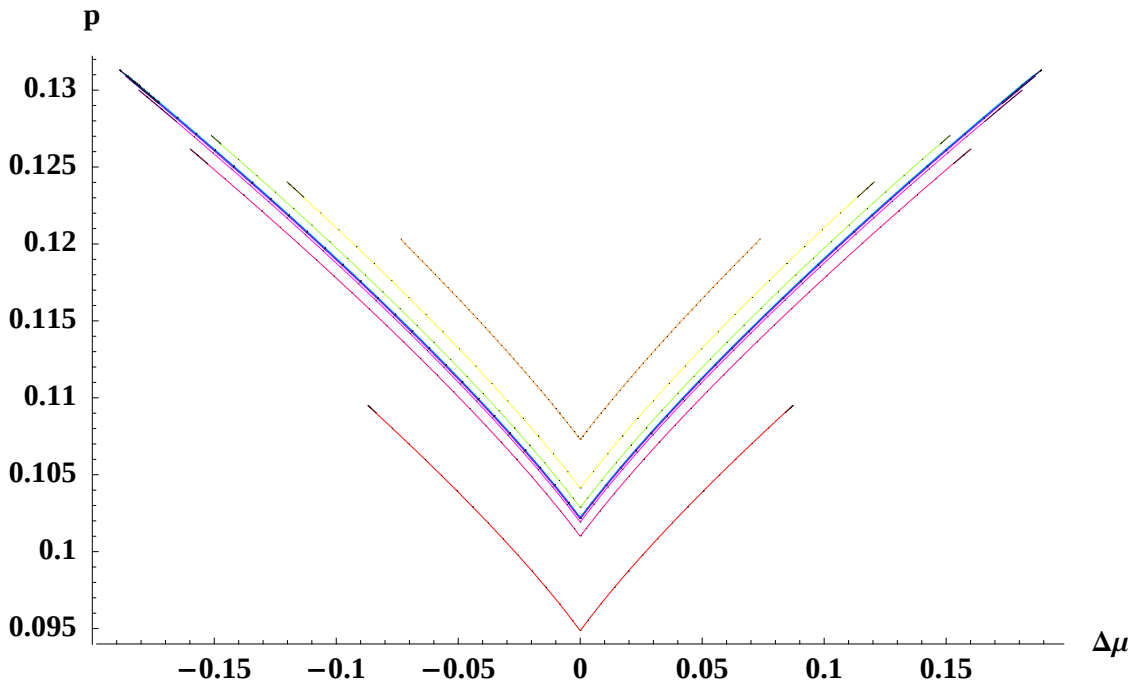

Figure 6.32: Projection of the triple lines of figure 6.31 onto the $(p, \Delta\mu)$-plane.

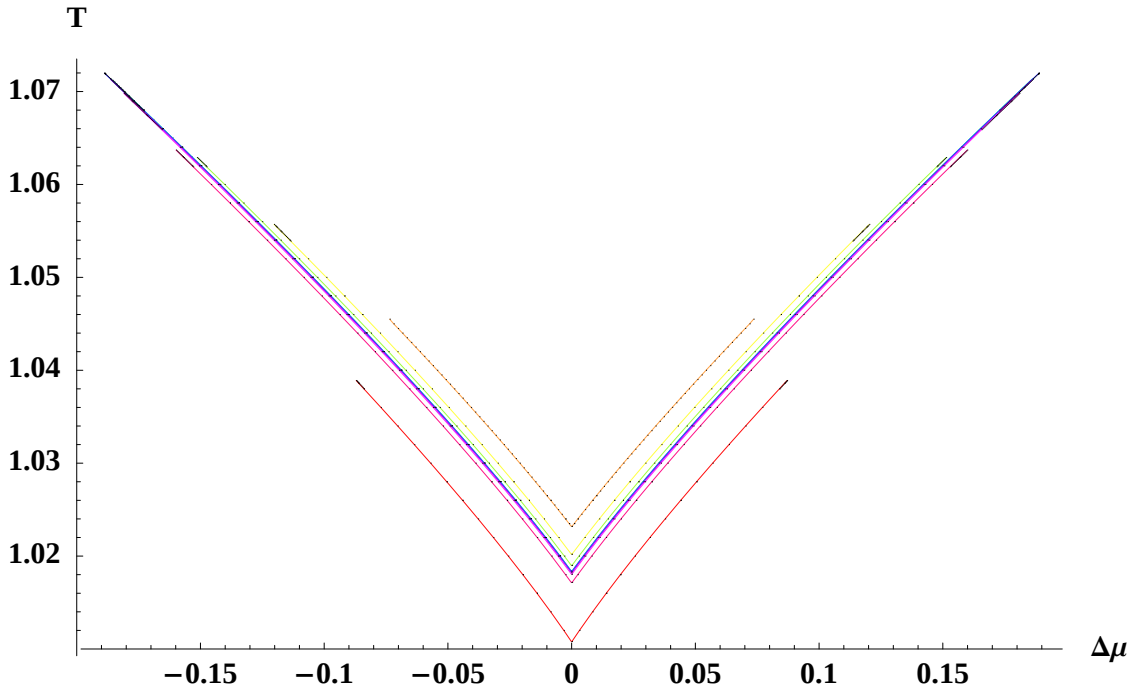

Figure 6.33: Projection of the triple lines of figure 6.31 onto the $(T, \Delta\mu)$-plane.

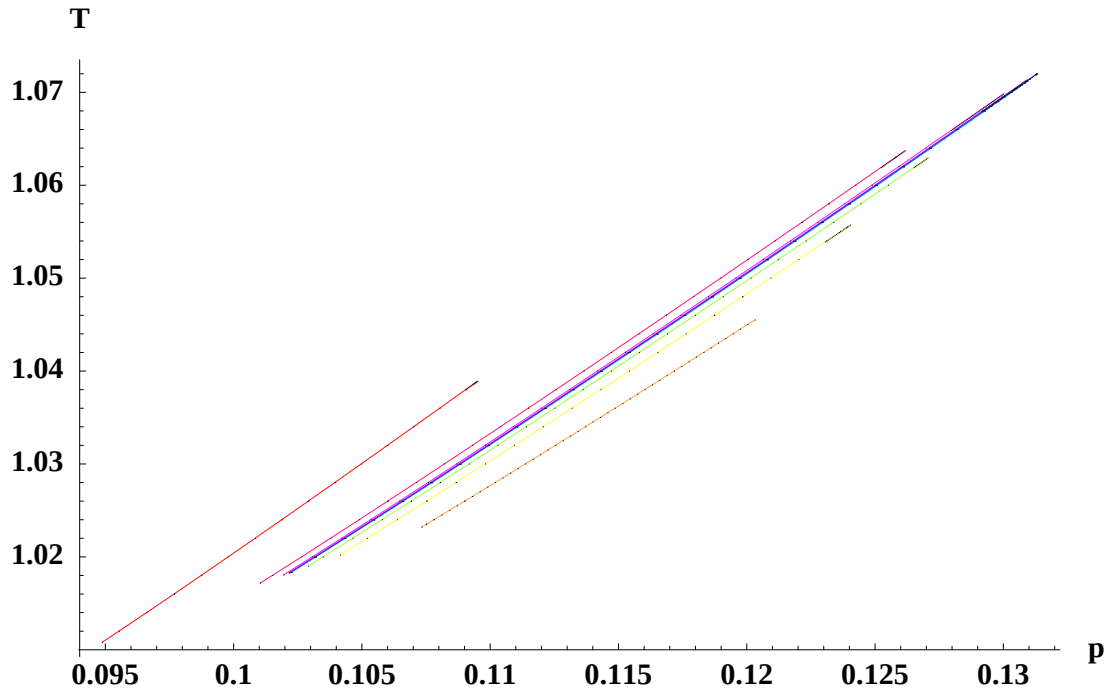

Figure 6.34: Projection of the triple lines of figure 6.31 onto the (T, p)-plane.

6.4 Conclusions

We have solved the Ornstein-Zernike equation with the mean spherical approximation as closure relation for the symmetrical binary Yukawa mixture and have obtained comprehensive phase diagrams in the (T, c, ρ)-space and the $(T, p, \Delta\mu)$-space. The former is a mixed field-density space whereas the latter is a field space.

We examined the phase behaviour for values of the ratio of the dislike to the like interaction strength $\delta = 0.67$ and $\delta = 0.68$. Both phase diagrams show type II behaviour but can be further classified by the form of the vapour-liquid critical line and the mixing-demixing critical lines. Therefore we call them type α and type β. For the former the vapour-critical line ends in critical end points and the mixing-demixng critical lines cover the whole concentration range, whereas for the latter it is the other way round.

The different behaviour of the two types also becomes manifest in the form of the triple lines, which themselves can be used to determine the value of δ where the two types go over in one another. Our estimate is $\delta = 0.678(0)$.

We have also identified different temperature regimes, where isothermal cuts have the same topology and have presented isothermal sections as examples for each of these regimes.

The field space representations allow to identify very easily properties like critical end points, tricritical points, triple lines, and quadruple points, whereas the mixed field-density space provides additional information like the form of tie lines.

The method we have used provides semi-quantitative results but is numerically not very expensive. Therefore it has been possible to obtain a comprehensive picture of type II phase diagrams which helps to deepen the understanding of the phase behaviour of the symmetrical binary mixture.

Chapter 7

Monte Carlo Results

We perform Metropolis Monte Carlo simulations for the symmetrical binary Yukawa mixture consisting of components A and B. The multicanonical sampling technique within the grand canonical ensemble allows to bridge free energy barriers and to sample coexisting phases in one simulation. To direct the computational effort to density and concentration fluctuations only transfer and flip moves are performed.

We use two different ways of finding a preweighting function (see figure 7.1) in the first place:

- The order parameter distribution in the critical region has due to finite size effects a double peak structure which is weak enough to be able to go back and forth between the coexisting phases in a simulation run. Therefore we need not apply multicanonical sampling which means that we use a flat weight function within our simulation. Histogram reweighting is applied to get the order parameter distribution, and therefore a new preweighting function, deeper in the coexistence region.
- Another possibility is to use the Wang-Landau algorithm which has the advantage that it is not restricted to the critical region. Again we use histogram reweighting to obtain new weight functions.

Coexistence points are estimated by applying the **equal peak area criterion** [45] to the corresponding order parameter probability distribution function. This method only provides reliable results far enough away from the critical region so that the peaks corresponding to the coexisting phases do not overlap.

The critical points themselves are obtained by comparison of the order parameter distribution function with the universal fixed point function corresponding to the 3d Ising class [42][43].

7.1 Simulation Details

The interaction potential is cut off at a distance $r_c = 3\sigma$ and therefore a long range correction is applied

$$\mathcal{U} = \sum_{i<j} \phi_c(r_{ij}) + (N_{\mathrm{A}}^2 + N_{\mathrm{B}}^2 + 2N_{\mathrm{A}}N_{\mathrm{B}}\delta)\frac{2\pi\varepsilon}{z^2}(1 - zr_c)e^{-z(r_c-\sigma)}. \tag{7.1}$$

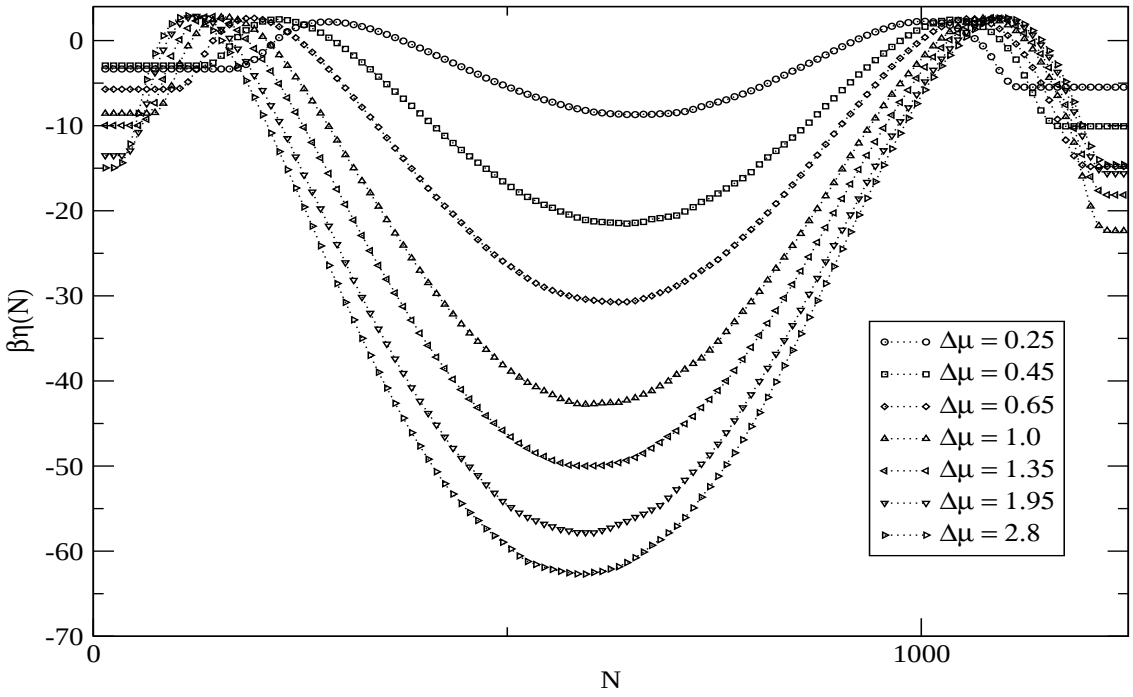

Figure 7.1: Examples of used weight functions ($l = 4$ and $T^{-1} = 0.96$; showing every 10th plot point).

The simulation box, for which periodic boundary conditions are applied, is divided into l^3 cubic cells, each of side r_c. The system sizes studied in this work correspond to $l = 4$ and $l = 7$.

We perform single and multi histogram reweighting to extra- and interpolate in the temperature T, in the ratio of dislike to like interaction strength δ, in the chemical potential $\mu_{\rm A}$ of component A, and in the field $\Delta\mu$.

The number density $\rho = N/V$ is an appropriate choice for the order parameter describing the vapour-liquid and the mixing-demixing transition. Therefore the preweighting function $\eta(N)$ only depends on the total particle number N and is incorporated in the acceptance ratios of the transfer moves

$$a(N \to N-1) = \min\left(1, \frac{N}{V} e^{-\beta[\mathcal{U}(\mathbf{r}^{N-1}) - \mathcal{U}(\mathbf{r}^N) - \mu + \eta(N-1) - \eta(N)]}\right) \tag{7.2}$$

$$a(N \to N+1) = \min\left(1, \frac{V}{N+1} e^{-\beta[\mathcal{U}(\mathbf{r}^{N+1}) - \mathcal{U}(\mathbf{r}^N) + \mu + \eta(N+1) - \eta(N)]}\right), \tag{7.3}$$

with $\mu = \mu_{\rm A}$ for the transfer of a particle of species A and $\mu = \mu_{\rm B}$ for transfer a particle of species B.

The demixing transition between an A rich and a B rich phase is best described by the order parameter $m = (N_{\rm A} - N_{\rm B})/N = 2c - 1$. The corresponding weight function is a function of the concentration $c = N/N_{\rm A}$ and therefore depends on the total particle number N and on the number of particles of species A, i.e. $N_{\rm A}$. The modified expressions for the acceptance ratios for

the transfer moves are given by

$$a(N_{\mathrm{A}} \to N_{\mathrm{A}} - 1) = \min\left(1, \frac{N}{V} e^{-\beta \Delta E^{-}}\right) \tag{7.4}$$

$$a(N_{\mathrm{A}} \to N_{\mathrm{A}} + 1) = \min\left(1, \frac{V}{N+1} e^{-\beta \Delta E^{+}}\right) \tag{7.5}$$

with

$$\Delta E^{-} = \mathcal{U}(\mathbf{r}^{N_{\mathrm{A}}-1}, \mathbf{r}^{N_{\mathrm{B}}}) - \mathcal{U}(\mathbf{r}^{N_{\mathrm{A}}}, \mathbf{r}^{N_{\mathrm{B}}}) - \mu_{\mathrm{A}} + \eta\left(\frac{N_{\mathrm{A}}-1}{N-1}\right) - \eta\left(\frac{N_{\mathrm{A}}}{N}\right) \tag{7.6}$$

$$\Delta E^{+} = \mathcal{U}(\mathbf{r}^{N_{\mathrm{A}}+1}, \mathbf{r}^{N_{\mathrm{B}}}) - \mathcal{U}(\mathbf{r}^{N_{\mathrm{A}}}, \mathbf{r}^{N_{\mathrm{B}}}) + \mu_{\mathrm{A}} + \eta\left(\frac{N_{\mathrm{A}}+1}{N+1}\right) - \eta\left(\frac{N_{\mathrm{A}}}{N}\right) \tag{7.7}$$

and we obtain for the flip moves

$$a(\mathrm{A} \to \mathrm{B}) = \min\left(1, e^{-\beta \Delta E^{\mathrm{A}\to\mathrm{B}}}\right) \tag{7.8}$$

with

$$\Delta E^{\mathrm{A}\to\mathrm{B}} = \mathcal{U}(\mathbf{r}^{N_{\mathrm{A}}-1}, \mathbf{r}^{N_{\mathrm{B}}+1}) - \mathcal{U}(\mathbf{r}^{N_{\mathrm{A}}}, \mathbf{r}^{N_{\mathrm{B}}}) - (\mu_{\mathrm{B}} - \mu_{\mathrm{A}}) + \eta\left(\frac{N_{\mathrm{A}}-1}{N}\right) - \eta\left(\frac{N_{\mathrm{A}}}{N}\right). \tag{7.9}$$

The corresponding expressions for the acceptance ratios for the transfer and flip moves of particles of species B can be easily derived.

We perform simulations at different sets of parameters which are compiled in table 7.1, 7.3, and 7.2 and sample the total particle number N, the particle number N_{A} of species A, the energy of like, and the energy of dislike particles every 500th sweep. In one sweep a flip and a transfer move are performed l^3 times, which means that we sampled the data every 64000 Monte Carlo steps for the system size corresponding to $l = 4$, and every 343000 Monte Carlo steps for $l = 7$. The number of samples collected in one simulation is of magnitude 10^6.

Wherever it is possible we make use of the symmetry of the system and obtain values for coexistence points and critical points for $c \leq 0.5$ and mirror the results at the $c = 0.5$ plane for the representations.

T	δ	μ_A	$\Delta\mu$
0.96	0.68	-3.3098	0.
0.96	0.68	-3.36993	0.1
0.96	0.68	-3.417298	0.15
0.96	0.68	-3.51679	0.25
0.96	0.68	-3.71688	0.45
0.96	0.68	-3.91722	0.65
0.96	0.68	-4.26781	1.0
0.96	0.68	-4.6181	1.35
0.96	0.68	-5.21849	1.95
0.96	0.68	-6.06879	2.8
0.976930	0.68	-3.370731	0.
0.98013	0.68	-3.38254	0.
0.98013	0.68	-3.41045	0.
1.0319	0.68	-3.6245	0
0.86	0.68	-5.61284	2.8

Table 7.1: Simulation parameters for the system size l=4.

T	δ	μ_A	$\Delta\mu$
0.975	0.67	-3.38877	0.06
0.97	0.67	-3.29884	0.02
0.97	0.68	-3.36738	0.04
0.981013	0.68	-3.39372	0.015
0.986	0.68	-3.395	0.010823

Table 7.2: Simulation parameters for the system size l=7.

T	δ	μ_A	$\Delta\mu$
0.960	0.68	-2.95	0.
0.991	0.68	-3.31	0.

Table 7.3: Simulation parameters for the demixing transition with system size l=7.

7.2 Results for $\delta = 0.68$

The isothermal cuts in figure 7.2 are obtained for a box length $l = 4$.

Figure 7.3 shows part of the isothermal cut for $T^{-1} = 0.98013$ and the density and concentration distribution functions corresponding to the specially marked coexistence points are shown in figure 7.4 and 7.5. The liquid peak of the density distribution function exhibits a weak double peak structure, which seems to be due to finite size effects close to a critical point at a lower temperature. This indicates that the mixing-demixing line does not cross over to the vapour liquid surface and that the phase diagram for $\delta = 0.68$ is of type β.

The figures 7.6 and 7.7 show results for coexistence lines ($\Delta\mu = 0$) and for critical points. The values of the critical points of figure 7.6 and 7.7 are compiled in the tables 7.4 to 7.7 and the matching of the corresponding order parameter distribution function and the universal fixed point function are presented in figures 7.8 to 7.11. Both functions have been shifted and scaled to gain unit variance which is denoted by $\overline{m}$ for the order parameter.

The distributions functions for the vapour-liquid transition in figures 7.8,7.9 and 7.10 become more and more asymmetric the closer they get to field range $[0.07, 0.115]$. This might be due to the triple line regimes at lower temperatures.

The matching of the distribution functions for the mixing-demixing transitions in figure 7.11 is only good enough to estimate critical points for $\Delta\mu$ lying in the interval $[0.01, 0.025]$.

In figure 7.11 we can see that the peak structure of the order parameter distribution for the demixing transition gets weaker for lower temperatures, which might be due to a tricritical point.

Values for critical points are presented without an error estimation and therefore no rounding takes place.

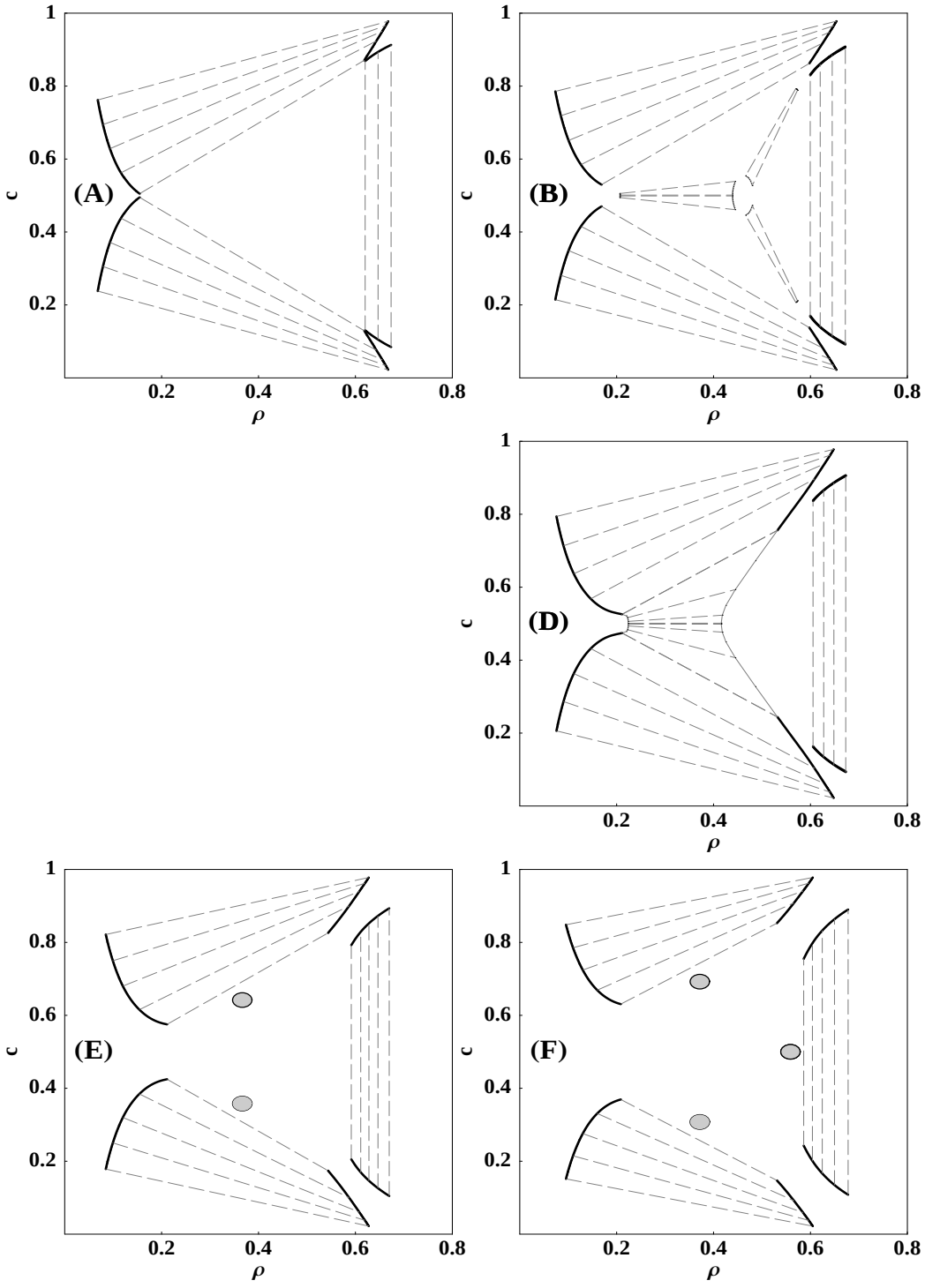

Figure 7.2: Isothermal cuts for $\delta = 0.68$ at $T \approx 0.999(\mathbf{A}), 1.014(\mathbf{B}), 1.020(\mathbf{D}), 1.041(\mathbf{E}), 1.064(\mathbf{F})$. The thin gray lines are coexistence curves strongly influenced by finite size effects and the dashed lines connect coexistence points and serve as a guide to the eye.

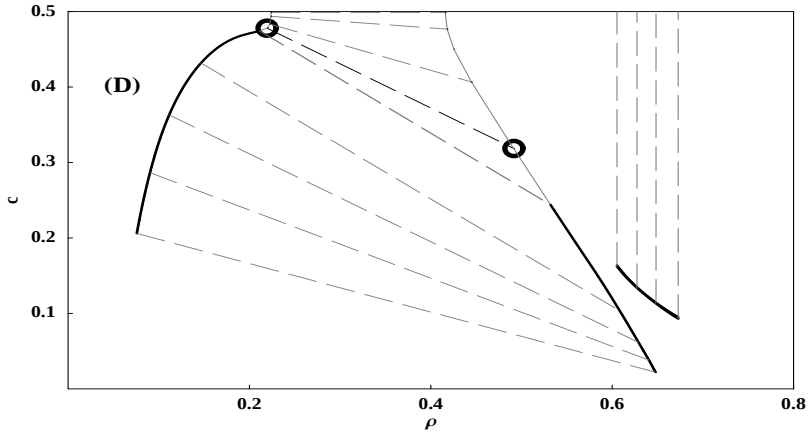

Figure 7.3: Isothermal cut for $T^{-1} = 0.98013$. The thin gray lines are coexistence curves strongly influenced by finite size effects and the dashed lines connect coexistence points and serve as a guide to the eye.

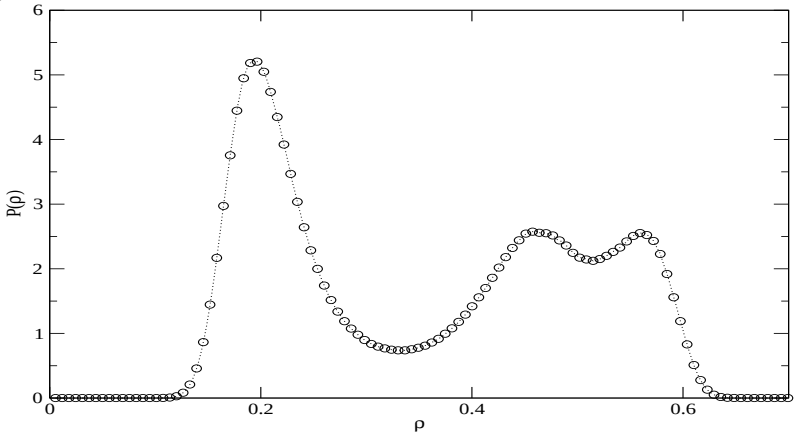

Figure 7.4: Number density probability distribution for the specially marked coexistence points of figure 7.3.

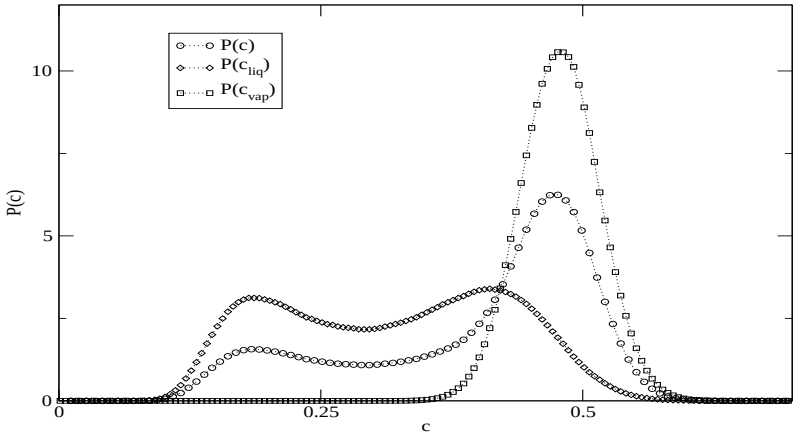

Figure 7.5: Concentration probability distribution for the specially marked coexistence points of figure 7.3.

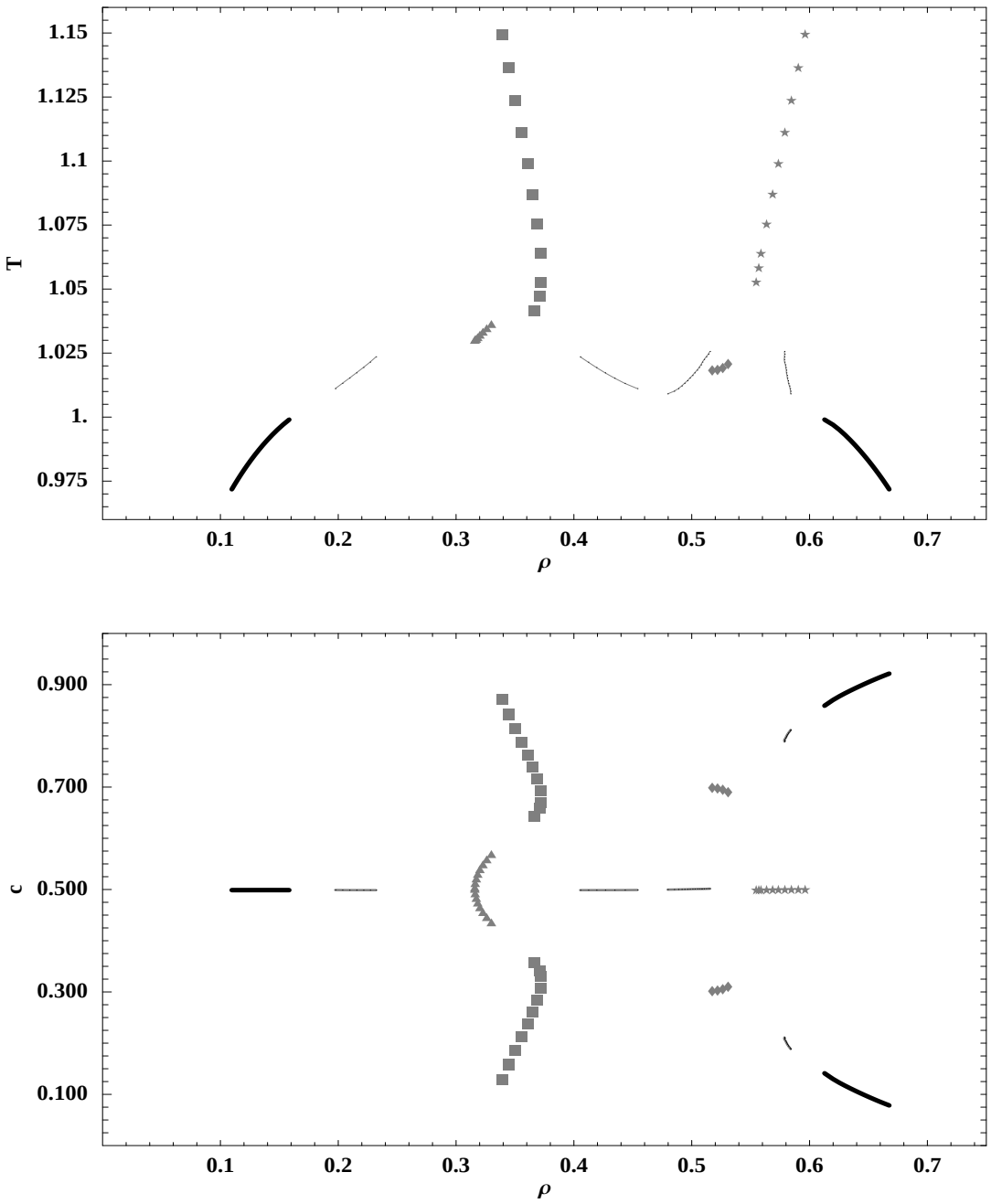

Figure 7.6: Projections of coexistence curves (l=4) and critical points (*stars* and *boxes* $l = 4$, *triangles* and *diamonds* $l = 7$). The thin gray coexistence curve is strongly influenced by finite size effects. The *triangles* and *boxes* denote vapour-liquid critical points, the *stars* denote demixing critical points, and the critical points of the transition between mixed and demixed liquid are denoted by *diamonds*.

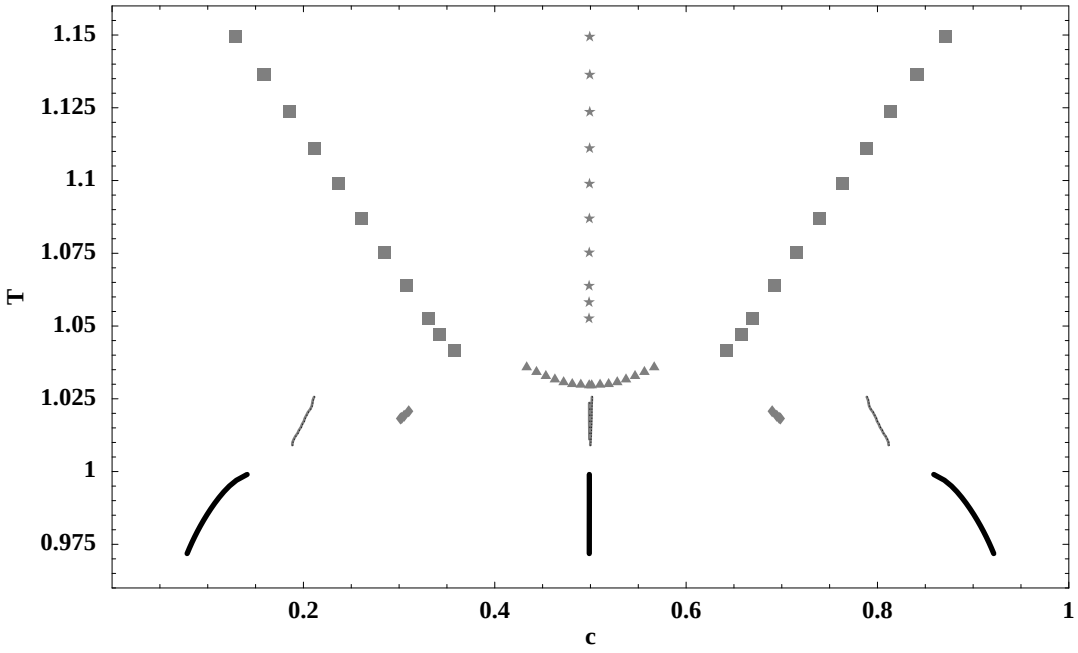

Figure 7.7: Same as in 7.6 projected onto the T-ρ plane.

ρ	c	T^{-1}	δ	μ_{A}	$\Delta\mu$
0.315899	0.498720	0.9712	0.68	-3.34974	0.00
0.316248	0.489943	0.9710	0.68	-3.35413	0.01
0.317190	0.480992	0.9708	0.68	-3.35878	0.02
0.318396	0.471979	0.9702	0.68	-3.36221	0.03
0.320229	0.462825	0.9693	0.68	-3.36478	0.04
0.322806	0.453386	0.9682	0.68	-3.36688	0.05
0.326022	0.443595	0.9669	0.68	-3.36846	0.06
0.329967	0.433351	0.9654	0.68	-3.36951	0.07

Table 7.4: Values for the vapour-liquid critical points ($l = 7$,*triangles*).

ρ	c	T^{-1}	δ	μ_{A}	$\Delta\mu$
0.339404	0.129408	0.870	0.68	-3.84502	0.990
0.344668	0.157994	0.880	0.68	-3.69874	0.800
0.344708	0.159023	0.880	0.68	-3.69374	0.795
0.350460	0.185905	0.890	0.68	-3.59203	0.649
0.355740	0.211972	0.900	0.68	-3.51587	0.528
0.360730	0.236829	0.910	0.68	-3.46129	0.428
0.365116	0.261082	0.920	0.68	-3.42332	0.344
0.369125	0.284347	0.930	0.68	-3.39887	0.273
0.371663	0.307657	0.940	0.68	-3.38511	0.212
0.371928	0.330865	0.950	0.68	-3.38071	0.160
0.371245	0.341948	0.955	0.68	-3.38170	0.137
0.366457	0.358047	0.960	0.68	-3.38291	0.114

Table 7.5: Values for the vapour-liquid critical points ($l = 4$, *boxes*).

ρ	c	T^{-1}	δ	μ_{A}	$\Delta\mu$
0.556930	0.498572	0.945	0.68	-3.037	-2.70381e-06
0.596229	0.499241	0.870	0.68	-2.307	-1.65290e-05
0.590439	0.499330	0.880	0.68	-2.415	-2.02925e-05
0.584580	0.499263	0.890	0.68	-2.520	-1.08064e-05
0.579040	0.499130	0.900	0.68	-2.621	-9.99252e-07
0.573533	0.498986	0.910	0.68	-2.719	+3.51564e-06
0.568650	0.498876	0.920	0.68	-2.813	+4.33229e-06
0.563505	0.498758	0.930	0.68	-2.905	+2.28111e-06
0.558734	0.498624	0.940	0.68	-2.994	-6.77226e-07
0.554704	0.498518	0.950	0.68	-3.080	-5.46676e-06

Table 7.6: Values for the demixing critical points ($l = 4$, *stars*).

ρ	c	T^{-1}	δ	μ_{A}	$\Delta\mu$
0.530875	0.310054	0.9797	0.68	-3.34547	0.010
0.526328	0.305261	0.9812	0.68	-3.36727	0.015
0.521904	0.302706	0.9819	0.68	-3.38227	0.020
0.517376	0.301452	0.9821	0.68	-3.39307	0.025

Table 7.7: Values for the mixing-demixing critical points ($l = 4$, *diamonds*).

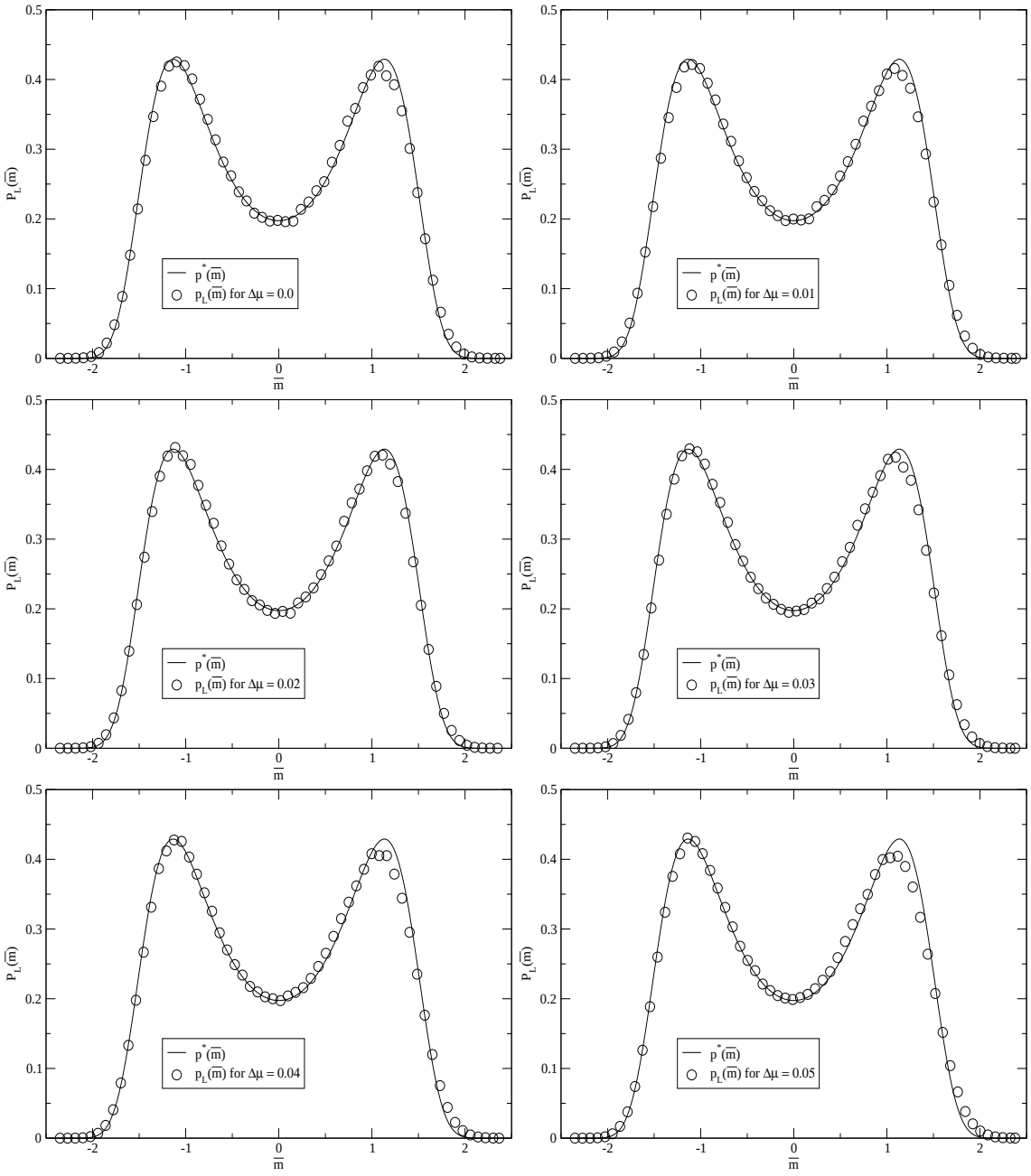

Figure 7.8: The scaled and shifted order parameter distribution functions of vapour-liquid critical points ($l = 7$, *triangles*) compared to the universal fixed point function for different values of $\Delta\mu$. $\overline{m}$ corresponds to the number density ρ.

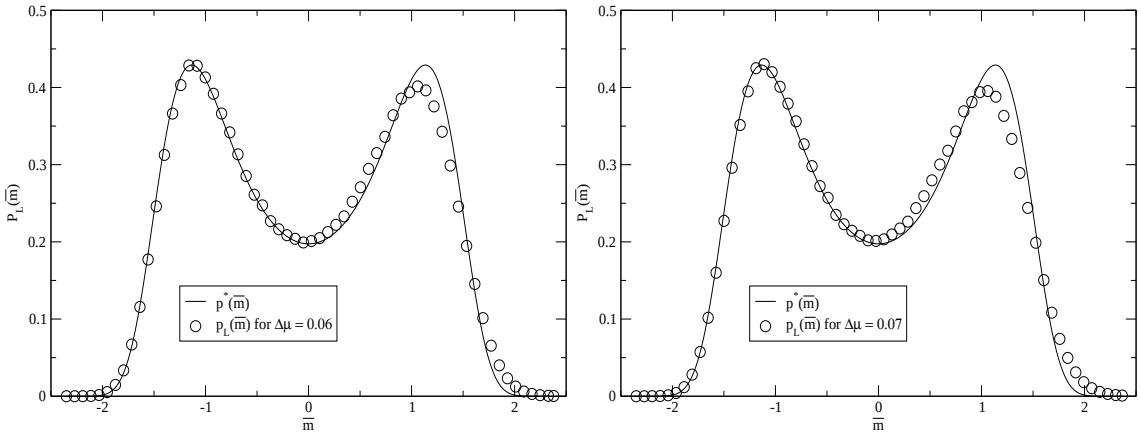

Figure 7.9: Same as in figure 7.8.

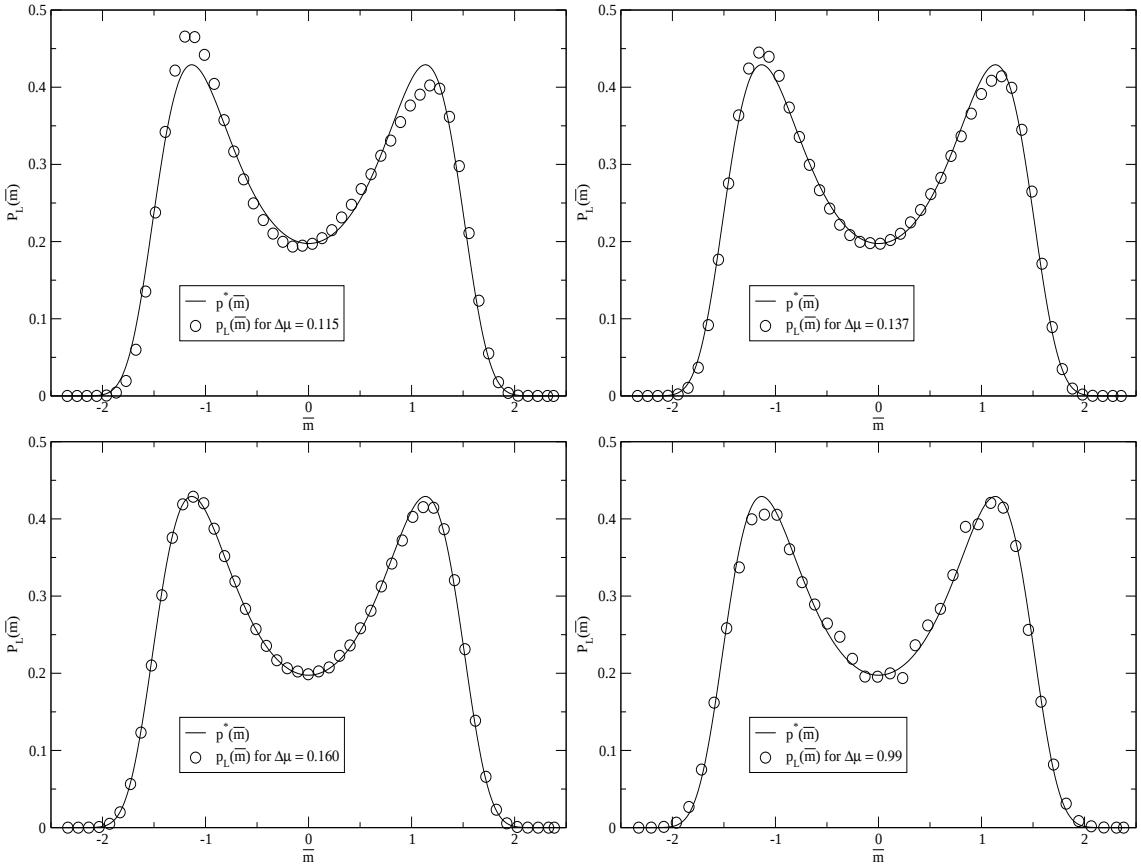

Figure 7.10: The scaled and shifted order parameter distribution functions of vapour-liquid critical points ($l = 4$, *boxes*) compared to the universal fixed point function for different values of $\Delta\mu$. $\overline{m}$ corresponds to the number density ρ.

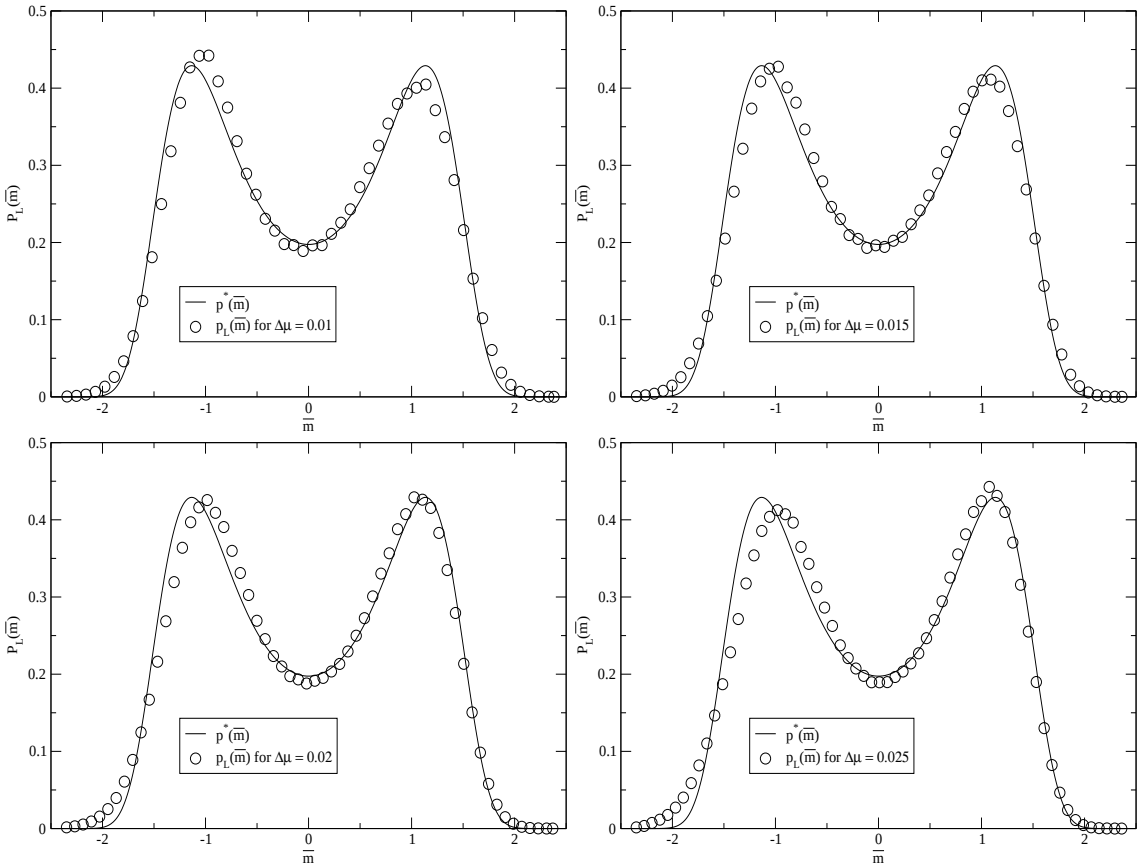

Figure 7.11: The scaled and shifted order parameter distribution functions of mixing-demixing critical points ($l = 7$, *diamonds*) compared to the universal fixed point function for different values of $\Delta\mu$. $\overline{m}$ corresponds to the number density ρ.

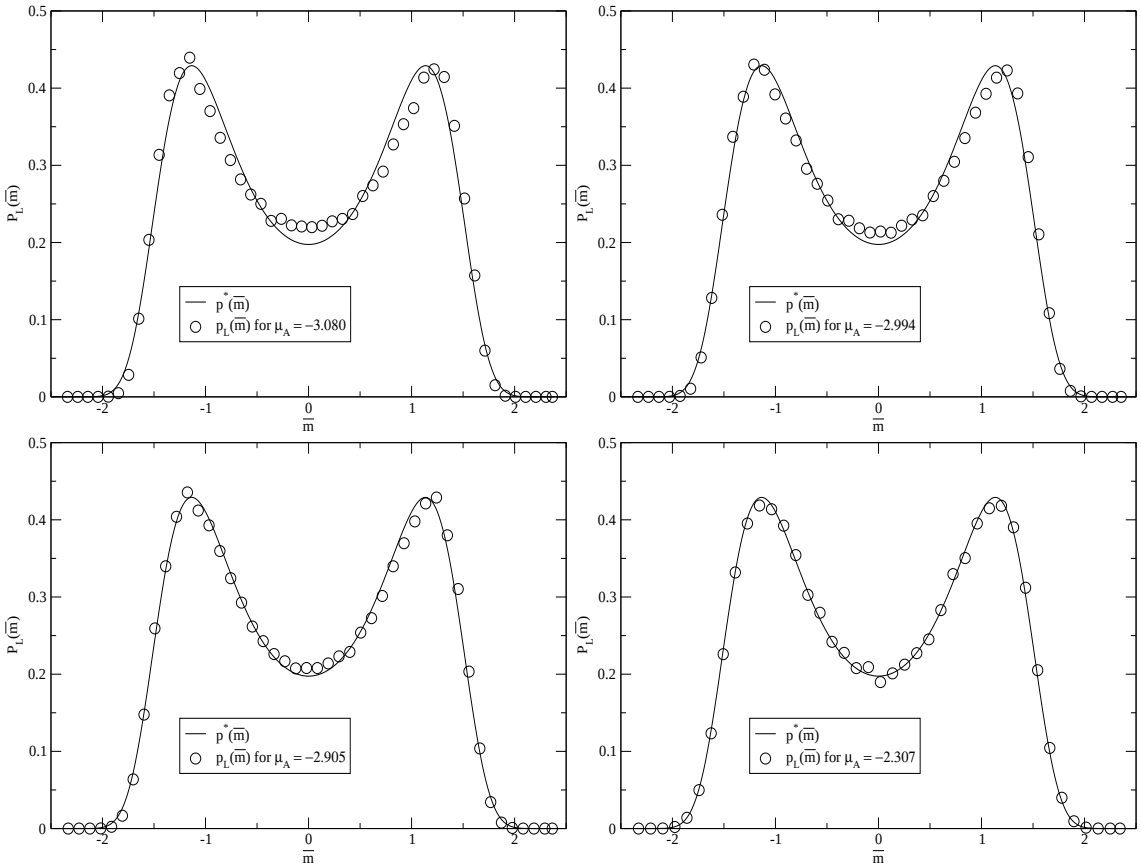

Figure 7.12: The scaled and shifted order parameter distribution functions of demixing critical points ($l = 4$, *stars*) compared to the universal fixed point function for different values of μ_{A}. $\overline{m}$ corresponds to the order parameter $m = 2c - 1$.

7.3 Conclusions

The symmetrical binary mixture is due to the rich phase behaviour a challenge for Monte Carlo simulation methods, which we have faced combining multicanonical sampling within the grand canonical ensemble and histogram reweighting methods.

We have discussed the complexities of type II phase diagrams in chapter 6, where we have found vapour-liquid, mixing-demixing, and demixing critical lines, triple lines, a quadruple point, and a tricritical point. Especially the finite size effects due to the different critical lines strongly affect the form of the probability distribution functions.

Critical points have been estimated by the comparison of the corresponding order parameter distribution function and the universal fixed point function appropriate to the 3d Ising universality class. Strictly speaking, field-mixing [46][47] effects have to be taken into account which is beyond the scope of this work.

Nevertheless, we have been able to show that the phase diagram for $\delta = 0.68$ belongs to type β and presented quantitative results for coexistence points and for vapour-liquid, mixing-demixing, and demixing critical points.

Appendix A

Coefficients

$$\xi_\nu = \frac{\pi}{6}\sum_i \rho_i \sigma_i^\nu \tag{A.1}$$

Parameters corresponding to the hard-sphere case:

$$A_j^0 = \frac{2\pi}{(1-\xi_3)^2}(1-\xi_3+3\sigma_j\xi_2) \tag{A.2}$$

$$B_j^0 = \frac{2\pi}{(1-\xi_3)^2}(-\frac{3}{2}\sigma_j^2\xi_2) \tag{A.3}$$

$$b_{ij}^0 = \frac{2\pi}{(1-\xi_3)^2}\left[\frac{3}{2}\sigma_i\sigma_j\xi_2\right] \tag{A.4}$$

Functions:

$$\theta_1(x) = 1-x-e^{-x} \tag{A.5}$$

$$\theta_2(x) = 1-x+\frac{1}{2}x^2-e^{-x} \tag{A.6}$$

Coefficients of equations (4.16):

$$M_m^{(a)} = 1+z\sigma_m \tag{A.7}$$

$$L_{mj}^{(a)} = 1+z\sigma_{mj}+\frac{1}{2}z^2\sigma_m\sigma_j \tag{A.8}$$

$$H_{lj}^{(a)} = zb_{lj}^0\theta_1(z\sigma_l) - A_j^0\theta_2(z\sigma_l) \tag{A.9}$$

$$G_{lj}^{(a)} = zA_l^0\theta_1(z\sigma_l) - \frac{4}{\sigma_j^2}B_j^0\theta_2(z\sigma_l) \tag{A.10}$$

$$F_{mlj}^{(a)} = L_{mj}^{(a)}G_{lj}^{(a)} - zM_m^{(a)}H_{lj}^{(a)} \tag{A.11}$$

$$E_{mlj}^{(a)} = (1+z\lambda_{jm})G_{lj}^{(a)} - zH_{lj}^{(a)} \tag{A.12}$$

$$D_{mjl}^{(a)} = \frac{1}{z^6}\left[\rho_m F_{mjl}^{(a)} + \delta_{mj}z^4(1-\frac{1}{2}e^{-z\sigma_j})\right] \tag{A.13}$$

$$C_{kmjl}^{(a)} = \frac{2\pi}{z^8}\rho_k\left[\rho_m(E_{mjl}^{(a)} - F_{mjl}^{(a)}e^{-z\sigma_m}) + \frac{1}{2}\delta_{mj}z^4(1-e^{-z\sigma_j})^2\right] \tag{A.14}$$

$$\tag{A.15}$$

$$A^{(4)}_{ij} = 2\pi K_{ij} \tag{A.16}$$

$$A^{(3)}_{lj} = \frac{1}{z^3}\rho_l H_{jl} - \delta_{lj} \tag{A.17}$$

$$A^{(2)}_{mjl} = \rho_l D^{(a)}_{mjl} \tag{A.18}$$

$$A^{(2)}_{kmjl} = \rho_l C^{(a)}_{kmjl} \tag{A.19}$$

$$H^{(b)}_{ij} = z b^0_{ij} + A^0_j \tag{A.20}$$

$$G^{(b)}_{ij} = z A^0_i - \frac{4}{\sigma_j^2} B^0_j \tag{A.21}$$

$$F^{(b)}_{mij} = L^{(a)}_{mj} G^{(b)}_{ij} - z M^{(a)}_m H^{(b)}_{ij} \tag{A.22}$$

$$E^{(b)}_{mij} = (1 + z\lambda_{jm}) G^{(b)}_{ij} - z H^{(b)}_{ij} \tag{A.23}$$

$$D^{(b)}_{mlj} = 2\pi\rho_l D^{(a)}_{mlj} \tag{A.24}$$

$$C^{(b)}_{kmjl} = \frac{2\pi}{z^6}\rho_m \left[\rho_k (E^{(b)}_{kij} - F^{(b)}_{kij} e^{-z\sigma_k}) - \frac{1}{2}\delta_{ik} z^4 e^{-z\sigma_i}\right] \tag{A.25}$$

$$B^{(5)}_{ij} = \frac{1}{z} A^0_j + b^0_{ij} \tag{A.26}$$

$$B^{(4)}_{lj} = \frac{2\pi}{z^3}\rho_l H^{(a)}_{lj} - 2\pi\delta_{lj} \tag{A.27}$$

$$B^{(3)}_{mij} = \frac{1}{z^4}\rho_m F^{(b)}_{mij} + \frac{1}{2}\delta_{im} \tag{A.28}$$

$$B^{(2)}_{kmlij} = \delta_{ik} D^{(b)}_{mlj} + \delta_{lm} C^{(b)}_{mkij} \tag{A.29}$$

$$B^{(1)}_{klmj} = 2\pi\rho_l C^{(a)}_{kmlj} \tag{A.30}$$

Coefficients of the factor correlation functions in equations (4.14) and (4.15):

$$C_{ij} = -\sum_l (\delta_{il} - \frac{2\pi}{z^2}\rho_l G_{il} e^{-z\sigma_i}) D_{lj} \tag{A.31}$$

$$f_{ij} = (C_{ij} + D_{ij}) e^{z\sigma_i} = \frac{2\pi}{z^2}\sum_l \rho_l G_{il} D_{il} \tag{A.32}$$

$$M_j = -\frac{1}{z^2}\sum_m \rho_m M^{(a)}_m D_{mj} - \frac{2\pi}{z^4}\sum_{mk} \rho_k\rho_m (1 - M^{(a)}_m e^{-z\sigma_m}) G_{mk} D_{kj} \tag{A.33}$$

$$N_j = \frac{1}{z^3}\sum_m L^{(a)}_{mj} D_{mj} + \frac{2\pi}{z^5}\sum_{mk} \rho_k\rho_m (1 + z\lambda_{jm} - L^{(a)}_{mj} e^{-z\sigma_m}) G_{mk} D_{kj} \tag{A.34}$$

$$A_j = A^0_j (1 + M_j) - \frac{4}{\sigma_j^2} B^0_j N_j \tag{A.35}$$

$$a_{ij} = A_j \tag{A.36}$$

$$b_{ij} = b^0_{ij}(1 + M_j) + A^0_i N_j \tag{A.37}$$

Expression needed for the calculation of the chemical potential $\frac{\Delta\mu_i}{k_B T}$:

$$\tilde{c}_{ij}(0) - c^0_{ij}(0) = (\overline{Q}_{ij} - \overline{Q}^0_{ij}) + (\overline{Q}_{ji} - \overline{Q}^0_{ji}) - \sum_{\rho_l} (\overline{Q}_{il}\overline{Q}_{jl} - \overline{Q}^0_{il}\overline{Q}^0_{jl}) \tag{A.38}$$

$$\overline{Q}_{ij} = \int_{\lambda_{ji}}^{\infty} Q_{ij}(r)\mathrm{d}r \tag{A.39}$$

$$\overline{Q}_{ij} = \frac{1}{6} a_{ij}\sigma_i^3 - \frac{1}{2} b_{ij}\sigma_i^2 - \frac{1}{z^2} C_{ij} M^{(a)}_i + \frac{1}{z^2} f_{ij} \tag{A.40}$$

$$\overline{Q}^0_{ij} = \frac{1}{6} a^0_{ij}\sigma_i^3 - \frac{1}{2} b^0_{ij}\sigma_i^2 \tag{A.41}$$

Appendix B

Tie Lines

Calculation of the tie lines

The system of volume V consists of two components labelled A and B. The total number of particles is N and N^A is the number of particles of species A. The density ρ and the concentration c are defined as

$$\rho = \frac{N}{V} \qquad c = \frac{N^A}{N}. \tag{B.1}$$

Two phases α and β which are in coexistence at the concentrations c^α and c^β and at the densities ρ^α and ρ^β are connected by so called tie lines. On a tie line the system consists of two phases α and β in thermodynamic equilibrium and moving along this line only the relative amounts of the phases change.

Assuming a point x of the tie line the system has the volume V_x and the total particle number N_x. The phase α has the volume V_x^α and N_x^α particles (with concentration c^α and density ρ^α). and the phase β has the volume V_x^β and N_x^β particles (with concentration c^β and density ρ^β). Therefore $N_x = N_x^\alpha + N_x^\beta$ and $V_x = V_x^\alpha + V_x^\beta$. The number of particles of species A at the point x of the tie line is called N_x^{A}.

The density ρ_x of the whole system is given by

$$\rho_x = \frac{N_x}{V_x} = \frac{N_x^\alpha + N_x^\beta}{V_x^\alpha + V_x^\beta} \tag{B.2}$$

and the overall concentration c_x is obtained by

$$c_x = \frac{N_x^{\mathrm{A}}}{N_x} = \frac{c^\alpha N_x^\alpha + c^\beta N_x^\beta}{N_x^\alpha + N_x^\beta}. \tag{B.3}$$

Fixing the volume $V_x = V$ where V is the volume of the system at phase coexistence we introduce a parameter γ

$$\gamma = \frac{V_x^\alpha}{V} \qquad 0 \le \gamma \le 1 \tag{B.4}$$

which parameterises the tie line:

$$\rho_x = \gamma\rho^\alpha + (1-\gamma)\rho^\beta \tag{B.5}$$

$$c_x = \frac{\gamma c_\alpha \rho^\alpha + (1-\gamma)c_\beta\rho^\beta}{\gamma\rho^\alpha + (1-\gamma)\rho^\beta} \tag{B.6}$$

Bibliography

[1] P. H. van Konynenburg and R. L. Scott
Philos. Trans. R. Soc. London **298** (1980) 495
Critical lines and phase equilibria in binary Van Der Vals Mixures

[2] P.C. Hemmer and D. Imbro
Phys. Rev. A **16** (1977) 380

[3] J.M. Tavaras, M.M. Telo da Gamma, P.I.CI Teixeira, J.J. Weis, and M.J.P Nijmeijer
Phys. Rev. E **52** (1995) 1915

[4] A. Oukousis and M. Baus
Phys. Rev. E **55** (1997) 7242

[5] M.A. Zaluska-Kotur and L.A. Turski
Phys. Rev. A **41** (1997) 3066

[6] H. Zhang and M. Widom
Phys. Rev. E **49** (1994) 3951

[7] B. Groh and S. Dietrich
Phys. Rev. E **50** (1994) 3814

[8] F. Schinagl, H. Iro, and R. Folk
Eur. Phys. J. B **8** (1999) 113

[9] M.J.P. Nijmeijer, A. Parola, and L. Reatto
Phys. Rev. A **41** (1990) 3966

[10] R.O. Sokolovskii
Phys. Rev. B **61** (2000) 36

[11] N. B. Wilding, F. Schmid, P. Nielaba
Phys. Rev. E **58** (1998) 2201-2212
Liquid-vapour phase behaviour of a symmetrical binary fluid mixture

[12] Elisabeth Schöll-Paschinger and Gerhard Kahl
Journal of Chem. Phys. **118** (2003) 7414
Self-consistent Ornstein-Zernike approximation for a binary symmetric fluid mixture

[13] E. Gutlederer
Diplomarbeit (2003)
Long-Range Behaviour of Pair Correlation Functions in Symmetric Binary Mixtures

[14] D. Pini, M. Tau, A. Parola, L. Reatto
Phys. Rev. E **67** (2003) 046116
Phase diagram of symmetric binary mixtures at equimolar and nonequimolar concentrations: A systematic investigation

[15] E. Arrieta, C. Jedrejek, K.N. Marsh
J. Chem. Phys. **86** (6) (1987) 3607-3626
Numerical MSA solution for binary Yukawa mixtures

[16] E. Arrieta, C. Jedrejek, K.N. Marsh
J. Chem. Phys. **95** (9) (1991) 6806-6837
Mean spherical approximation algorithm for multicomponent multi-Yukawa fluid mixtures: Study of vapour-liquid, liquid-liquid, and fluid-glass transitions

[17] J. S. Høye and L. Blum
J. Stat. Phys. **16** (1977) 399

[18] J. S. Høye and L. Blum
J. Stat. Phys. **19** (1978) 317

[19] Daan Frenkel and Berend Smid
Academic Press, Sand Diego 1996
Understanding Molecular Simulation

[20] M. E. J. Newman and G. T. Barkema
Clarendon Press, New York 1999
Monte Carlo Methods in Statistical Physics

[21] David P. Landau and Kurt Binder
Cambridge University Press, Cambridge 2000
A Guide to Monte Carlo Simulations in Statistical Physics

[22] Bernd A. Berg and Thomas Neuhaus
Phys. Rev. Let. **68** (1992) 9
Multicanonical Ensemble: A New Approach to Simulate First-Order Phase Transitions

[23] Alan M. Ferrenberg and Robert H. Swendson
Phys. Rev. Let. **61** (1988) 2635

[24] Alan M. Ferrenberg and Robert H. Swendson
Phys. Rev. Let. **63** (1989) 1195
Optimized Monte Carlo Data Analysis

[25] Nigel B. Wilding
Am. J. Phys. **69** (2001) 1147
Computer simulation of fluid phase transitions

[26] J.M. Yeomans
Clarendon Press, Oxford 1992
Statistical Mechanics of Phase Transitions

[27] R.B. Griffiths and J.C.Wheeler
Phys. Rev. A **2** (1970) 1047
Critical points in multicomponent systems

[28] J.S. Rowlinson and F. L. Swinton
Butterworth, London 1982
Liquids and Liquid Mixtures

[29] L.S. Ornstein and F. Zernike
Proc. Akad. Sci. (Amsterdam) **17** (1914) 793

[30] J. P. Hansen and I. R. McDonald
Academic Press, New York 1986
Theory of Simple Liquids

[31] C. Caccamo
Phys. Rep. (1996) 274
Integral Equation Theory
Description of phase equilibria in classical fluids

[32] J. L. Lebowitz and J. Percus
Phys. Rev. **144** (1966) 217

[33] R.J. Baxter
J. Chem. Phys. **52** (1970) 4559

[34] G. Pastore
Mol. Phys. **55** (1988) 187

[35] N.F. Carnahan and K.E. Starling
J. Chem. Phys. **51** (1969) 635

[36] E. Lomba, J.-J. Weis, N. G. Almarza, F. Bresme and G. Stell
Phys. Rev. E **49** (1994) 5169

[37] L. E. Reichl
John Wiley & Sons, New York 1998
A Modern Course in Statistical Physics

[38] G. G. Torrie and J. P. Valleau
J. Comput. Phys. **23** (1977) 187-199
Nonphysical sampling distributions in MC free energy estimation: Umbrella Sampling

[39] Fugao Wang and D. P. Landau
Phys. Rev. E. **64** (2001) 056101-1
Determining the density of states for classical statistical models:
A random walk algorithm to produce a flat histogram

[40] Micheal E. Fisher and Micheal N. Barber
Phy. Rev. Let. **28** (1972) 1516
Scaling Theory for Finite-Size Effects in Critical Region

[41] John L.Cardy (editor)
North Holland, Amsterdam 1988
Finite Size Scaling

[42] R. Hilfer and N. B. Wilding
J. Phys. A **28** (1995) 281
Are critical finite size scaling functions calculable from knowledge of an appropriate critical exponent?

[43] M.M. Tsypin and H.W.J. Blöte
Phys. Rev. E **62** (2000) 73
Probability distribution of the order parameter for the three-dimensional Ising-model universality class: A high-precision Monte Carlo study

[44] Wolfram Research Inc.
www.wolfram.com

[45] C. Borgs and R. Kotecky
Phys. Rev. Lett **68** (1992) 1734

[46] A. D. Bruce and N.B. Wilding Phys. Rev. Lett. **68** (1992) 193
Scaling Fields and Universality of the Liquid-Gas Critical Point

[47] Nigel B. Wilding
Phys. Rev. E **52** (1995) 602
Critical-point and coexistence-curve properties of the Lennard-Jones fluid: A finite-size scaling study

Acknowledgements

I want to thank ...

Gerhard Kahl for his support, friendliness, and encouragement.
Nigel B. Wilding for his hospitality, generosity, and support.
Bianca, Dieter, Gernot, and Maria for their friendship and their help.
Helen and Graham for their friendliness and for their helpfulness.

... and ...

my parents Rosi and Walter for their confidence in me and my decisions, for their manifold support, and for their love.
my sister Manuela and my brother Mario for their faith in me.
my friends Wolfgang, Reinhard, and Philipp for knowing me so well.
Pippa for being there for me, when I really needed someone.

I want to thank Trixi for her support, her encouragement, her understanding, and her love.

Danksagung

Ich danke ...

Gerhard Kahl für seine Unterstützung, Freundlichkeit und Ermutigung.
Nigel B. Wilding für seine Gastfreundschaft, Großzügigkeit und Unterstützung.
Bianca, Dieter, Gernot und Maria für ihre Freundschaft und ihre Hilfe.
Helen und Graham für ihre Freundlichkeit und ihre Hilfsbereitschaft.

... und ...

meinen Eltern Rosi und Walter für ihr Vertrauen in mich und meine Entscheidungen, für ihre vielfältige Unterstützung und ihre Liebe.
meiner Schwester Manuela und meinem Bruder Mario für ihr Vertrauen in mich.
meinen Freunden Wolfgang, Reinhard und Philipp dafür, dass sie mich so gut kennen.
Pippa dafür, dass sie für mich da war, als ich wirklich jemanden gebraucht habe.

Ich danke Trixi für ihre Unterstützung, ihre Ermutigungen, ihr Verständnis und ihre Liebe.

To boldly go in phase-space where no one has gone before ...